Reliability Assessment of Drag Embedment Anchors and Laterally Loaded Buried Pipelines

by

© Amin Aslkhalili

A thesis submitted to the

School of Graduate Studies

In partial fulfillment of the requirements for the degree of

Master of Engineering

Faculty of Engineering and Applied Science

Memorial University of Newfoundland

October 2020

St. John's, Newfoundland

Abstract

Drag embedment anchors and buried subsea pipelines are two important elements of the offshore field developments that are used for station-keeping of floating facilities and transferring the hydrocarbons, respectively. The lateral soil resistance against the drag anchors and pipelines are mobilized in a similar fashion with identical conventional design equations. This is fundamentally caused by similar lateral projection of the anchor and pipe geometries. The reliability assessment of the drag embedment anchors as a key component of mooring systems, and the lateral response of trenched pipelines as crucial structural elements are significantly important due to a range of uncertainties involved in the design process. Despite the similar design equations for lateral soil resistance against the moving anchor and pipe, these elements are subjected to different kinds of loadings and uncertainties that are expected to affect their reliability indices. In this study, the reliability of drag embedment anchors and laterally displaced pipelines were conducted and compared to investigate the extent of similar fashions in the lateral response of these two elements to large displacements. Both uniform and non-homogeneous soil domains were considered and compared to evaluate the impact of more realistic design scenarios. Macro spreadsheets were developed for iterative limit state and kinematic analyses and obtaining the holding capacity of drag embedment anchors. The lateral force-displacement responses of the buried pipelines were extracted from published centrifuge model tests and incorporated into finite element models in ABAQUS. Automation Python scripts were developed to perform a comprehensive series of numerical analyses and post-process the outputs to construct the required databases. Response surfaces were developed and probabilistic analyses were conducted by using the first order reliability method (FORM) to obtain the reliability indices and failure probabilities.

Comparative studies were conducted to obtain an equivalent annual probability of failure between the pipelines and drag anchors. The study showed that the similar conventional approaches for modeling of the anchors and pipelines lateral displacement might be acceptable for homogeneous soil domains. However, the reliability indices were significantly affected by defining non-homogenous soil domains. It was observed that the magnitude of the reliability indices in the layered soil strata and trenched/backfilled conditions could be significantly reduced. This, in turn, revealed the need for improving the current design codes to incorporate more realistic conditions. The proposed probabilistic approach was found robust to optimize the subsea configuration of the anchors and pipelines and improve the reliability indices. The study revealed several important trends in anchors and pipeline-seabed interactions and provided an in-depth insight into its impact on reliability assessment and a safe and cost-effective design.

Acknowledgment

First of all, I would like to thank my supervisor, Dr. Hodjat Shiri, for his valuable guidance, supports, and the belief that he had in me to allow me to be a part of his research team. He was beside me in every step of this journey, and I would never forget what he had taught me.

My best regards go to Dr. Sohrab Zendehboudi, my co-supervisor, who helped me through this path.

I want to gratefully acknowledge the financial support of this research by Wood PLC via establishing the Wood Group Chair in Arctic and harsh environment engineering at Memorial University, the NL Tourism, Culture, Industry and Innovation (TCII) via CRD collaborative funding program, the Natural Sciences and Engineering Research Council of Canada (NSERC) via Engage funding program, the in-kind technical supports and advice of TechnipFMC, NL, Canada, the Memorial University of Newfoundland through VP start-up fund, and the school of graduate studies (SGS) baseline fund.

Last but foremost, my sincere thanks go to my Mother, Father, and beloved wife (Setareh). They lovingly encouraged me through my studies and supported me emotionally in every day of this stressful journey. I am thankful for having you beside me.

Contents

List of Figures

List of Tables

List of Symbols and Abbreviations

A_s	Area of shank
A_t	Fluke tip area
b_c	Effective chain width
b_f	Fluke width
b_s	Shank width
C_{ub}	Backfill soil undrained shear strength
C_{un}	Native soil undrained shear strength
d	Nominal chain diameter, Trench depth
D	Pad-eye embedment depth, Pipe outer diameter
d_a	Attachment depth
d_{ai}	Initial fluke depth
$d_{a_{eff}}$	Effective attachment depth
d_c	Depth of overlaying clay layer
d_f	Fluke thickness
d_s	Average depth of the shank
d_t	Depth of fluke's tip
d_{sb}	Embedment depth of back lower point of shank
d_{sf}	Embedment depth of front lower point of shank
du_a	The absolute displacement of the anchor
du_s	Soil wedge displacement
du_{sa}	Displacement of the soil relative to the anchor
d_w	Wave direction
d_{wc}	Current direction relative to wave
d_{ww}	Wind direction relative to wave
E_n	Normal circumference parameter
E_n	Tangential circumference parameter
F	Form factor (Neubecker and Randolph 1996)
f_y	Yield stress of pipe
$f(X)$	Joint probability function of X
F	Friction force
F_f	The fluke force
F_{fb}	The force on the back of the fluke
F_{fc1}	Normal fluke clay force
F_{fc2}	Shear fluke clay force
F_{fs}	Sand fluke force
$F_R(r)$	Cumulative distribution of load
F_s	The shank force
$F_S(s)$	Cumulative distribution of capacity
F_{sc1}	Normal shank clay force
F_{sc2}	Shear shank clay force
F_{sc3}	Side shank clay force
F_{ss}	Sand shank force
F_t	Fluke tip force
$G(X)$	Limit state function, Performance function
$G(R,S)$	Limit state function
$G(u_R,u_S)$	Transformed limit state function to standard normal space
$G'(u_R,u_S)$	Approximation of transformed limit state function
h	Back edge of the fluke
H	Depth of fluke tips
H_s	Significant wave height
L_f	Fluke length
L_f	Caisson length (Silvia-Gonzalez et al. 2013)
L_s	Shank length

M	Magnitude of the earthquake
N_c	Bearing capacity factor of clay
N_q	Standard bearing capacity factor and bearing capacity for sand
N_{qs}	Shank bearing factor in sand
N_t	Bearing factor of fluke tip in sand
p_F	Probability of failure
p_{Fa}	Annual probability of failure
P_{u1}	First peak of lateral soil force per unit length of pipe
P_{u2}	Second peak of lateral soil force per unit length of pipe
Δ_{P1}	Displacement at P_{u1}
Δ_{P2}	Displacement at P_{u2}
q	Bearing pressure
q_{sand}	Demonstrative of standard sand strength
Q	Normal soil reaction on chain segment
Q_d	Peak of downward vertical soil force per length of pipe
Q_{eff}	Effective profile of resistance
Q_u	Peak of upward vertical soil force per length of pipe
$\bar{Q}$	Average bearing resistance per unit length of chain over embedment depth
Δ_{qd}	Displacement at Q_d
Δ_{qu}	Displacement at Q_u
R	Anchor capacity at mudline, Soil reaction
$R(X)$	Load function
R_a	Anchor capacity at pad-eye
R_d	Design anchor capacity at mudline
$R_{d,a}$	Design resistances at the pad-eye
r_i	Distance between point i and anchor shackle
s	Length of chain
s_{ug}	Undrained shear strength gradient
s_{u0}	Surface undrained shear strength
$S(X)$	Capacity function
SF	Side friction
t	Pipe thickness
T	Line tension
T_a	Line tension at the pad-eye
T_a'	Revised anchor capacity at the pad-eye
T_d	Design line tension at mudline
$T_{d,a}$	Design tensions at the pad-eye
$T_{dyn,max}$	Mean maximum dynamic line tension
$T_{dyn,max-C}$	Characteristic mean maximum dynamic tension
T_{mean}	Mean line tension
T_{mean-C}	Characteristic mean line tension
T_o	Chain tension at mudline
T_p	Spectral peak period
T_u	Peak of axial soil force per length of pipe
T^*	Normalized tension
Δt	Extreme sea state duration, Displacement at T_u
u_R	Rosenblatt transformation of load
u_S	Rosenblatt transformation of capacity
u^*	Most probable point
U_{10}	Wind velocity
U_c	Surface current velocity direction
w, w_c	Chain self-weight per unit length, Trench width
W_a	Anchor dry weight
W_a'	Sub anchor weight
W_s	The mobilized soil mass
W_{sc}	Weight of soil wedge

x_a	Anchor horizontal displacement
X	Absolute displacement of point i, Set of uncertain parameters, Probability density function
x*	Horizontal distance normalised by D
Δx	Absolute penetration increments of the origin
Y	Absolute displacement of point i
Δy	Absolute penetration increments of the origin
Z	Depth below mudline
z*	Depth normalised by D
α_h	Strain hardening parameter
α_{gw}	Girth weld factor
α_s	Side shear factor
β	Inclination of fluke, reliability index, The angle of pipe-fault intersection
β_{annual}	Annual reliability index
β_F	First order reliability index
β_i	Initial fluke angle
γ	Clay soil unit weight
γ_ε	Resistance strain factor
γ'	Effective unit weight of soil
γ_c'	Clay effective unit weight
γ_{dyn}	Partial safety factor on dynamic line tension
γ_{mean}	Partial safety factor on mean line tension
γ_s'	Sand effective unit weight
δ	Coefficient of variation
δ_c	Seabed surface depth
δ_{fs}	Average fault movement
ε_c	Compression strain
ε_d	Design compression strain
η_a	Anchor efficiency
θ	Line tension angle
θ_a	Line tension angle at the pad-eye
θ_f	Fluke wedge angle
θ_{fs}	Fluke-shank angle
θ_i	Polar coordinate angle of point i
θ_o	Line tension angle at mudline
Δθ	Rotation increments of the origin
λ	Failure wedge angle, mean annual rate of extreme sea states, Occurrence rate
μ	Chain-soil friction coefficient, Mean
σ_h	Hoop stress
$\emptyset'$, $\emptyset_p'$	Soil friction angle
$\emptyset_p$	Sand peak friction angle
Θ	Vector of environmental variables
ψ	Dilation angle
$\Phi^{-1}(\,)$	Inverse of the cumulative standard normal function

Chapter 1. Introduction

1.1 Background and Motivation

Offshore field developments require drag embedment anchors as a critical component of the mooring system and buried subsea pipelines for station-keeping the floating structures, and hydrocarbons transportation. Similar lateral projection of the anchor and pipe geometries results in the similarity between the lateral soil resistance against the drag anchors and pipelines, which are organized using conventional design equations (Dickin, 1994; Ng, 1994). The broad range of uncertainties involved in the design process imposes the reliability assessment of crucial structural elements such as the drag embedment anchors and the lateral response of trenched pipelines. These structural elements encounter different types of loadings and uncertainties, which affect their reliability indices. In the current study, the reliability of drag embedment anchors and laterally displaced pipelines were explored and compared in both homogeneous and non-homogenous soil to investigate the similarity extent of lateral response of these two elements under large displacements. The following sections provide a brief introduction about the drag embedment anchors and buried pipelines:

1.1.1 Drag Embedment Anchors

Floating facilities such as operation vessels, semi-submersibles, Spars, and FSPOs, etc. are used to extraction and production of hydrocarbon from offshore reserves. The ideal solution for station keeping of floating facilities is using catenary mooring systems combined with seabed anchors. Different types of anchors could be used with mooring systems like suction anchors, pile anchors, screw-in anchors, plate anchors, deadweight anchors, and drag embedment anchors. Nevertheless, the drag embedment anchors are considered to be the most attractive method due to their cheap and straightforward installation procedure and could be used for temporary and permanent

mooring systems. Despite convenient installation, the evaluation of holding capacity in drag embedment anchors is challenging due to their complex geometry and uncertain interaction between the seabed and anchors.

In order to have safe floating facilities and offshore environments, it is essential to fulfilling the reliability of the mooring and anchoring system. This requirement has increased by expanding offshore exploration and extraction toward the deep waters and harsh environments that need high capacity anchors and high strength components in the mooring system. On the other hand, the complex behavior of seabed with the anchor and environmental loads along with the unavailability to inspect, maintain and, monitor of drag anchors highlights the importance of reliability assessments to reduce the probability of failure in the system as much as possible.

The reliability assessment of drag embedment anchor families is dramatically less developed compared to other anchor types, e.g., suction anchors. In the literature, there are numerous of studies focused on the reliability assessment of various anchor types including suction anchors (Choi, 2007; Valle-molina et al., 2008; Clukey et al., 2013; Silva-González et al., 2013; Montes-Iturrizaga and Heredia-Zavoni, 2016; Rendón-Conde and Heredia-Zavoni, 2016). However, due to complicated interaction between the seabed and anchors, limited access to holding capacity databases, and the difficulties associated with performing computational analyses to estimate the reliability of drag embedment anchor families. (Moharrami and Shiri, 2018) studied the reliability of drag embedment anchors in clay, but there are no reliability investigations in the sand or layered seabed. For estimation of holding capacity, there are some design codes (e.g., API RP 2SK, 2008) which only recommend a unique procedure for homogenous (clay or sand) and layered seabed. In the layered seabed, this simplification will dramatically affect the reliability of the system, and the level of risk will not be appropriately estimated.

1.1.2 Subsea Pipelines

Buried pipelines considered as one of the most attractive ways for transportation of hydrocarbons and other contents in onshore and offshore environments. In Canada, as stated by the Canadian Energy Pipeline Association (CEPA), 130,000 km of underground transportation pipelines operate daily to transmit 97 percent of Canada's consumption of crude oil and natural gas from production plants to markets across North America (www.cepa.com). Both offshore and onshore buried pipelines pass through different types of soils where the integrity of pipes may be threatened by a variety of subsea geohazards and the resulted ground movements, which could cause significant damages and leading to their failure. European Gas pipeline Incident data Group (EGIG) stated the fourth primary reason for pipeline failures is ground movements, and pipe rupture is the consequence of almost half of these incidents (EGIG, 2005). Ground movements initiate relative lateral movements between soil and pipe that may cause extra loading on the buried pipelines. In designing subsea pipelines, understanding the behavior of buried pipelines under loading is an important engineering consideration.

Trenching the buried pipelines is a known and common construction practice during the installation of subsea pipes. Due to excavation or supplying the required soil inside the trench from other areas with different geotechnical properties, the backfill material which fills the trench would not have the same properties as the native trench soil has. Therefore, the soil around the buried pipelines is not homogenous anymore and comprised of backfill and native soil, which have different soil resistance against the pipe during different phases of pipe movement through the soil. From the state of design point of view, the current design guidelines utilize discrete nonlinear springs for each orthogonal loading axis (x, y, and z) for representing the soil resistance in the axial, vertical and lateral direction on buried pipelines (ASCE, 1984; PRCI, 2009; ALA, 2005;

DNV, 2007). In the most design guidelines except PRCI (2009), the surrounding soil is assumed to be homogenous and the effect of the trench is neglected. There are some studies in the literature which covers the impact of the trench and backfill on the lateral interaction of soil-pipe in clay (C-CORE, 2003; Phillips et al., 2004). The results of those studies are incorporated in the PRCI (2009) design guideline, which could help to have a better understating and calculation of lateral force-displacement relations in clay.

The geometry and the geotechnical properties of the backfill and native soil of the trench directly affects the lateral force-displacement of trenched pipelines. Therefore, in order to have a safe and cost-effective trenched pipeline design at the same time, it is required to perform reliability analysis to find out the most optimum and reliable trench geometry and see the effect of using guidelines which neglect consideration of trench effects against more advanced methodologies (covering the trench effects) on the reliability of the system.

1.2 Research Objectives

The research objectives were set to fill some of the key knowledge gaps. These objectives were successfully achieved throughout the study:

- Develop numerical and analytical models to obtain the holding capacity of anchors and the dynamic mooring line tensions as the input parameters for the probabilistic modeling and reliability assessment of drag embedment anchors in sand. There was no study in the literature to have considered the sand seabed.
- Extend the developed reliability analysis model to study the effect of complex layered seabed soil strata.

- Develop a three-dimensional finite element model integrated with a probabilistic model for reliability assessment of the fault-induced lateral pipe/soil interaction in homogeneous seabed stratum.
- Extend the developed model to capture the effect of trenching/backfilling on lateral pipe response to the ground movement.
- Compare the reliabilities of the drag embedment anchors and the laterally displaced pipelines with the effect of non-homogeneous seabed soil strata.

1.3 Thesis Organization

The thesis was prepared in a paper-based format. The outcomes are presented through six chapters. Chapter 1 describes the background, motivation, objectives, and organization of the thesis. Chapter 2 includes a critical literature review. It is worth mentioning that each chapter is a manuscript and has its independent literature review. However, to facilitate reading the thesis, the literature review of various chapters were properly integrated and presented in Chapter 2. Chapter 3 presents a journal paper published in "Safety in Extreme Environments" (Springer). The paper investigates the reliability assessment of drag embedment anchors in sand that has never been done in the past. Chapter 4 is a comprehensive conference paper accepted for oral presentation in the 73rd Canadian Geotechnical Conference (GeoCalgary 2020). The paper presents the reliability assessment of drag embedment anchors in complex layered seabed soil stratum. In this chapter, the reliability indices of the anchors in layered seabed was compared with the sand seabed to investigate the effect of non-homogeneous soil conditions. Chapter 5 is a journal manuscript that discusses developing a three-dimensional FE model to capture the pipe/soil interaction with the incorporation of the trench effects. A platform was developed in this chapter to conduct a probabilistic model, assess the reliability of buried pipelines in clay, and investigate the optimum trench geometry. Chapter 6

summarizes the key findings and observations made throughout the study. The comparative reliability of drag embedment anchors and subsea pipelines were also discussed. Moreover, recommendations were provided for future studies.

Chapter 2. Literature Review

2.1 Mooring and Anchoring System

The floating facilities were emerged during the recent years by developments of offshore hydrocarbon discoveries toward deeper waters. The advancement of floating facilities such as semi-submersible platforms, floating production, storage, and offloading (FSPO) facilities has resulted in the exploration and production of hydrocarbon fields located in water deeper than 400 m. As stated by U.S. Energy Information Administration (www.eia.gov), offshore oil resources provide nearly 30 percent of global oil production. Before these developments, the fixed structures, including monopods, concrete gravity structure (CGS), and steel jackets structures were able to discover and exploit the resources limited to 300 m water depth (O'Neill, 2000). Different offshore structure representation is in Figure 2-1.

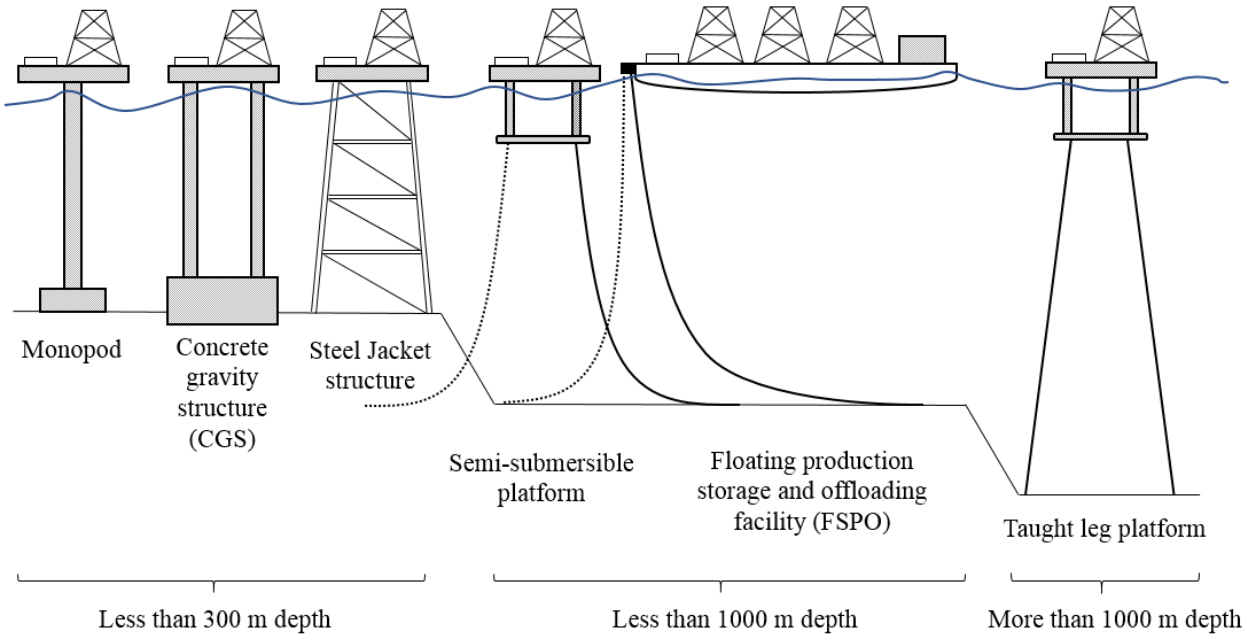

Figure 2-1. Different offshore structures

Two distinct groups of mooring systems, including the catenary mooring lines and the taut line mooring, are employed for anchoring of floating structures. The depth of water defines which mooring system group would be used. The floating structure should be surrounded by groups of mooring lines for station keeping of the floating structure. The catenary mooring line system is suitable for the shallow to deep water depth (less than 1000 m). In this alignment, the catenary lines arrive at the seabed horizontally and only subjected to horizontal force. It should be pointed out that the weight of the mooring line becomes a design limitation by increasing the water depth. Therefore, the taut line mooring system is used for deep to very deep waters (more than 1500 m). Taut lines arrive seabed at an angle and cause horizontal and vertical forces at the same time (O'Neill, 2000). A schematic of catenary mooring lines and taut lines are indicated in Figure 2-2.

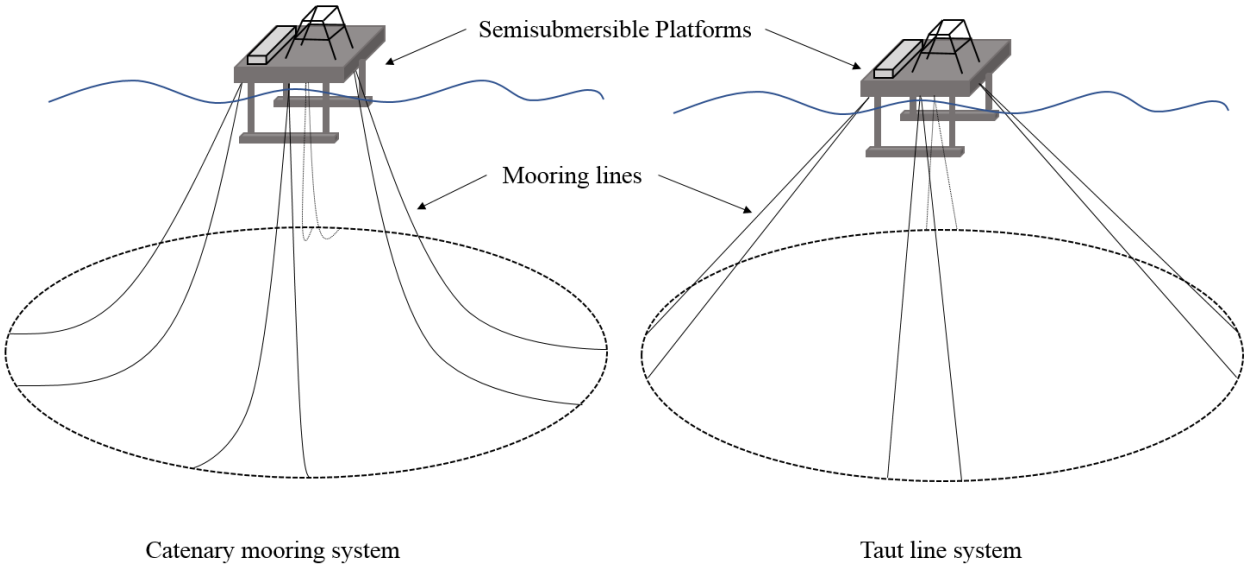

Figure 2-2. Different mooring system

There are different types of anchoring choices such as gravity (deadweight), pile, plate, suction, and drag embedment anchors that could be integrated with the mooring system to keep the floating

facilities in their position. Some of the concerns that need to be considered for selecting the anchoring solution are summarized below:

- The nature and size of the floating structure
- The magnitude and nature of environmental loads (waves, winds, currents) on the structure
- The type of the mooring line system which is a function of water depth
- The standard tolerance of position movement for the structure during the design lifetime
- The properties of the seabed
- Any particular concern related to the installation and handling of the anchoring system

The drag embedment anchors have some features which make them an ideal anchoring option; some of these qualities are mentioned here:

- Cost-effective and straightforward installation procedure
- Ability to retrieve and reinstall make them ideal for anchoring of systems with short- or medium-term floating structures such as drilling rigs, semi-submersible exploration, construction barges and subsea pipeline laying barges
- Having high holding capacity and weight efficiency (the ratio of holding capacity to dry weight of anchor)

In addition to all those features, there are some minor disadvantages related to drag embedment anchors. They are only suitable for the catenary mooring system as they have low vertical resistance. The drag embedment anchors are inappropriate for use in hard or rocky seabed due to their nature and installation procedure. In addition to these minor issues, the incredibly complicated geometry of drag embedment anchors makes them hard to have an accurate prediction

of anchor behavior through the soil, and estimation of their real holding capacity is complicated (O'Neill, 2000).

2.1.1 Drag Anchor Behaviors

As mentioned earlier, drag embedment anchors are integrated with a catenary mooring line to resist the applied load on the floating facility. Therefore, to have a precise interpretation of drag anchor behavior, it is required to consider the influence of the connected chain to the behavior of anchor (Fulton and Stewart, 1994; Craig, 1994). A fully installed drag anchor with chain system is presented in Figure 2-3 which d_a is the anchor padeye depth, d_t is fluke tip depth, β is fluke angle to horizontal, θ_a is chain and anchor padeye attachment angle to horizontal, T_a is the line tension at padeye, θ_0 and T_0 are the chain angle to horizontal and chain tension at mudline.

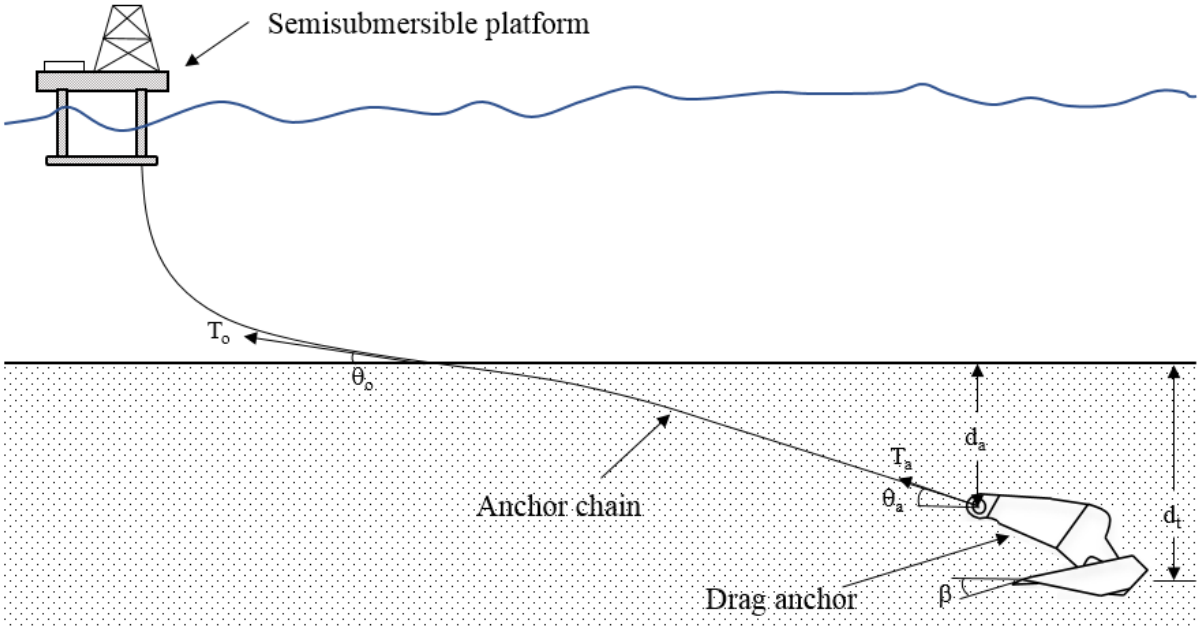

Figure 2-3. The typical arrangement of drag anchor and chain

2.1.2 Anchor Chain

Three critical points in the anchor chain behavior that should be considered are presented here:

- The line tension angle (θ_a) at the padeye, which defines the relative magnitude of horizontal to vertical components of applied force on the anchor. The line tension angle (θ_a) need to be kept as small as possible in designs as the drag anchors are supposed to have a significant horizontal resistance compared to the vertical one.
- The frictional capacity of the buried chain needs to be thoroughly analyzed as the anchor capacity produced at anchor padeye is strongly dependent on the frictional capacity of the buried chain (Degenkamp and Dutta, 1989).
- The diameter of the chain has a direct relationship with the frictional capacity and, consequently, the holding capacity of anchor.

A lot of researchers have been conducted on developing a method to analyze anchor-chain behavior. The procedure proposed by Vivatrat et al. (1982) and produced by Degenkamp and Dutta (1989) has been utilized and employed in a series of drag embedment anchor software such as Stewart Technology Associate (1995), DNV (2000). Subsequently, the proposed method was utilized by Neubecker and Randolph (1995, 1996a) as an initial step for a theoretical study related to anchor-chain behavior in homogenous soil and developed by (O'Neill, 2000) for the layered seabed.

2.1.3 Theoretical Anchor Models

During the last ninety years, a lot of studies and investigations have been done to understand the behavior of drag anchors and holding capacity in different seabed criteria. Those studies have been categorized into three main groups to have a better understanding of what has been done before.

The first group is drag anchor behavior through experimental investigations, the second group is developed drag anchor theories, and the last one is design and modeling tools for drag anchors.

a) Drag Anchor Behavior Through Experimental Investigations

The experimental investigations have been done in the laboratory or field tests. The purpose of those investigations was to find a relation between the holding capacity of anchors and the geometrical properties of anchors in different soils by the construction of the empirical database. For example, the NCEL 1987 is one of the most popular field tests, and its results were largely used in industry as a standard design. NCEL (1987) has design charts that correlate the holding capacity against the anchor weight.

By introducing the geotechnical centrifuge tests at the start of the 90s, a new method of experimental tests, especially for drag embedment anchors was introduced as they need long drag lengths to reach their maximum holding capacity. The results of these tests were utilized for the evaluation and development of theoretical methods for understanding drag anchors' behavior in different seabed criteria. For instance, Neubecker (1995) and O'Neill (2000) conducted a series of centrifuge drag anchor tests in clay and layered soils, respectively.

b) Development of Drag Anchor Theories

Drag anchor theories related to cohesive, non-cohesive soils are developed differently and have different applications. In comparison between anchors in cohesive and non-cohesive soils, if all other factors are kept the same, the drag anchors in cohesive soil achieve higher embedment depth compared to non-cohesive soils. It indicates that failure mechanisms in cohesive soils (clay) are fully limited and local to the anchor. Still, non-cohesive soils (sand) have an active soil wedge failure mechanism that goes to the seabed surface. Therefore, the geotechnical forces applied to

the anchor in clay soil are not a function of anchor orientation and only dependent to anchor's local bearing and shear resistances, and the local undrained shear strength of clay.

Stewart (1992) proposed a theoretical method for drag anchor behavior in clay, which had two main phases. The first part is a calculation procedure that estimates the major force components on the fluke and shank of the anchor to determine the net moment on the anchor based on the center of each force. The second part is related to determining the kinematic of the anchor-based on the calculated net moment and the assumption that the anchor always moves parallel to its fluke, which is supported by Dunnavant and Kwan (1993). Based on this study, other researchers developed the drag anchor theory to calculate the ultimate holding capacity and trajectory of anchor in clay soil, e.g., Neubecker and Randolph (1996a), Thorne (1998), and O'Neill et al. (2003).

The general procedure proposed for modeling the drag anchor behavior in the sand is mostly similar to the clay method, which comprised of static and kinematic analysis to calculate the geotechnical forces on the anchor components and incremental displacements to compute the embedment path of the anchor. On the other hand, in non-cohesive soils, geotechnical forces are higher, penetration depth is lower and, the failure mechanism is extended to the soil surface. Because the governing geotechnical theory for the calculation of acting forces in non-cohesive soils completely differs from the cohesive soils.

Saurwalt (1974) proposed the first model to identify the static forces on the drag anchor in the sand by idealizing the drag anchor with a buried inclined plate. Tabatabaee (1980) and LeLievre and Tabatabaee (1981) improved the Saurwalt's work to come up with a procedure to accurately estimate the holding capacity of anchor for a given depth and orientation in the sand. The first complete kinematic model of anchor trajectory in sand using a minimum work approach was

developed by Neubecker and Randolph (1996b). Using the static and kinematic of drag anchors in the sand, Neubecker and Randolph (1996c,1996b) formed the model to describe the behavior of drag anchors in sand.

Despite drag anchor behavior in homogenous soils, there were no studies related to the behavior of anchor in layered soils before the O'Neill approach. O'Neill (2000) developed the theory of anchor behavior in the layered seabed (uncemented sand over cemented sand and clay over sand) using the procedures in clay only and sand only.

c) Design and Modelling Tools for Drag Anchors

All methods above are utilized to come up with some convenient tools for the prediction of anchor behavior in different criteria. These methods are categorized into three different groups. The first one is design charts, which predict the holding capacity versus anchor weight in different soils. For instance: NCEL, Vryhof Stevpris, IFP charts. The second one is design code rules, which have some recommendations for designing the drag anchor in different criteria, e.g., American Petroleum Institute's (API) and Det Norske Veritas (DNV). The last one is software designs which able to predict the behavior of anchors in different soil media and are available commercially such as, STA-Anchor, DIGIN, UWA-Anchor.

2.2 Buried Subsea Pipelines

As indicated in Figure 2-4, buried subsea pipelines are subjected to movements of seafloor caused by gravity forces, hydraulic forces, tectonic activity, mudslides, and slumping (Poulos, 1988, Audibert et al., 1979). These movements could cause instability in the soil surrounding the pipeline, which may result in rapid and significant displacement of adjacent soil. The resultant stresses of soil movement depend on different parameters such as soil type, the geometry of

pipeline, the existence of trench around the pipe, trench geometry, and native soil and backfill properties. The scholars have been working to achieve a better understanding of the soil-pipe interaction, and these studies divided into two broad groups. The first group includes investigations that consider the soil around the pipeline as a homogenous field. The second group contains studies that cover the effect of a trench on the pipe-soil interactions.

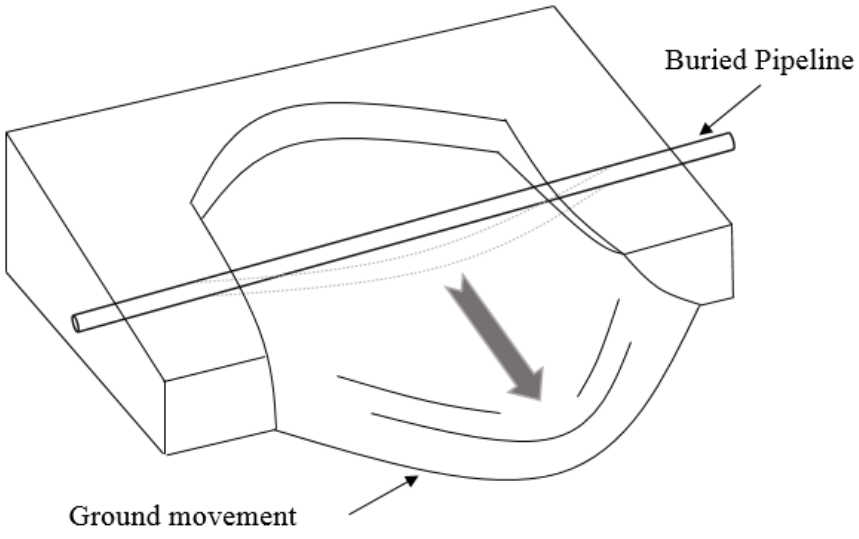

Figure 2-4. Buried pipeline subjected to ground movement

2.3 Lateral Pipeline Soil Interaction

There are a large number of physical model tests and numerical studies which focus on the lateral interaction of buried pipes with the surrounding soil in the sand. The physical studies try to understand the lateral resistance of pipeline using the centrifuge or other experimental methods and obtain soil failure mechanism using different techniques such as the particle image velocimetry (PIV). Some of these studies are mentioned here (Trautmann and O'Rourke, 1985; Daiyan et al., 2011; Almahakeri et al., 2013; Burnett, 2015). Besides physical models, the numerical studies in the literature use different constitutive models and finite element software to make a better

understanding of this complex problem (Yimsiri et al., 2004; Guo and Stolle, 2005; Yimsiri and Soga, 2006; Xie et al., 2013; Jung et al., 2013).

Despite studies related to pipe soil interaction in the sand, there are only a few theoretical and experimental pieces of research to find out the lateral resistance of pipeline in clay. As pipelines have some mutual behavioral characteristics with plate anchors and pipe, some of the studies related to pipe-soil interaction in clay are developed based on plate anchor or pile theories. For instance, these studies are done based on plate anchor theory (Tschebotarioff, 1973; Luscher et al., 1979; Rowe and Davis, 1982; Das et al., 1985; Das et al., 1987; Merifield et al., 2001) and the following researches are developed using piles principles (Hansen and Christensen, 1961; Reese and Welch, 1975; Bhushan et al., 1979; Klar and Randolph, 2008).

A limited number of studies in clay have proposed an independent model to investigate the lateral interaction between soil and pipe (Audibert and Nyman, 1977; Ng, 1994; Paulin, 1998; Oliveira et al., 2010).

The effect of a trench on the lateral response of the pipe is not well developed. Paulin (1998), C-CORE (2003), Phillips et al. (2004), Kianian and Shiri (2019) are only researchers that integrated the effect of a trench and backfill on the lateral pipe-soil interaction in clay.

2.4 Reliability Assessment

Geotechnical engineering always deals with risk and decision making under uncertainty. Even before the development of any geotechnical disciplines, the people who were dealing with soils, rocks, and geological phenomena were aware of this fact. Any geotechnical engineering project comprised of three phases: the first step is site exploration, the second step is the required soil testing to define the material properties, and the last one is analyzing the response of soil/rock mass under the applied load. The uncertainty about loads and uncertainty related to foundation

response are two significant uncertainties that could be arisen in our geotechnical projects during all these three phases.

The risked based design and using reliability methods is a practical approach to deal with those uncertainties and having a more realistic estimation of the real problem. The risk and reliability methods are used more broadly in offshore structures compared to onshore ones due to the following reasons, higher construction costs in offshore, the lower ability for maintenance and service of the structure, and a higher level of uncertainty in offshore due to existence of dynamic loads (wave, wind, current).

A short review of the utilized reliability tools used in this study is presented in the following sections.

2.5 Reliability Analysis Methods

The goal of a probabilistic study is to find out how the uncertainty of input parameters in problems affects the outputs. The first step of performing probabilistic research is developing a model to solve the problem and calculating the required outputs. After generating the solving model, a limit state function will be defined based on the conditions of the problem to separate the failure and the safe zone. Selecting a favorable reliability tool among the existing ones (Monte Carlo simulation, first and second-order reliability method) will be the next step to carry out the probabilistic study. It should be mentioned that in a particular geotechnical problem, there are a large number of parameters that have uncertainty and could be evaluated in probabilistic studies. Even though based on the purpose of each study, some of them are selected and their uncertainties will be quantified to see how they will affect the outputs of the problem. The FORM method, which considers as one of the most crucial reliability tools will be discussed in the next section.

2.5.1 First Order Reliability Method (FORM)

In a reliability study, assume $X = \{X_1, X_2, \dots, X_n\}$ represents a set of uncertain parameters involved in the problem where $X_1, X_2, \dots, X_n$ are the probability density function of each parameter, and $f(X)$ denotes the joint probability function of X. The limit state function in which distinct safe and failure regions are indicated by $G(X)$ and the failure happens whenever $G(X)$ is less than or equal to zero. Based on these definitions, the probability of failure could be defined as equation 2-1:

$$P_f = Prob[G(X) < 0] = \int_{G(X)\leq 0} f(X)\, \mathrm{dX} \tag{2-1}$$

Due to difficulties in the calculation of this integral different approximation approaches have been developed (Madsen et al., 1986). One of the most consistent computational methods is the first order reliability method (FORM) (Bjerager, 1991).

As stated in equation 2-2, the limit state function $G(X)$, could be expressed as a function of $R(X)$ and $S(X)$ which are stands for load and capacity:

$$G = R(X) - S(X) \tag{2-2}$$

The probability of failure could be calculated using the approximations of the limit state function G, which is a function of R and S, $G(R, S)$. The procedure of the FORM method consists of three steps (Bjerager, 1991):

I. Transforming limit state function $G(R, S)$ into the standard normal space
II. Approximating the modified function in the standard normal space
III. Computing the corresponding probability of failure to the approximate transformed function

In the first step, for statically independent variables (X) the Rosenblatt transformation (equation 2-3) is being used for converting the limit state function $G(R,S)$ to standard normal space $G(u_R,u_S)$ which the vector (R,S) is transferred to (u_R,u_S). Where, $\Phi^{-1}(\,)$ is the inverse of the cumulative standard normal function and $F_R(r)$, $F_S(s)$ are the cumulative distribution functions of the load and capacity.

$$u_R = \Phi^{-1}\big(F_R(r)\big), u_S = \Phi^{-1}\big(F_S(s)\big) \tag{2-3}$$

In the second step, the transferred limit state function to standard normal space $G(u_R,u_S)$ is approximated to $G'(u_R,u_S)$ using the first-order Taylor series expansion. More details about this transformation could be found in the following literatures (Hasofer and Lind, 1974; Fiessler et al., 1979; Ditlevsen, 1981; Hohenbichler and Rackwitz, 1981). The expansion point (u^*) for the Taylor series states the point on the limit state function that has the minimum distance to the origin of reduced variables, which represents the most probable failure point. There are different algorithms for finding the most probable point (u^*) in the literature and the comparison between these methods is provided by Liu and Der Kiureghian (1991).

The last step is computing the reliability of the fitted limit state function $G'(u_R,u_S)$. For this goal, it is required to evaluate the probability content that corresponds to the region outside the assumed failure surface $G'(u_R,u_S)$ (Zhao and Ono, 1999). In the FORM method, the reliability index is defined as the distance between the origin of reduced space and most probable point (u^*). Finally, the probability of failure could be calculated using equation 2-4, which correlates the first order reliability index to the likelihood of failure:

$$P_f = \Phi(-\beta_F) \tag{2-4}$$

Figure 2-5 shows a graphical view of the reliability index and the above-mentioned three steps.

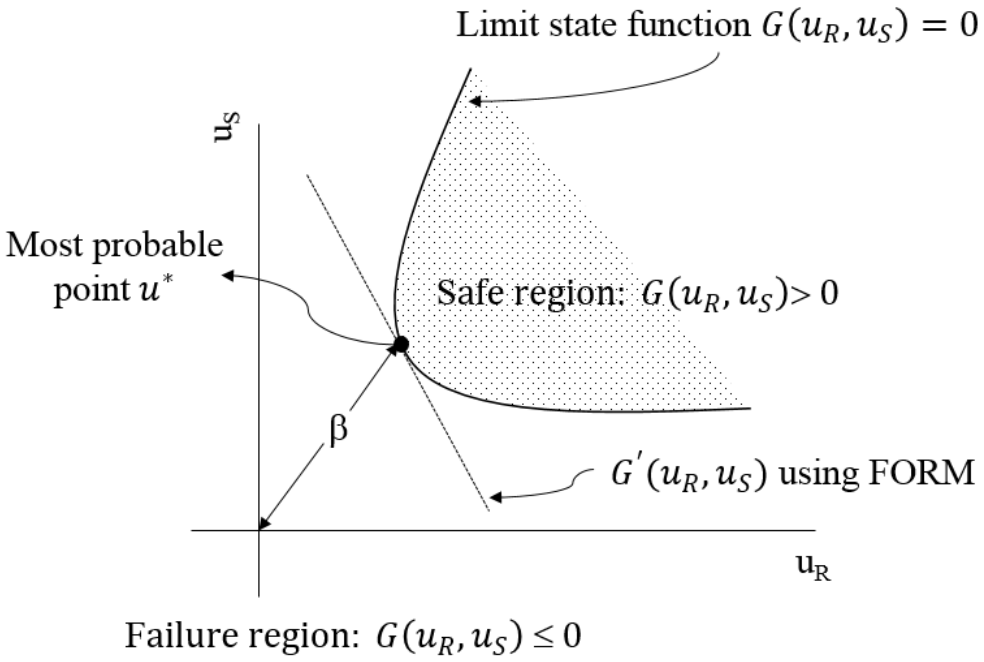

Figure 2-5. The graphical interpretation of the reliability index and three steps for the FORM calculation method

2.5.2 Response Surface Method

Sometimes in engineering problems, the function that relates the uncertain input parameters to outputs of our problem is not easy to develop or implicitly known. For instance, assume the outputs of a problem are extracted from a large finite element model, which each run takes a long time and it is not possible to have enough runs for developing the function. Or there is a limited experiment result that relates the inputs and outputs without any explicit function. If a reliability study needs to be done in these cases in which there is no explicit function between inputs and outputs, the response surface method could help to develop a relationship between inputs and outputs based on the limited available data resources. In the eighties, the response surface method was started to utilize the reliability assessments of engineering problems (Rackwitz, 1982; Felix and Wong, 1985; Lucia Faravelli, 1990). Subsequently, a large number of studies have been done around the

response surface methods and different procedures were developed for applying it to various engineering problems.

Chapter 3. Reliability Assessment of Drag Embedment Anchors in Sand for Catenary Mooring Systems

Amin Aslkhalili[1], Hodjat Shiri[1], Sohrab Zendehboudi[2]

1. Civil Engineering Dept., Faculty of Engineering and Applied Science, Memorial University of Newfoundland, A1B 3X5, St. John's, NL, Canada.

2. Process Engineering Dept., Faculty of Engineering and Applied Science, Memorial University of Newfoundland, A1B 3X5, St. John's, NL, Canada.

This chapter was published as a journal paper in the "Safety in Extreme Environments-Springer (2019)" Volume1, Pages39–57, https://doi.org/10.1007/s42797-019-00006-5

Abstract

The reliability of drag embedment anchors in sandy seabed was assessed for catenary mooring systems. The anchor holding capacity was obtained by performing a series of iterative limit state and kinematic analyses through developing an advanced macro spreadsheet. Series of coupled dynamic mooring analyses were conducted for a semisubmersible platform using OrcaFlex software. The dynamic mooring line tensions were obtained by incorporation of the uncertainties in environmental loads, metocean variables, and stress distribution along the catenary mooring lines into the response surface. A probabilistic model was developed for holding capacity of the selected drag anchors. An iterative procedure was performed by adopting the first order reliability method (FORM) to calculate the failure probabilities. The study showed significant dependence of the anchoring system reliability on geometrical configuration of the selected anchor families, the seabed soil properties, and the environmental loads. It was observed that the reliability-based development of in-filed testing procedures proposed by design codes can have significant contribution to achieving a more cost-effective and safer design.

Keywords: Reliability analysis; Drag embedment anchor; Catenary mooring; Response surface; Numerical method; Sand seabed

3.1 Introduction

Drag embedment anchors are widely used as a cost-effective solution for temporary and permeant station keeping of floating structures. By growing offshore exploration and productions, the number of incidents in floating facilities induced by the failure of mooring system has been increased, subsequently (Wang et al., 2010; Duggal et al., 2013). This has caused the industry to further emphasize on reliability assessment of the mooring systems and their key components in various types of seabed sediments. Drag embedment anchors are amongst the crucial components of the mooring systems that are used with catenary and taut leg mooring systems.

Different anchoring solutions might be used to provide an efficient and reliable mooring system such as suction anchors, propellant embedded anchors, screw-in anchors, plate anchors, deadweight anchors, pile anchors, and drag embedment anchors. However, the latter one is one of the most attractive options that are simple and cheap to install but challenging to evaluate the holding capacity (Neubecker and Randolph, 1996a; Aubeny and Chi, 2010) due to complex and uncertain interaction with the seabed (see Figure 3-1).

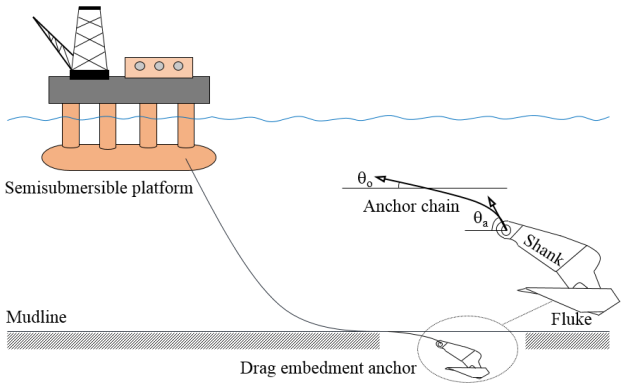

Figure 3-1. Detail of drag embedment anchor in the catenary mooring system

The current practice proposed by design codes (e.g., API RP 2SK, 2008) recommends a unique procedure for in-field evaluation of the holding capacity of drag embedment anchors in both sand and clay. This approach may lead to a different level of reliabilities and cost impacts, consequently. Therefore, to improve the current practice, it is mandatory to perform comparative reliability studies for the performance of drag anchors in both sand and clay. There are several studies in the literature that have considered the reliability assessment of various anchor families such as suction anchors (Choi, 2007; Valle-molina et al., 2008; Clukey et al., 2013; Silva-González et al., 2013; Montes-Iturrizaga and Heredia-Zavoni, 2016; Rendón-Conde and Heredia-Zavoni, 2016). However, having limited access to in-field holding capacity databases, the complicated interaction between the anchor and the seabed, and the need for the extensive amount of costly computational analyses have resulted in limitations to assess the reliability of these important Anchor families. There is only one study that has investigated the reliability of drag anchor in clay (Moharrami and Shiri, 2018), but there is no study in the sand yet.

The current study contributed to filling of this knowledge gap by combining advanced coupled mooring analysis and iterative limit state solutions for anchor kinematics in sand seabed that is quite common in the offshore region. Comparisons were made between the reliability index provided by the same group of anchors in sand and clay. In addition, an equalization study was conducted to determine the different group of anchor families in sand and clay that result in an identical reliability index. The holding capacity of anchors was calculated by developing an Excel spreadsheet and incorporation of the limit state analysis proposed by Neubecker and Randolph (1996a). There are several studies on the prediction of drag anchors capacity by analytical and empirical solutions (Neubecker and Randolph, 1996a; Thorne, 2002; O'Neill et al., 2003; Aubeny and Chi, 2010). However, the adopted solution (Neubecker and Randolph, 1996a) benefits from

several advantages such as simplified prediction of the anchor capacity and trajectory, incorporation of chain-sand interaction, and comprehensive validation against the experimental studies (Neubecker and Randolph, 1996a; Neubecker and Randolph, 1996b; O'Neill et al., 1997). This model has been widely used in several studies in the literature (Neubecker and Randolph, 1996b; Neubecker and Randolph, 1996c; O'Neill et al., 2003) and recommended by design codes (e.g., API RP 2SK, 2008).

The mooring line tension was obtained by performing dynamic mooring analysis using OrcaFelx software and a generic semisubmersible platform. Reliability assessment was performed by using first-order reliability method (FORM) through developing a probability model for anchor holding capacities that is further explained in the coming sections.

The study provided an excellent insight into the problem and prepared the ground for improving the current state-of-practice from reliability and cost-effectiveness standpoints.

3.2 Methodology

The reliability analysis was conducted by calculation of the anchor capacity against the mooring line tensions. The model proposed by Neubecker and Randolph (1996a) was used to analyze chain-soil and anchor-soil interactions in the sand and predict the anchor capacity at the mudline and shank pad-eye. The anchor model was programmed in an Excel spreadsheet VBA Macro (Visual Basic Application). OrcaFlex software package was employed to model a generic semisubmersible platform in the Caspian Sea to obtain the characteristic mean and maximum dynamic line tensions for a 100 years return period sea states. Various key parameters were incorporated in the estimation of anchor capacities including peak friction at the seabed, dilation angle, soil density, fluke and shank bearing capacity factors, anchor geometrical configurations, line tension angle at mudline, and side friction factor. The response surfaces were used to determine the mean and expected

maximum dynamic line tensions. First order reliability method (FORM) was used to assess the reliability of anchors connected to the catenary mooring line. The DNV design code (DNV-RP-E301, 2012) was used to define the partial design factors on the mean and maximum dynamic line tensions and capacities.

3.3 Modeling Drag Embedment Anchor

Drag embedment anchors are commonly connected to the chain and then the mooring line. The resistance that soil provides against the anchor and the frictional capacity of the chain is the primary source of ultimate anchor capacity. Both of these key components were modeled in the current study to achieve a sufficient level of accuracy in the calculation of total holding capacity.

3.4 Soil-Chain Interaction

Analysis of the embedded anchor chain is vital for two main reasons. First, the frictional capacity between the chain and the soil that can significantly contribute to the ultimate anchor capacity. Second, the angle between the anchor and the chain at the pad eye that has an important effect on the soil-chain interaction. In the present study, a stud chain was considered, and the methodology proposed by Neubecker and Randolph (1995) was adopted to implement the chain-soil interaction. Figure 3-2 shows the free body diagram of a differential segment of the chain that was adopted force equilibrium analysis (Neubecker and Randolph, 1995a). The parameter T is the line tension; θ is the inclination from the horizontal; F is the friction force, and Q is the typical soil reaction on chain segment.

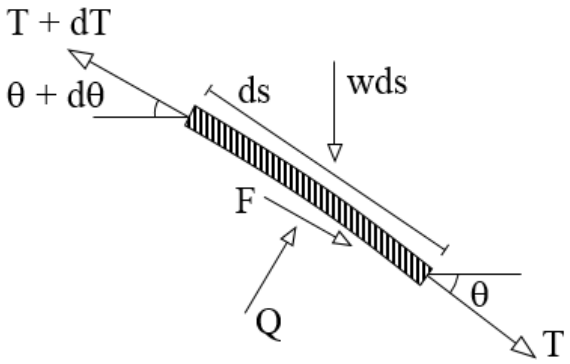

Figure 3-2. Force equilibrium of chain element

According to Figure 3-2, the tangential and normal equilibriums can be written as:

$$\frac{dT}{dS} = F + WSin\theta \tag{3-1}$$

$$T\frac{d\theta}{dS} = -Q + WCos\theta \tag{3-2}$$

It is possible to describe the normal (Q) and tangential (F) soil resistances acting on the chain as soil pressures:

$$Q = (E_n d)q \tag{3-3}$$

$$F = (E_t d)f \tag{3-4}$$

where d is the nominal chain diameter, E_n and E_t are circumference parameters. In non-cohesive soils, the bearing pressure q can be expressed by:

$$q = N_q \gamma' z \tag{3-5}$$

where q is bearing pressure;N_q is the standard bearing capacity factor; γ' is the effective unit weight of the soil; z is depth. These governing equilibrium equations are non-linear which makes

difficulties in finding the solution. Therefore, to simplify the equation, the chain was assumed to be weightless (Neubecker and Randolph, 1995a). Although, it is possible to account for the chain weight by a secondary effect i.e., reducing the profile of normal resistance per unit length by an amount equal to the chain weight per unit length. However, Neubecker and Randolph (1995) showed that the contribution of the chain weight has a minor effect on ultimate capacity. The governing equilibrium equations for weightless chain now become:

$$\frac{dT}{dS} = F \tag{3-6}$$

$$T\frac{d\theta}{dS} = -Q \tag{3-7}$$

where the relationship between F and Q can be written as (Neubecker and Randolph, 1995a):

$$F = \mu Q \tag{3-8}$$

where μ is the frictional coefficient which is between 0.4 and 0.6. By substitution of the equations 3-6 and 3-7 into equation 3-8, the governing formula can be obtained:

$$\frac{dT}{dS} + \mu T\frac{d\theta}{dS} = 0 \tag{3-9}$$

Equation 3-9 can be written in the following form to give the expression for the load development along the chain:

$$T = T_a e^{\mu(\theta_a - \theta)} \tag{3-10}$$

Now substituting equation 3-10 into equation 3-7 and considering the small values of θ leads to:

$$\frac{T_a}{2}(\theta_a^2 - \theta^2) \approx \int_z^D Q dz = (D - z)\bar{Q} \tag{3-11}$$

where Q is the average bearing resistance (per unit length of chain) over the depth range of z to D. Equation 3-11 allows the change in chain angle to be estimated directly regarding the chain tension at the attachment point, T_a and the average bearing resistance. Since the chain angle is close to the zero at the seabed, the equation 3-11 can be simplified as below:

$$\frac{T_a\theta_a^2}{2} = D\bar{Q} \tag{3-12}$$

Combining equation 3-10 with equation 3-12 results in an equation that describes frictional development along the chain:

$$\frac{T_o}{T_a} = e^{\mu(\theta_a)} = e^{\mu\sqrt{T^*/2}} \tag{3-13}$$

where T_o is chain tension at mudline; T^* is normalized tension that is given by:

$$T^* = \frac{T_a}{D\bar{Q}} \tag{3-14}$$

Assuming a soil layer with bearing capacity proportional to depth, for a surface chain angle equal to zero, Neubecker and Randolph (1995) proposed the following equation for chain profile:

$$z^* = e^{-x^*\left(\sqrt{2/T^*}\right)} = e^{-x^*\theta_a} \tag{3-15}$$

where z* and x* are depth and horizontal distance normalized by D, respectively.

Incorporating the anchor chain weight into the formulation to obtain a higher accuracy for general tension capacity, the following formulation was obtained:

$$T = T_a e^{\mu(\theta_a - \theta)} + \mu w s \tag{3-16}$$

where w is chain self-weight per unit length; and s is the length of chain.

Figure 3-3 illustrates the validation of the closed form chain profile given in equation 3-16 with the existing experimental results (Bissett, 1993). The proposed equation is in a good agreement with a real chain profile, where the bearing resistance is approximately proportional to depth.

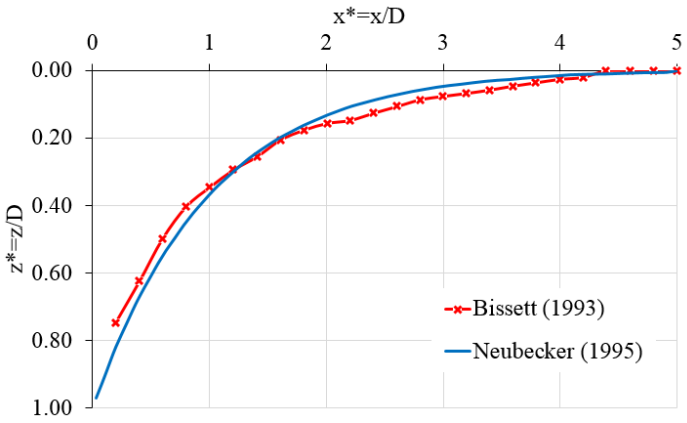

Figure 3-3. Comparison of chain profile in sand

3.5 Anchor Holding Capacity

In the present study, the drag anchor was assumed to move through the soil in a quasi-static condition. Although the anchor has some finite velocity, the magnitude of this velocity is small so that the inertial considerations can be neglected. To obtain the anchor holding capacity, the limit state model proposed by Neubecker and Randolph (1996a) was adopted. Figure 3-4 shows the three-dimensional wedge failure mechanism for calculation of the anchor capacity at pad eye (T_a).

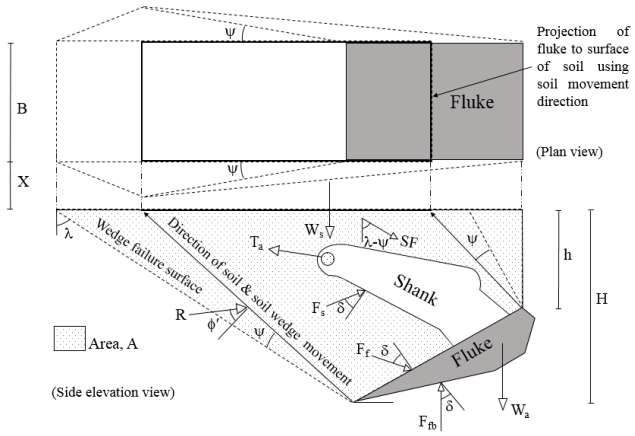

Figure 3-4. The three-dimensional failure wedge in plan and side view and force system of the anchor

Using the force equilibrium system shown in Figure 3-4, the first step is to calculate the cross-section area of the wedge:

$$A = \frac{H^2-h^2}{2tan\beta} + \frac{H^2 tan\lambda}{2} \tag{3-17}$$

where H is the depth of fluke tips; h is the back edge of the fluke; β is the inclination of the fluke, and λ is the failure wedge angle. The lateral extent of failure wedge can be calculated by:

$$X = \frac{Htan\psi}{cos\,(\lambda-\psi)} \tag{3-18}$$

where ψ is the dilation angle. Now, the mobilized soil mass can be obtained based on the known values of X and A:

$$W_s = \gamma BA + \frac{2}{3}\gamma XA \tag{3-19}$$

where W_s is the mobilized soil mass; B is the width of the fluke. The side friction (SF) should be determined to satisfy limit equilibrium formulation:

$$SF = \frac{\gamma L(H+h)^2(sin\emptyset' - sin\,\psi)}{4cos\psi(1-sin\emptyset' sin\psi)} \tag{3-20}$$

where $\emptyset'$ is the soil friction angle.

Using the force equilibrium system shown in Figure 3-4, the shank force could be driven from the standard bearing capacity as below:

$$F_s = A_s \gamma d_s N_{qs} \quad (3\text{-}21)$$

where F_s is the shank force; A_s is the area of the shank; d_s is the average depth of the shank; and N_{qs} is the bearing factor for the shank. There are still two unknown forces acting on the soil wedge i.e., the fluke force (F_f) and soil reaction (R). By considering horizontal and vertical force equilibrium, the unknown forces can be simply determined. Now, using the force equilibrium of the anchor alone, the unknown forces in the back of the fluke (F_{fb}) and the chain tension (T_a) can be calculated based on horizontal and vertical force equilibrium. This procedure was iteratively continued with different values of the failure wedge angle (λ) to find out the minimum upper bound estimate of the anchor holding capacity (T_a).

It is worth mentioning, the anchor geometry used in analytical solution is an idealized form of the real anchor geometry, which is quite complex. It was observed during the current study, that changing the geometry idealization approach might have remarkable impact on the ultimate holding capacity and consequently the reliability index. In the current study, the anchor geometry was idealized using the methodology proposed by Neubecker and Randolph (1996a). However, further studies are needed to propose an idealization methodology with improved accuracy resulting in a closer holding capacity to the in-filed tests.

3.6 Anchor Kinematics

The anchor trajectory is a key parameter that can be used for interpretation of the obtained holding capacities and reliability indices in the later stages. The solution proposed by Neubecker and

Randolph (1996c) for prediction of the anchor trajectory was adopted, where three main conditions were set to ensure kinematic admissibility of the anchor model. These conditions put constraints on the absolute and relative displacements of the anchor and the soil wedge and hence are helpful in defining the kinematics of the system. First, the soil wedge will move at the dilation angle to the failure surface. Second, displacement of the soil relative to the anchor (du_{sa}) must be parallel to the upper face of the flukes. Third, the anchor must maintain contact with the soil behind it by traveling in a direction parallel to the back of the fluke. The third condition applies when there is a force on the rear of the flukes so that when this force becomes zero, the anchor is free to travel away from the soil behind it and this condition is meaningless. These three conditions for anchor and soil displacements fully describe the kinematics of the system so that for a given anchor displacement the magnitudes and directions of the soil displacement and the relative anchor-soil displacement can be easily calculated. The minimum work approach was applied and the penetration Δy and rotation $\Delta\theta$ were considered to obtain the incremental anchor displacements. Further details of the anchor kinematic model can be found in Neubecker and Randolph (1996c).

3.7 Developing Iterative Macro for Prediction of Anchor Performance

The static limit state and kinematic models were coded into an Excel spreadsheet using VBA macros to calculate the ultimate holding capacity of the anchor-chain system and the anchor trajectory. The developed spreadsheet performed a series of iterative analyses with the calculation procedure outlined in Figure 3-5.

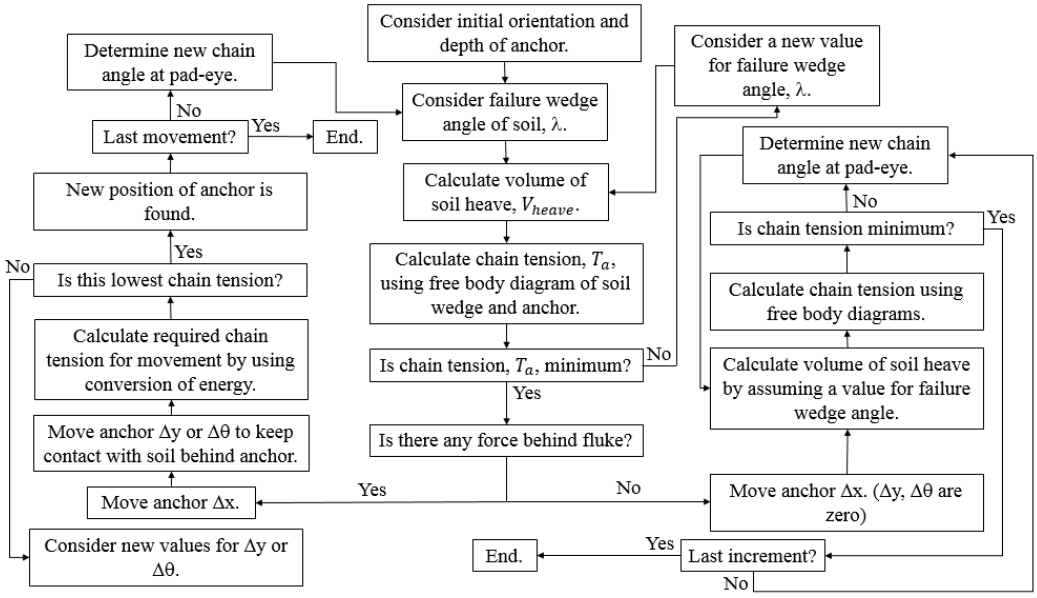

Figure 3-5. Analysis flow chart for embedment history of drag anchors

The proper performance of developed Excel spreadsheet was validated against the published experimental and analytical studies (Neubecker and Randolph, 1996b) and showed a perfect agreement (see Figure 3-6). Also, comparisons were made against the design codes (NCEL, 1987) and referenced manufacturers datasheets (Vryhof Anchors, 2010) (see Figure 3-7).

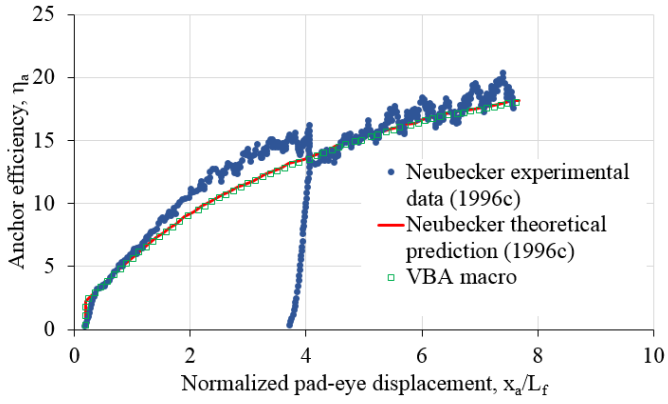

Figure 3-6. Comparison of results for anchor efficiency

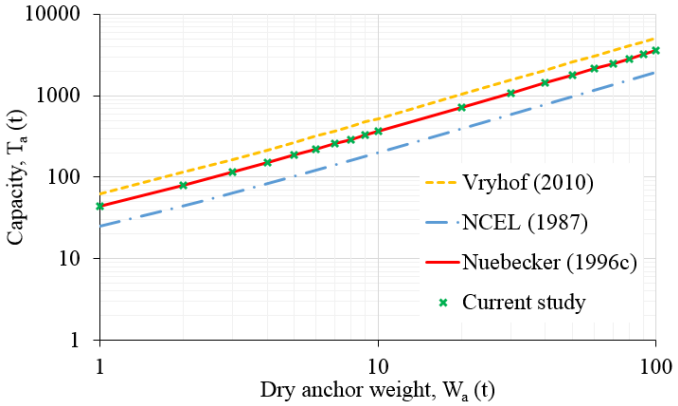

Figure 3-7. Comparison of results for anchor holding capacity

The input parameters of the validation case study are given in Table 3-1.

Table 3-1. Soil and anchor input parameters in the current analysis

Parameter	Value
Anchor dry weight, W_a (kN)	98.06
Fluke length, L_f (m)	3.41
Fluke width, b_f (m)	5.99
Fluke thickness, d_f (m)	0.51
Shank length, L_s (m)	5.55
Shank width, b_s (m)	2.31
Fluke-Shank angle, θ_{fs} (°)	32
Effective chain width, b_c (m)	0.24
Chain self-weight, w_c (kN/m)	2
Chain soil friction coefficient, μ	0.4
Peak friction angle, ϕ_p (°)	35
Residual friction angle, ϕ_r (°)	25
Dilation angle, ψ (°)	8.5
Effective unit weight, γ' (kN/m3)	10

3.8 Anchors Used in the Current Study

Two types of popular anchors that are widely used for temporary and permanent mooring of floating systems, i.e., Stevpris Mk5 and Mk6, were used in the current study for reliability studies. These anchors have a fluke length to fluke thickness ratios (L_f/d_f) of 6.67 and 3.09 respectively.

Figure 3-8 illustrates the plan and side views of these anchors with geometrical properties given in Table 3-2. In addition, the selection of these anchors enabled making comparisons with earlier studies that have used similar anchors (Moharrami and Shiri, 2018).

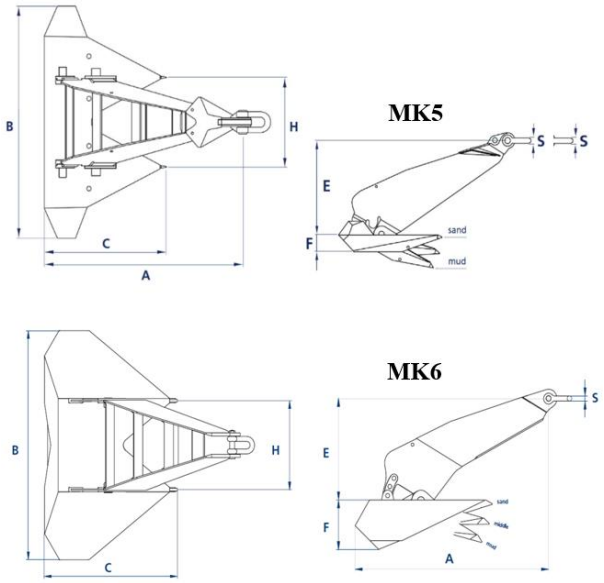

Figure 3-8. Schematic of the modeled anchor in the present study

Table 3-2. Main dimensions for 12 t anchors (Vryhof Anchors, 2010)

	Mk5 (L_f/d_f = 6.67)	**Mk6** (L_f/d_f = 3.09)
A (mm)	5908	5593
B (mm)	6368	6171
C (L_f), (mm)	3624	3961
E (mm)	3010	2642
F (d_f), (mm)	543	1282
H (mm)	2460	2394
S (mm)	150	140
Fluke-shank angle(θ_{fs}), (°)	32.00	32

Table 3-3 shows the calculated values of the holding capacities or design resistances ($R_{d,a}$) and the corresponding line tension angles (θ_a) at the pad-eyes. The soil properties for these series of analysis are selected from Table 3-1.

Table 3-3. Properties of the modeled drag anchors

Anchor type	L_f/d_f	L_f (mm)	d_f (mm)	$R_{d,a}$ (kN)	θ_a (˚)
Mk5	6.67	4297	644	2275	13.0
Mk6	3.09	4534	1468	2267	12.9

3.9 Finite Element Mooring Analysis

A generic semisubmersible platform located in the Caspian Sea was considered with eight leg catenary spread mooring system for dynamic mooring analysis (see Figure 3-9). Each mooring line comprised of three different parts, i.e., the upper, middle and lower segments. The upper and lower segments were made of chain, while the central segment was wire rope. A water depth of 700 m was assumed and a finite element model was developed using OrcaFlex software to obtain the dynamic line tensions at the touchdown points (TDP). Performing a three hours' time domain simulation, the most critically loaded line was detected for the environmental loads with a 100 years return period (i.e., H_s = 9.5 m, T_P = 12.8 s, and U_{10} = 29 m/s). Figure 3-10 shows the adopted head sea response amplitude operator (RAO) of the platform.

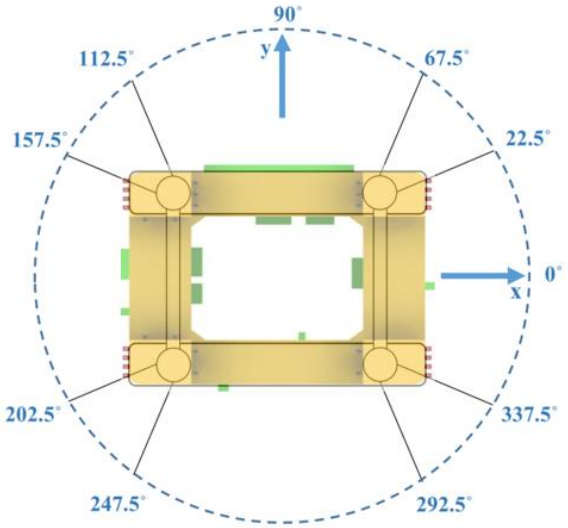

Figure 3-9. Schematic plan view of the mooring line arrangement

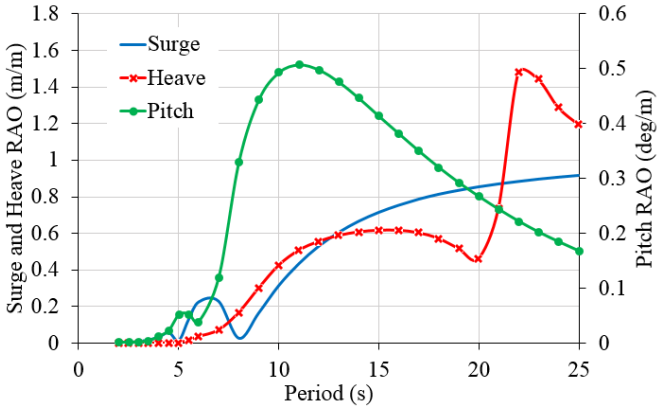

Figure 3-10. Generic semisubmersible RAO, the head sea

The key outcome of dynamic mooring analysis is summarized in Table 3-4 including T_d (design line tension), θ_o (line angle at mudline), $T_{mean\text{-}C}$ (characteristic mean tension), and $T_{dyn,max\text{-}C}$ (characteristic mean maximum dynamic tension) that will be used for reliability assessment in the next section.

Table 3-4. Catenary mooring system characteristic

H_s (m)	T_P (s)	U_{10} (m/s)	$T_{mean\text{-}C}$ (kN)	$T_{dyn,max\text{-}C}$ (kN)	T_d (kN)	θ_o (°)
9.5	12.8	29	846	623	2493	1.3

3.10 Reliability Analysis

First order reliability method (FORM) was adopted through an iterative procedure to obtain the probabilistic results by incorporation of uncertainties in seabed soil properties and environmental loads. The probabilistic modeling of anchor capacity was conducted by using the limit equilibrium method proposed by Neubecker and Randolph (1996a). The embedment profile and the frictional capacity of the chain were also accounted for in the calculation of ultimate holding capacities. The response surface approach and appropriate probability density functions were used to take into consideration the uncertainties of the environmental loads and metocean variables including significant wave height, spectral peak period, wind velocity, and consequently the stress distribution throughout the catenary lines. A target failure probability of 10E-5 was set assuming a consequence class of 2 as per recommendations made by DNV-RP-E301 (2012). Further details are provided in the coming sections.

3.11 Limit State Function

In order to establish the limit state function, care should be taken on considering the contribution of the frictional chain capacity and its effect of the complexity of the reliability analysis. If the limit state function is formulated at the pad-eye, the statistical dependence between the applied load and the capacity of the anchor must be determined, and the complexity of the reliability analysis will be significantly increased. On the other hand, the current study aims to focus on uncertainties existed in the evaluation of anchor capacity rather than the chain capacity. Therefore, an alternative approach that has also been used by other researchers (Choi, 2007; Silva-González et al., 2013) was adopted to prevent unnecessary complication in the reliability analysis. The limit state function was formulated at mudline, but the chain-soil interaction impacts were considered in the calculation of the ultimate holding capacity. This approach facilitated the reliability analysis

by keeping the variables independence between the line tension and the capacity of the anchor at the mudline. Therefore, the limit state function was written as follows (DNV-RP-E301, 2012):

$$M = R_d - T_d \tag{3-22}$$

where R_d is the design anchor and chain system capacity at mudline.

The design line tension at mudline (T_d) was defined as (DNV-RP-E301, 2012):

$$T_d = T_{mean-C} \cdot \gamma_{mean} + T_{dyn-C} \cdot \gamma_{dyn} \tag{3-23}$$

where T_{mean-C} is the mean line tension due to pretension and mean environmental loads; T_{dyn-C} is the dynamic line tension due to low frequency and wave frequency motions; γ_{mean} is the partial safety factor for the mean line tension; and $\gamma_{dyn\text{-}c}$ is the partial safety factor for the dynamic line tension. The values of γ_{mean} and $\gamma_{dyn\text{-}c}$ for consequence class 2 and the dynamic analysis were taken as 1.40 and 2.10, respectively (DNV-RP-E301, 2012). Both $T_{mean\text{-}C}$ and $T_{dyn,max\text{-}C}$ are expressed at the mudline as functions of the significant wave height (H_s), peak period (T_p), and wind velocity (U_{10}) representing an extreme sea-state. Consequently, the limit state function can be written as:

$$M\left(R, H_s, T_p, U_{10}\right) = R_d - T_{mean-C} \cdot \gamma_{mean} - T_{dyn,max-C} \cdot \gamma_{dyn} \tag{3-24}$$

The anchor capacity and load tensions are evaluated in the direction of the mooring line at the touchdown point, where the anchor line starts to embed (i.e., at an angle θ_o with the horizontal direction). The probability of failure P_F during a given extreme sea state was defined as:

$$p_F = P\left[M\left(R, H_s, T_p, U_{10}\right) \leq 0\right] \tag{3-25}$$

By using a Poisson model for the occurrence of extreme sea states (Silva-González et al., 2013),

the annual probability of failure P_{Fa} was written as an exponential function of the probability of failure P_F :

$$p_{Fa} = 1 - exp(-\lambda p_F) \quad (3\text{-}26)$$

where λ is the ratio of the number of extreme sea states to their observation period (in years); for small values of λ_{P_F}, the annual probability of failure is $P_{Fa} \approx \lambda_{P_F}$.

3.12 Probabilistic Modelling of Anchor Capacity

The crucial factors that were used to construct the anchor capacities database were including the peak friction angle (ϕ_p), the dilation angle (ψ), and the soil density (γ'). The mean value of peak friction angle (μ_{ϕ_p}) for lognormal distribution was set to 35° with a coefficient of variation (δ_{ϕ_p}) equal to 0.05 to take into consideration the uncertainty due to systematic test variations and spatial variations of the soil properties (Basha and Babu, 2008; Anchor manual, 2010). A normal distribution with a mean value (μ_ψ) of 8.49° and a coefficient variance (δ_ψ) of 0.28 was adopted for the sand dilation angle (ψ) that was calculated by using Bolton's empirical equation for sand (Bolton, 1986; Phoon, 1999; Simoni and Houlsby, 2006). The soil density was represented by a normal distribution with a mean value ($\mu_{\gamma'}$) of 10.07 and a coefficient variance ($\delta_{\gamma'}$) of 0.02 (Neubecker, 1995; Phoon, 1999; Simoni and Houlsby, 2006). To construct the capacity database, 5000 simulations were conducted by adopting different values of ϕ_p, ψ and γ'.

Figure 3-11 shows the fitted distribution and the histograms of the anchor capacities at mudline for MK5 and MK6 anchors with L_f equal to 3.624 (Left) and 3.961 (Right).

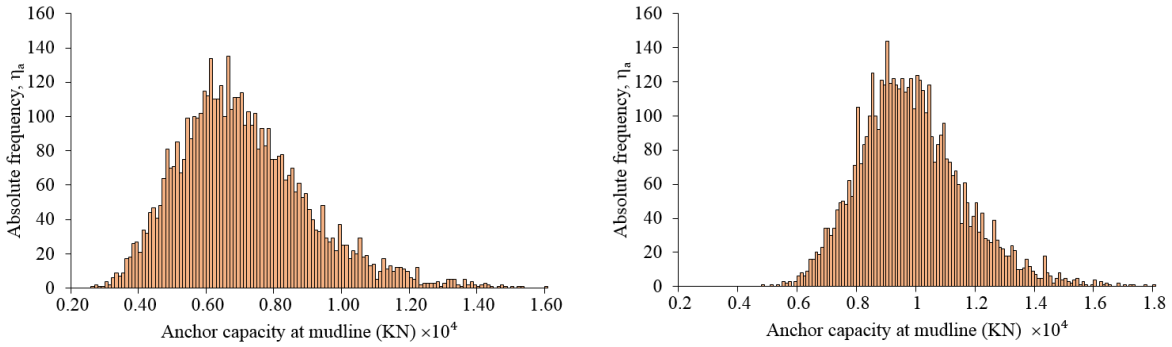

(a)

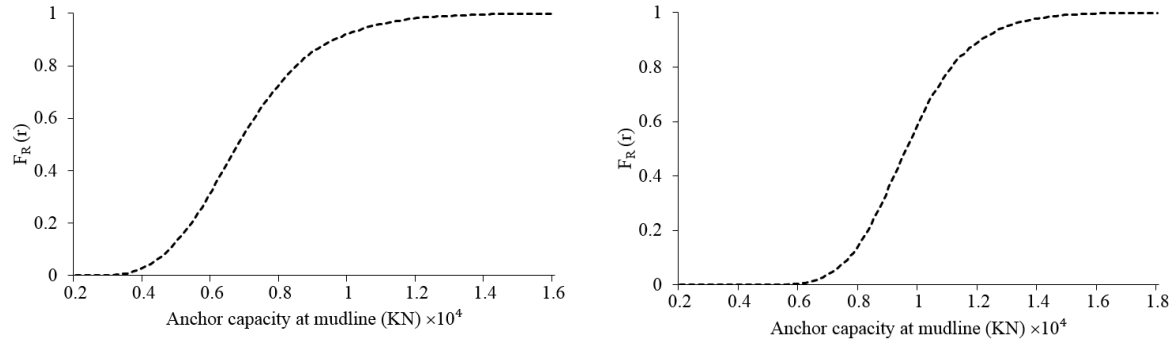

(b)

Figure 3-11. Histograms of simulated and fitted capacities at mudline, (a) absolute frequency, (b) Cumulative frequency

Table 3-5 shows the mean (μ), standard deviation (σ), coefficient of variation (δ), and median value (m) of anchor capacities at pad-eye and mudline for MK5 (with fluke lengths of 2.707, 3.166, 3.41 and 3.624 m) and MK6 (with fluke lengths of 2.958, 3.46, 3.728 and 3.961 m). The mean capacity at mudline is 10 - 14% higher than the mean capacity at pad-eye. Commonly in all anchor models, when the fluke length and fluke thickness increase, the differences between capacity at the pad-eye and mudline increase. The same conclusion can be driven for differences between median capacities at the pad-eye and the mudline, but in some anchor models (MK6 with L_f = 3.961m) the difference between median at the mudline and pad-eye decreases by an increment of

fluke length and thickness. The coefficients of variation of the capacity at pad-eye and mudline are about 23-27% for all MK5 anchor families and are about 16-18% for all MK6 anchor families.

Table 3-5. Statistical properties of anchor capacity at pad-eye and mudline

Model	L_f/d_f	L_f (m)	Padeye				Mudline				μ_{Ra}/μ_R
			μ_{Ra} (KN)	σ_{Ra} (KN)	δ_{Ra}	m_{Ra} (KN)	μ_R (KN)	σ_R (KN)	δ_R	m_{Ra} (KN)	
MK5	6.67	2.707	2283.1	506.6	0.222	2419.0	2650.5	618.8	0.233	2801.0	0.86
MK5	6.67	3.166	3754.2	978.8	0.260	4001.0	4314.8	1174.1	0.272	4620.0	0.87
MK5	6.67	3.410	4874.1	1273.2	0.261	5183.5	5590.7	1522.7	0.272	5970.0	0.87
MK5	6.67	3.624	6093.6	1636.5	0.268	6506.0	6978.8	1949.2	0.279	7485.0	0.87
MK6	3.09	2.958	2876.4	429.2	0.150	2917.0	3357.1	524.4	0.156	3411.5	0.86
MK6	3.09	3.460	5149.2	885.5	0.172	5246.0	5983.4	1070.7	0.178	6095.0	0.86
MK6	3.09	3.728	6702.5	1101.0	0.164	6822.2	7768.5	1327.9	0.170	7434.0	0.90
MK6	3.09	3.961	8451.4	1505.3	0.178	8588.0	9779.6	1805.6	0.184	9958.5	0.86

The variation of the mean and standard deviation of anchor capacity versus the fluke length for the MK6 anchor family at pad-eye and mudline are illustrated in Figure 3-12 to show the capacity distribution.

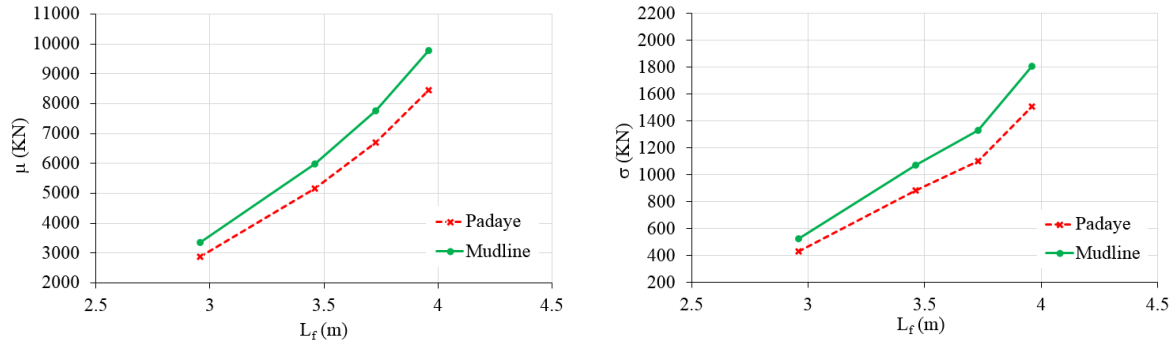

Figure 3-12. The mean and standard deviation of anchor capacity versus fluke length; MK6

3.13 Probabilistic Modelling of Line Tension

The response surfaces were developed using an approach proposed by Silva-González et al. (2013), where a Gaussian process was adopted to define the dynamic line tensions(Sarkar and Eatock Taylor, 2000; Choi, 2007). The maximum expected dynamic line tension during the extreme sea state (presented by a random vector of r uncertain environmental variables (Θ)) was expressed based on the model proposed by Davenport (1964):

$$E[T_{dyn,max}]_\theta = \mu_{Tdyn,max} = \left[\sqrt{2ln\,(\nu_\Theta \Delta t/2)} + \frac{0.5772}{\sqrt{2ln\,(\nu_\Theta \Delta t/2)}}\right]\sigma_{T,\Theta} \quad (3\text{-}27)$$

where Δt is the duration, $\nu_\Theta = \nu(\Theta)$ and $\sigma_{T,\Theta} = \sigma(\Theta)$ are the mean crossing rate and the standard deviation of the dynamic line tension, respectively. A second order polynomial expansion was used to represent both the line tension T_{mean}, and the predicted maximum dynamic line tension at mudline $T_{dyn,\,max}$ by using Θ:

$$Y(\Theta) = c + a^T\Theta + \Theta^T b\Theta \quad (3\text{-}28)$$

Where Y(Θ) is the response of interest, and Θ is the r × 1 vector of environmental variables. The following unknown coefficients c, a (r ×1) and b (r ×r) were determined by response analysis. To develop response surfaces, seven key environmental parameters were investigated on the mooring

system in the Sardar-e-Jangal gas field in the Caspian Sea. A database of 8100 different combinations was built using divergent environmental variables such as significant wave height (H_s), the direction of the wave (d_w), the velocity of wind (U_{10}), peak period (T_p), route of wind (d_{ww}), the speed of surface current (U_c), and current path relative to wave direction (d_{wc}). The mooring line with the highest load was taken into consideration to obtain the response surfaces. Figure 3-13 illustrates the response surfaces of both mean and maximum expected dynamic line tension for the domains of the peak wave period and significant wave height.

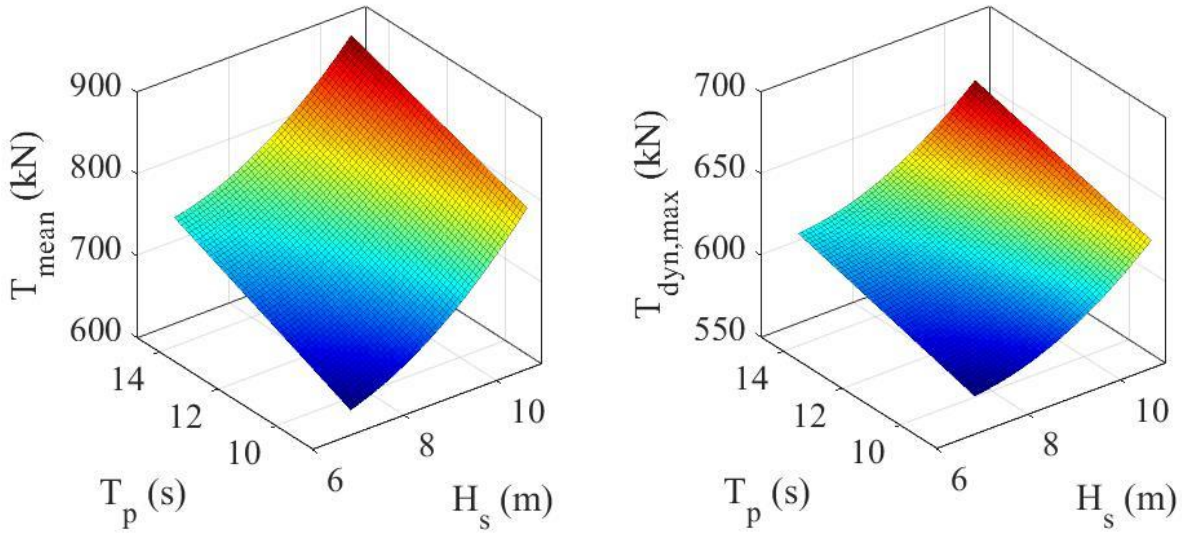

Figure 3-13. Response surfaces for T_{mean} and $T_{dyn,\ max}$

The extreme sea states were identified by using a storm event. A time interval was determined around the peak period using clustering and de-clustering (t_{peak} - $\Delta T_{cluster}$, t_{peak} - $\Delta T_{cluster}$). In the defined interval, the extreme sea state happens if the sea state at t_{peak} experiences a significant wave height higher than a threshold amount ($H_s \geq H_s^{th}$).

Other environmental variables were considered based on t_{peak}. The extreme ecological quantities of the Caspian Sea were determined according to the three-hour time series during a 24 years

observation period provided by metocean studies (Private communications, unpublished results). Using a set of 24 extreme sea states throughout the hindcast time series and using the peak over threshold method, the marginal probability distributions of $\Theta = [H_s, T_p, U_{10}]^T$ were generated. The magnitude of the mean annual rate, λ, was 30/24 = 1.25 per year based on the maximum probability estimate. The marginal distributions with the best fitting, the maximum probability estimate parameters; and the correlation coefficients for three crucial environmental variables are provided in Table 3-6 and Table 3-7.

Table 3-6. Distribution parameters of environmental variables

Variable	Probability distribution	Distribution parameters	
H_s	Weibull	Scale	9.5351
		Shape	10.1552
T_p	Lognormal	μ_{lnT_p}	2.4966
		σ_{lnT_p}	0.1196
U_{10}	Lognormal	$\mu_{lnU_{10}}$	3.4827
		$\sigma_{lnU_{10}}$	0.1095

Table 3-7. Estimated correlation coefficients

	H_s	T_p	U_{10}
H_s	1.0	0.9728	0.9905
T_p	0.9728	1.0	0.9935
U_{10}	0.9905	0.9935	1.0

3.14 Results of Reliability Analysis

First order reliability method (FORM) was used to carry out the reliability analyses. In this study to ignore the convergence problems in FORM method, a narrow and appropriately weighted

Gaussian distribution was used to model the finite probability at a lower bound capacity (Melchers et al., 2003). The variation of the annual reliability index as a function of dry anchor weight and fluke length are shown in Figure 3-14, where each point on the plot (a) corresponds to an equivalent point in the plot (b) and vice versa. For instance, point 4 in both parts of Figure 3-14 represents an MK5 anchor with L_f = 3.961 m and W_a = 12 t with an annual reliability index of 3.92.

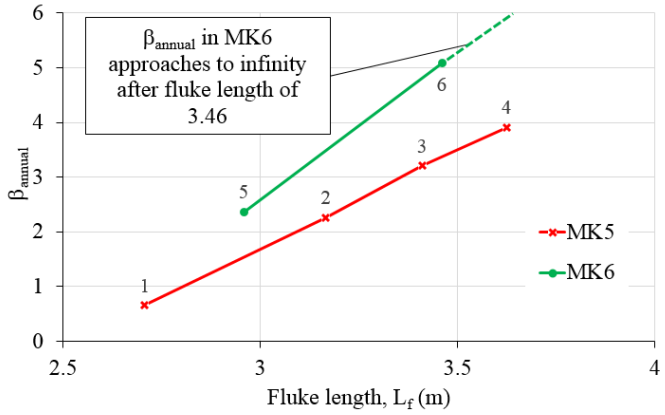

(a)

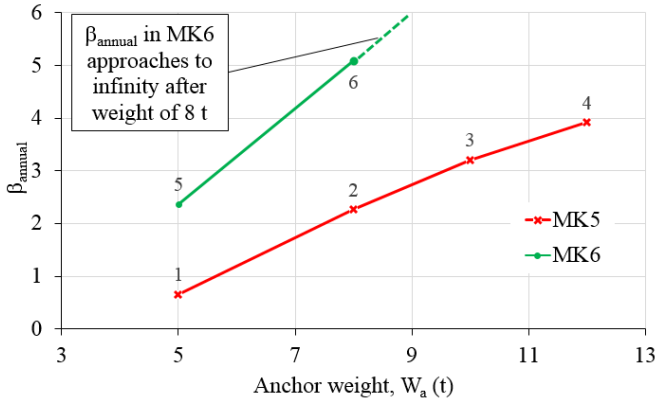

(b)

Figure 3-14. Annual reliability index versus (a) fluke length, and (b) anchor weight

As shown in Figure 3-14, to achieve specified target reliability, different anchor families with different fluke lengths and weights are available. For example, for desired reliability index of β_{annual}

= 2, either MK5 with L_f = 3.46 m and W_a = 8 t (point 2) or MK6 with L_f = 2.95 m and W_a = 5 t (point 5) could be used. Figure 3-14 shows that for the anchors with the fairly close magnitude of fluke length but different weights (from MK5 and MK6), the corresponding reliability levels are remarkably different. For instance, the 10 tones MK5 and 8 tones MK6 anchors with L_f values of 3.41 m (point 3) and 3.46 m (point 6) have a reliability index of 3.2 and 5.08, respectively. This shows that despite the clay (Moharrami and Shiri, 2018) the anchor weight is less influential in the sand, so a lighter MK6 anchor gives higher holding capacity, higher reliability index, and consequently lower failure probability (reduces from 0.0119 to 1.5×10^{-7}) compared with a heavier MK5 anchor. These ranges of failure probability are commonly used for ultimate limit state design in offshore systems (DNV-OS-E-301, 2010; DNV-OS-F201, 2010; DNVGL-ST-F101, 2019). As observed in Figure 3-14, the fluke length has a significant effect on reliability indices in both anchor families; the larger fluke length, the higher holding capacity, the higher reliability index, and the lower probability of failure.

Figure 3-15 illustrates the logarithmic variation of failure probability (log (P_{Fa})) versus anchor weight and fluke length with a linear curve fit for MK5 and MK6. The curves' slopes in Figure 3-15 indicate the required increment of anchor weight and fluke length to decrease the annual probability of failure for one order of magnitude (by a factor of 10). These results can be used in a life cycle cost-benefit analysis, where the modeling initial cost is required as a function of the probability of failure. The initial cost can increase by increasing material mass and volume, which are associated with anchor weight and fluke length, and therefore deduction in failure probability. By observing both curves in Figure 3-15, the slopes of MK6 are remarkably higher than MK5, so that a small deviation in fluke length and fluke weight results in a considerable change in failure probability and reliability index. These required increasing rate of the anchor weight and the fluke

length for MK5 are 1.8542, 0.2702 and for MK6 are 0.6408, 0.1072, respectively. Therefore, to improve the reliability index from 2.26 to 3.91, a 24% increase in weight and 9% increase in fluke length are needed in MK5, and an 8% increase in weight and 4% increase in fluke length is required in MK6.

As shown in Figure 3-15, in MK6 anchor families, beyond an anchor weight of 8 t and fluke length of 3.46 m the annual reliability index and the logarithm of failure probability approaches the infinity that is shown by dashed lines.

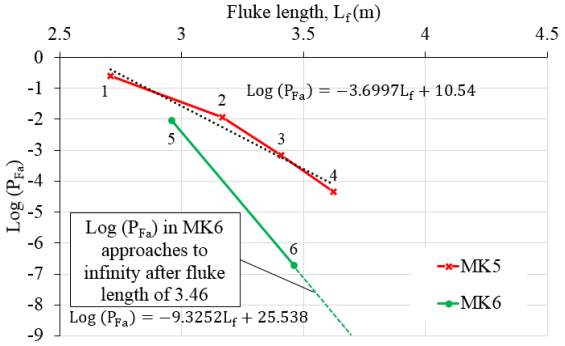

(a)

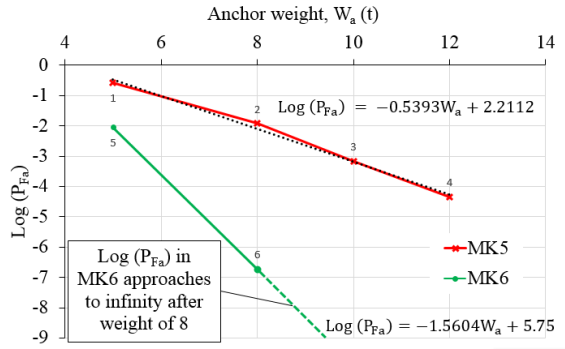

(b)

Figure 3-15. The logarithm of failure probability versus (a) fluke length, and (b) anchor weight

3.15 Equivalent Reliability Study in Sand and Clay

The reliability assessment results obtained from the current study in the sand was compared with the earlier published studies in clay (Moharrami and Shiri, 2018) to provide an in-depth insight into the problem. The comparative reliability assessment was conducted to determine the anchor classes (commonly referred to by their weight in practice) resulting in similar reliability indices. Figure 3-16 shows the comparative reliability indices obtained for different anchor weights from MK5 and MK6 families in sand and clay. The plots show the anchor classes in sand and clay that result in a fairly close magnitude of reliability indices. For instance, an 8 t MK5 anchor in the sand (point 1) results in an almost same reliability index (2.26 and 2.48) given by a 15 t MK5 anchor in clay (point 5). In MK6, the reliability indices of anchors heavier than 8 t are infinity, so there are only two points for sand.

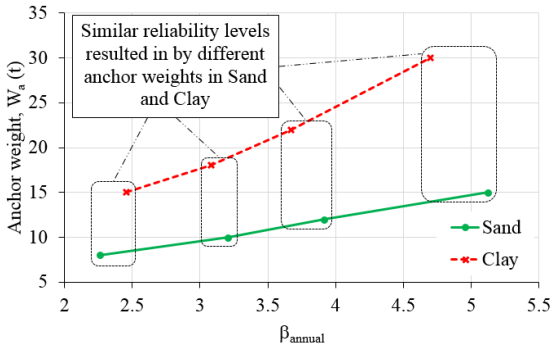

(MK5)

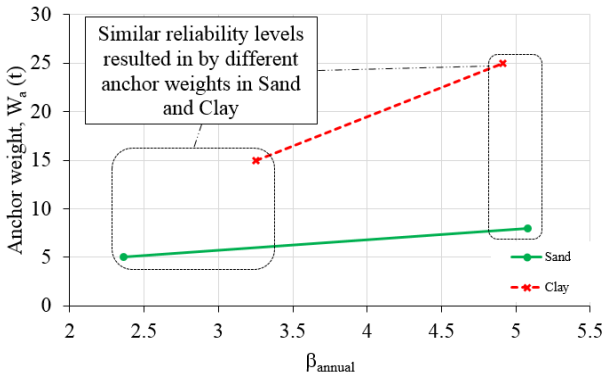

(MK6)

Figure 3-16. Equivalent anchor class (weight) comparison between sand & clay

Table 3-8 provides the map of equivalent anchor classes in sand and clay resulting in a fairly close reliability index.

Table 3-8. Equivalency map of anchor classes in sand and clay with a close reliability indices

Sand \ Clay		Anchor Classes in Clay				
		15 t	18 t	22 t	25 t	30 t
Anchor Classes in Sand	5 t	MK6			MK6	
	8 t	MK5				
	10 t		MK5			
	12 t			MK5		
	15 t					MK5

Further studies can be conducted to determine the equivalency map between the different anchor groups, e.g., MK3, MK5, MK6, and even other anchors in the market. This kind of information can provide better insight for operators and designers to select the required anchors with the desired level of reliability that may vary depending on project conditions.

3.16 Conclusions

The reliability of drag embedment anchors in the sand was investigated for catenary mooring systems and compared with earlier studies in clay. The reliability analyses were carried out by adopting the first order reliability method (FORM) using two popular Stevpris anchor families,

MK5 and MK6. The limit state function was established at the mudline, while the chain-soil interaction effects were accounted for in the calculation of ultimate holding capacities. Fully coupled time domain analyses were conducted to simulate the station keeping of a generic semisubmersible platform in the Caspian Sea and obtain the dynamic mooring line tensions. Response surface method was adopted for probabilistic modeling of the line tensions at mudline. An Excel spreadsheet containing VBA macros was developed and validated to predict the ultimate anchor capacity and the anchor trajectory down the seabed by incorporation of a popular limit state model in the sand. The variation of annual reliability indices and the logarithm of the failure probabilities versus the fluke length and the anchor weight were obtained and compared with existing studies. Several important trends were observed, some of which are summarized as follows:

The geometrical configuration of the anchors, particularly the fluke length, are the most influential parameters in determining the reliability indices. The anchor weight has a beneficial contribution to achieving a higher level of reliability but to a less extent. A well-designed anchor geometry can significantly dominate the weight effect. For instance, some lighter MK6 anchors result in a higher reliability index compared to heavier MK5 models due to their superior geometrical design.

The costly in-field testing procedure recommended by design codes for estimation of the anchor capacities are unique for all of the anchor families, seabed soil types, environmental loads, and operation conditions. This approach ignores the reliability effects affected by a wide range of inherent uncertainties and limits the cost-effectiveness of the proposed solutions. Further reliability-based refinement of the proposed procedures can have significant cost effects on offshore projects.

The existing anchor solutions are developed based on simplified anchor geometries. The idealization of anchor geometry may have a significant impact on reliability results. However, the impact is not significant in comparative studies. Further investigations are required to determine the best practice for the idealization of anchor geometry in analytical solutions.

A target reliability index for a given anchor family in clay can be achieved by a heavier anchor compared to the sand. It is challenging to determine a corresponding set of soil parameters in clay and sand to result in an identical reliability index. However, further studies in this area can be beneficial in proposing a more cost-effective infield testing procedure.

It is worth mentioning that the reliability models for assessing the anchor capacities can be significantly improved by having access to the in-field test databases and corresponding seabed soil properties, and the statistics of failures. These kinds of information are mandatory for obtaining absolute reliability indices or failure probabilities. However, the closed form solution is highly beneficial for performing comparative studies and improving the recommended practices.

Acknowledgments

The authors gratefully acknowledge the financial support of this research by Wood PLC via establishing the Wood Group Chair in Arctic and harsh environment engineering at Memorial University, the NL Tourism, Culture, Industry and Innovation (TCII) via CRD collaborative funding program, the Natural Sciences and Engineering Research Council of Canada (NSERC) via Engage funding program, Memorial University of Newfoundland through VP start-up fund and school of graduate studies (SGS). The technical advice of Mr. Mohammad Javad Moharrami is also kindly acknowledged.

References

API RP 2SK, 2008. Design and Analysis of Stationkeeping Systems for Floating Structures.

Aubeny, C.P., Chi, C., 2010. Mechanics of Drag Embedment Anchors in a Soft Seabed. J. Geotech. Geoenvironmental Eng. 136, 57–68. https://doi.org/10.1061/(ASCE)GT.1943-5606.0000198

Basha, B.M., Babu, G.L.S., 2008. Target reliability based design optimization of anchored cantilever sheet pile walls. Can. Geotech. J. 45, 535–548. https://doi.org/10.1139/t08-004

Bissett, M.J., 1993. Soil resistance to chain anchor movement.

Bolton, M.D., 1986. Discussion: The strength and dilatancy of sands. Géotechnique 37, 219–226. https://doi.org/10.1680/geot.1987.37.2.219

Choi, Y.J., 2007. Reliability Assessment of Foundations for Offshore Mooring Systems under Extreme Environments.

Clukey, E.C., Gilbert, R.B., Andersen, K.H., Dahlberg, R., 2013. Reliability of Suction Caissons for Deep Water Floating Facilities 1991, 456–474. https://doi.org/10.1061/9780784412763.035

Davenport, A.G., 1964. Note on the Distribution of the Largest Value of a Random Function With Application To Gust Loading. Proc. Inst. Civ. Eng. 28, 187–196. https://doi.org/10.1680/iicep.1964.10112

DNV-OS-E-301, 2010. Position Mooring. Offshore Standard.

DNV-OS-F201, 2010. Dynamic Risers. Offshore Standard.

DNV-RP-E301, 2012. Design and Installation of Fluke Anchors.

DNVGL-ST-F101, 2019. Submarine Pipeline Systems. Offshore standartd.

Duggal, A., Ma, K., Shu, H., Smedley, P., L'Hostis, D., 2013. A Historical Review on Integrity Issues of Permanent Mooring Systems 3. https://doi.org/10.4043/24025-ms

Melchers, R.E., Ahammed, M., Middleton, C., 2003. FORM for discontinuous and truncated probability density functions. Struct. Saf. 25, 305–313. https://doi.org/10.1016/S0167-4730(03)00002-X

Moharrami, M.J., Shiri, H., 2018. Reliability assessment of drag embedment anchors in clay for catenary mooring systems. Mar. Struct. 58, 342–360. https://doi.org/10.1016/j.marstruc.2017.12.005

Montes-Iturrizaga, R., Heredia-Zavoni, E., 2016. Reliability analysis of mooring lines using copulas to model statistical dependence of environmental variables. Appl. Ocean Res. 59, 564–576. https://doi.org/10.1016/j.apor.2016.07.008

NCEL, 1987. Drag embedment anchors for navy moorings. Naval Civil Engineering Laboratory, Port Hueneme, Calif., Techdata Sheet 83-08R.

Neubecker, S.R., 1995. The behaviour of drag anchor and chain systems, PhD Thesis, Department of Civil Engineering, The University of Western Australia.

Neubecker, S.R., Randolph, M.F., 1996a. The performance of drag anchor and chain systems in cohesive soil. Georesources Geotech. 14, 1–7.

Neubecker, S.R., Randolph, M.F., 1996b. The kinematic behaviour of drag anchors in sand. Can. Geotech. J. 33, 584–594. https://doi.org/https://doi.org/10.1139/t96-084-306

Neubecker, S.R., Randolph, M.F., 1996c. The static equilibrium of drag anchors in sand. Can. Geotech. J. 33, 574–583.

Neubecker, S.R., Randolph, M.F., 1995. Profile and frictional capacity of embedded anchor chains. Geotech. Eng. 121, 797–803.

O'Neill, M.P., Bransby, M.F., Randolph, M.F., 2003. Drag anchor fluke–soil interaction in clays. Can. Geotech. J. 40, 78–94. https://doi.org/10.1139/t02-096

O'Neill, M.P., Randolph, M.F., Neubecker, S.R., 1997. A Novel Procedure For Testing Model Drag Anchors, in: Proceedings of the 7th International Offshore and Polar Engineering Conference.

Phoon, K.K., 1999. Characterization of geotechnical variability. Can. Geotech. J. 624, 612–624.

Private communications, n.d. with Kinsale Energy Ltd.

Rendón-Conde, C., Heredia-Zavoni, E., 2016. Reliability analysis of suction caissons for moored structures under parameter uncertainties. Struct. Saf. 60, 102–116. https://doi.org/10.1016/j.strusafe.2016.02.004

Sarkar, A., Eatock Taylor, R., 2000. Effects of mooring line drag damping on response statistics of vessels excited by first- and second-order wave forces. Ocean Eng. 27, 667–686. https://doi.org/10.1016/S0029-8018(99)00014-1

Silva-González, F., Heredia-Zavoni, E., Valle-Molina, C., Sánchez-Moreno, J., Gilbert, R.B., 2013. Reliabilitystudy of suction caissons for catenary and taut-leg mooring systems. Struct. Saf. 45, 59–70. https://doi.org/10.1016/j.strusafe.2013.08.011

Simoni, A., Houlsby, G.T., 2006. The direct shear strength and dilatancy of sand-gravel mixtures. Geotech. Geol. Eng. 24, 523–549. https://doi.org/10.1007/s10706-004-5832-6

Thorne, C.P., 2002. Penetration and Load Capacity of Marine Drag Anchors in Soft Clay. J. Geotech. Geoenvironmental Eng. 124, 945–953. https://doi.org/10.1061/(asce)1090-0241(1998)124:10(945)

Valle-molina, C., Heredia-zavoni, E., Silva-gonzález, F.L., 2008. Reliability analyses of suction caissons for FPSO systems, in: International Conference on Offshore Mechanics and Arctic Engineering. pp. 1–6.

Vryhof Anchors, 2010. Anchor manual. Krimpen ad Yssel, The Netherlands.

Wang, L.Z., Guo, Z., Yuan, F., 2010. Quasi-static three-dimensional analysis of suction anchor mooring system. Ocean Eng. 37, 1127–1138. https://doi.org/10.1016/j.oceaneng.2010.05.002

Chapter 4. Reliability Assessment of Drag Embedment Anchors in Layered Seabed, Clay over Sand

Amin Aslkhalili[1], Hodjat Shiri[2]

1. 2. Civil Engineering Dept., Faculty of Engineering and Applied Science, Memorial University of Newfoundland, A1B 3X5, St. John's, NL, Canada.

This chapter is a conference paper accepted for oral presentation in 73rd Canadian Geotechnical Conference (Geo-Calgary2020), Paper number 71.

Abstract

Drag embedment anchors combined with catenary mooring systems are widely used for temporary and permeant station keeping of the offshore floating facilities. With growing exploration and production of offshore reserves, the number of mooring failure incidents in floating facilities has been increased. This implies the significance of the reliability assessment of the mooring system components and particularly drag embedment anchors as one of the key elements. The currently used anchor design codes consider only homogeneous seabed soil condition. It is widely accepted that the presence of the layered seabed may significantly affect the ultimate holding capacity of anchors. Therefore, it is expected that layered seabed condition affects the reliability indices of these anchors as well. However, there are only a few published studies that have investigated homogeneous seabed soil condition ignoring the effect of layered soil strata. In this study, the reliability of drag embedment anchors was comprehensively investigated in the layered seabed (clay over sand). An advanced calculation tool was developed to obtain the holding capacity of the anchors by combining a series of iterative limit state and kinematic analysis. A time-domain dynamic mooring analysis was conducted by assuming a semisubmersible platform to obtain the dynamic line tensions. The uncertainties of the environmental loads, metocean variables, seabed soil properties were incorporated into a first-order reliability analysis (FORM) to obtain the failure probabilities. A probabilistic model established for determination of holding the capacity for nominated drag anchor families. The study revealed a significant effect of the layered soil condition in reliability assessment by lowering the magnitude of reliability indices. The improvement of the recommendations provided by design codes by incorporation of the complex seabed condition was found necessary for a safer and cost-effective anchor design.

Keywords: Drag embedment anchors; Reliability assessment; Surface response; Layered seabed soil; Probabilistic modeling; Dynamic mooring analysis

4.1 Introduction

Catenary mooring systems along with seabed anchors are often used for station keeping of a wide range of offshore floating facilities such as operation vessels, semi-submersibles, Spars, FPSOs, etc. Different types of anchors are used in a mooring system such as suction anchors, pile anchors, screw-in anchors, plate anchors, deadweight anchors, and drag embedment anchors. However, the latter one is amongst the most popular seabed anchoring solutions that are used for both temporary and permanent mooring systems. Temporary mooring systems are usually used with construction vessels and floating exploration units. These systems are retrieved at the end of the operation. The permanent mooring systems are used for floating production facilities and are remained in the seabed by ending the unit operation life (Figure 4-1).

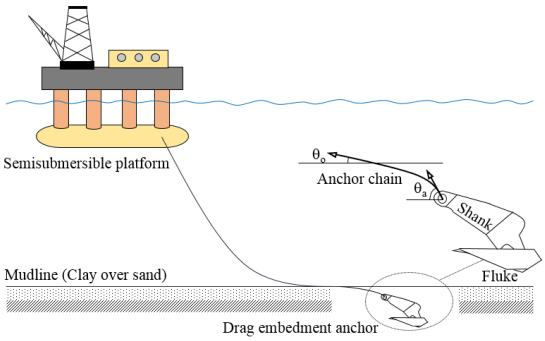

Figure 4-1. Drag embedment anchor configuration with a catenary mooring line

The operational and environmental safety of the floating facilities significantly depends on the reliability of mooring and anchoring systems. Expanding the offshore explorations and operations towards the deep waters and harsh environments has resulted in developing high capacity anchoring and mooring solutions with high-strength components. However, the number of mooring system related incidents in harsh environments involving floating facilities (on an average of more than two incidents per year reported by Duggal et al. 2013) continues to raise concerns in

the industry in general. On the other hand, large uncertainties in seabed parameters and environmental loads combined with the inaccessibility for monitoring, inspection, and maintenance mandates the reliability assessment of drag anchors to minimize their likelihood of failure.

It becomes more challenging when the seabed soil strata comprise of layered conditions such as clay over sand, sand over clay, sand over sand, etc., since depending on the anchor trajectory in the layered soil, the ultimate holding capacity may significantly vary (M. P. O'Neill et al., 1997). In layered seabed condition, the existing design codes recommend the same capacity assessment procedure as homogeneous soil. This simplification may affect the reliability of the drag anchors and impose some level of risk to the project. This important aspect has never been studied in the past and needs investigations to facilitate refining the design code recommendations for layered soil.

The holding capacity of drag embedment anchors has been widely investigated (Dunnavant and Kwan, 1993; Neubecker, 1995; Neubecker and Randolph, 1996; O'Neill et al., 1997; O'Neill, 2000; O'Neill et al., 2003). The reliability of some of the anchor families such as suction caissons have been widely investigated in the literature (Clukey et al., 2013; Choi, 2007; Valle-molina et al., 2008; Silva-González et al., 2013; Montes-Iturrizaga and Heredia-Zavoni, 2016; Rendón-Conde and Heredia-Zavoni, 2016). However, there are only two studies (to the best of the authors' knowledge) on the reliability of drag embedment anchors (Moharrami and Shiri, 2018; Aslkhalili et al., 2019) both of which have considered a single homogeneous layer of clay and sand, respectively.

In this study, the influence of layered seabed on reliability and the likelihood of failure of drag embedment anchors supporting the catenary mooring lines were comprehensively investigated.

Clay over sand stratum was considered, which is commonly found in offshore territories. A generic semisubmersible platform in the Flemish Pass Basin, Newfoundland Offshore (Eastern Canada), was simulated by fully coupled time-domain analyses to obtain the dynamic tensions of mooring lines. The response surface method was employed for conducting a probabilistic model of the line tensions at the mudline. The probabilistic modeling of anchor capacity was conducted using a limit state equilibrium and kinematic approach to characterize the fluke-soil interaction and failure states. The embedded profile and the frictional capacity of the anchor chain at the seabed were also considered in the calculation of the ultimate holding capacity. The uncertainties of the environmental loads, metocean variables, and consequently, the stress distribution throughout the catenary lines was accounted for using the response surface method. The first-order reliability method (FORM) was used through an iterative procedure to obtain probabilistic failures.

It was observed that the layered soil condition with different configurations and soil properties could have a significant effect on reliability indices, compared with the homogeneous seabed soil. This can affect the reliability of the currently proposed sequential procedures recommended by design codes to obtain the anchor capacity through performing filed trials. The study revealed the significance of considering the layered seabed soil stratum in the evaluation of ultimate holding capacity and the need for improving the existing design codes.

4.2 Methodology

The reliability study was conducted based on a limit state function assessing the anchor holding capacity against the dynamic mooring line tensions at mudline. The anchor response in the layered soil (clay over sand), along with the soil-chain interaction was obtained by adopting the limit state equilibrium and kinematic approach and the procedure proposed by O'Neill et al. (1997). An Excel spreadsheet VBA Macro (Visual Basic Application) was programmed to calculate the holding

capacity of anchor incorporating the effect of the soil-chain interaction. In order to obtain the mean and maximum dynamic line tensions, mooring analysis was conducted using OrcaFelx by assuming a generic semisubmersible platform in the Flemish Pass Basin, NL offshore (Canada), and the sea states with a 100 years return period.

Stevpris Mk5 and Mk6 anchors were considered for reliability studies with the key parameters including undrained shear strength, effective clay unit weight, fluke and shank bearing factor, clay and sand boundary layer depth, effective sand unit weight, sand friction angle, dilation angle, anchor geometrical configurations, line tension angle at mudline, and side friction factor. The response surface method was used to function the mean and predicted maximum of dynamic line tension using uncertain metocean variables. The reliability analysis was conducted by using the first order reliability method (FORM). The required data related to partial design factors for capacities and the mean and maximum dynamic line tensions were obtained from DNV-RP-E301 (2012).

4.3 Modeling Drag Anchor in Layered Soil

4.3.1 Chain-Soil frictional capacity

The frictional capacity between the soil and the embedded chain has a significant contribution to the anchor performance, penetration trajectory, and the ultimate holding capacity (Neubecker and Randolph, 1995a). The model proposed by O'Neill et al. (1997) was adopted to calculate the soil-chain frictional capacity in layered soil. This model has been developed by extension of the earlier studies conducted by Neubecker and Randolph (1995b). Figure 4-2 shows the force equilibrium of the chain, where Q is the soil bearing resistance normal to the chain, T is the line tension, F is the friction force, and θ is inclination angle from the horizontal line.

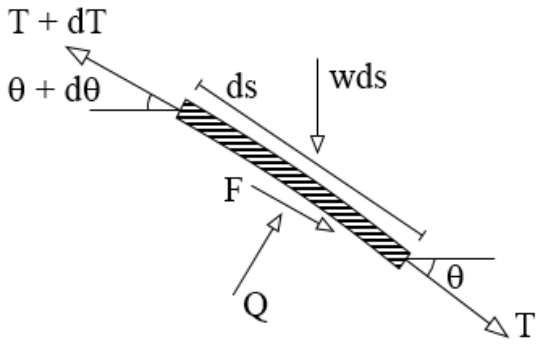

Figure 4-2. Force equilibrium of the chain element

The primary parameter for calculation of chain bearing capacity is the soil bearing resistance (Q). In a layered soil, this parameter needs to be calculated for sand-only and clay-only strata. O'Neill (2000) proposed the following expressions for the effective resistance profiles in homogenous seabed soil:

$$Q_{eff}(z) = N_c b_c (s_{u0} + s_{u0} z) - W_c \qquad \text{for clay} \qquad (4\text{-}1)$$

$$Q_{eff}(z) = N_c b_c \gamma_s' z - W_c \qquad \text{for sand} \qquad (4\text{-}2)$$

Where N_c and N_q are bearing capacity factors for clay and sand, b_c is effective chain weight, w_c is chain self-weight, s_{u0} is surface undrained shear strength, s_{ug} is undrained shear strength gradient, γ_s' is sand effective unit weight, and z represents depth.

In a layered soil profile, the effective profile resistance in the sand which is overlaid by clay, the overburden pressure applied by clay layer needs to be considered. O'Neill (2000) proposed the following set of equations for effective resistance profile for clay over sand:

$$Q_{eff}(z) = N_c b_c (s_{u0} + s_{u0} z) - W_c \qquad \text{for } \delta_c \le z < d_c$$

$$Q_{eff}(z) = N_q b_c\left[\gamma_c^{'} d_c + \gamma_c^{'}(z - d_c)\right] - W_c \qquad \text{for } d_c \le z < d_a \tag{4-3}$$

Where $\gamma_c^{'}$ is clay effective unit weight, d_c is the depth of overlaying clay layer, and δ_c is seabed surface depth.

It is challenging to find an analytical solution for equation 4-3 due to different chain embedment depth. Therefore, O'Neill (2000) adopted a substitutive numerical solution by assuming a zero inclination at the mudline:

$$\left[\theta_a^2 - \frac{2}{T_a}\int_z^{d_a} Q(z)dz\right]^{0.5} = \theta \approx -\frac{dz}{dx} \tag{4-4}$$

where, T_a, θ_a, and, d_a are chain load, the inclination of the pad-eye, and attachment depth, respectively. The chain angle at the shank pad-eye, θ_a, can be obtained by:

$$\frac{T_a\ \theta_a^2}{2} = \int_0^{d_a} Q(z)dz = d_a\bar{Q} \tag{4-5}$$

Knowing the chain angle at pad-eye, and the embedded chain profile, the incremental chain load along the chain length can be estimated as:

$$T \approx T_a e^{\mu(\theta_a - \theta)} + \mu w_c\left(x + \frac{d_{a_{eff}}\theta_a}{4}\right) \tag{4-6}$$

Figure 4-3 shows the load development throughout the embedded weighty and weightless chains. The plot shows the limited contribution of the chain weight to its ultimate capacity.

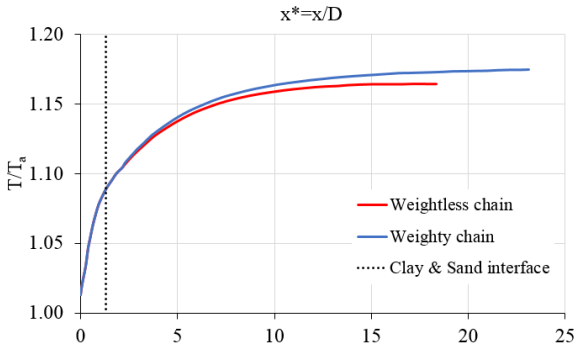

Figure 4-3. Embedded chain load behavior in clay over sand layered soil

4.3.2 Anchor Holding Capacity

The holding capacity of drag embedment anchor in layered soil (clay over sand) was obtained by combining the limit equilibrium and kinematic solutions for homogeneous clay and sand layers (O'Neill, 2000). Four main scenarios were defined to cover three different domains of clay-only, sand-only, and clay over sand seabed:

The anchor is entirely in the clay layer and has not yet entered the sand.

The anchor fluke tips have just passed the sand-clay interface.

The anchor fluke has fully or significantly embedded in the sand layer, but all or part of the shank is still in the clay layer.

The anchor fluke and shank are entirely embedded in the sand layer beneath the clay.

The first episode was adopted from Neubecker and Randolph (1996b) with no modification. The episode was identified by incremental checking of the fluke tip depth, d_t, which needed to be less than the clay layer depth, d_c. When the fluke tip passes the clay-sand interface ($d_t > d_c$), the second episode starts. In this episode, the clay-only domain is still dominant, but the effect of the fluke tip

encountered with the sand layer was considered. O'Neill (2000) proposed the following equation for calculation of fluke tip force that was added to T_a to obtain the revised anchor capacity, T_a':

$$F_t = A_t q_{sand} N_t \tag{4-7}$$

where A_t is the projected area of fluke tips on a perpendicular plane to moving direction, q_{sand} is the standard sand strength, and N_t is bearing factor of fluke tip in the sand. The direction of F_t assumed to be parallel to the direction of movement.

The standard sand strength, q_{sand}, was obtained by:

$$q_{sand} = \gamma_c' d_c + \gamma_s' (d_t - d_c) \tag{4-8}$$

As the anchor embeds further in the seabed, it reaches a point which the dominant mechanism changes to sand. The exact position of transition point is not well known; nevertheless, O'Neill (2000) proposed, as the bottom depth of front shank face, d_{sf}, transcends depth of clay-sand interface, d_c, the governing mechanism changes to sand-dominant behavior. Modifications were done to the sand-dominant mechanism to use in this episode: first, adding the normal and shear forces of clay on the fluke and shank, second, incorporating the clay overburden pressure. Figure 4-4 shows the modified acting forces on a drag anchor which has the sand-dominant mechanism.

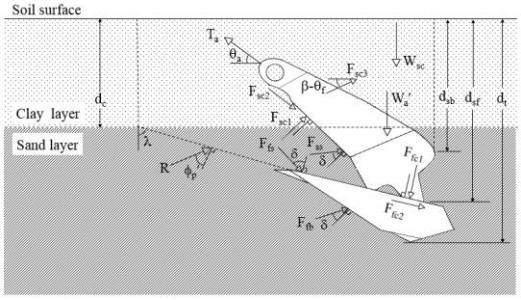

Figure 4-4. Force system of anchor-soil in clay over sand

As indicated in Figure 4-4, the clay normal and shear fluke force, F_{fc1} and, F_{fc2}, are perpendicular and parallel to the top fluke face and they could exist when shank front depth and shank back depth be respectively, greater and less than clay depth layer ($d_{sf} \geq d_c$, $d_{sb} < d_c$). The clay normal, F_{sc1}, and shear, F_{sc2}, act normal and oriented to the front shank face, and they exist when pad-eye depth is less than clay layer depth ($d_a < d_c$). The clay side shank force, F_{sc3}, acts parallel to moving direction. The weight of soil wedge, W_{sc}, side friction, SF, and, the sand shank force, F_{ss}, need to be modified compared to sand only force system and the updated functions used in calculations. The modified formulations of all these forces can be found in O'Neill (2000).

The fourth episode is achieved by deep penetration of the anchor, where the fluke and shank are completely embedded within the sand layer. The calculation procedure for this episode is the same as the third episode by two corrections. First, the fluke and shank clay forces become zero; second, the influence of sand layer is considered for determination of the inclination angle at the attachment point of chain and pad-eye.

The force-free body diagram of the anchor in clay over sand layered soil was determined by using the forgoing four episodes and their relevant modified forces. The unknown parameters are soil resistance, R, sand fluke force, F_{fs}, the force behind the flukes, F_{fb}, and the chain tension, and T_a which was calculated by using soil failure wedge, the anchor force free-body diagram, and applying vertical and horizontal force equilibriums.

It is worth mentioning; the ultimate holding capacity is sensitive to the anchor geometry idealization approach that is used in an analytical solution. In this study, the idealization method proposed by Neubecker and Randolph (1996c) was adopted. Aslkhalili et al. (2019) have discussed the influence of anchor geometry idealization impact on its holding capacity and consequently, the reliability indices.

The anchor embedment trajectory in the layered soil (clay over sand) was obtained by using the methodology proposed by Neubecker and Randolph (1996a) and extended by O'Neill et al. (1997). The adopted methodology has been developed based on a minimum work approach. The anchor, at some point in the soil with ultimate forces acting on it needs a certain amount of work to be translated and rotated to some new geometry in the soil. A series of assumed displacements and rotations are automatically tried to obtain the incremental relocation dissipating the least amount of work. The corresponding displacement increment with the least dissipated energy is assumed to be the anchor trajectory with the least resistance against the anchor relocation. More details of the proposed kinematic model for the layered soil (clay over sand) could be found in Neubecker and Randolph (1996a) and O'Neill (2000).

4.3.3 Developing Calculation Spreadsheet

The ultimate holding capacity and the trajectory of the anchor-chain system was calculated by developing an Excel spreadsheet equipped with VBA macros. Figure 4-5 shows the iterative calculation flowchart.

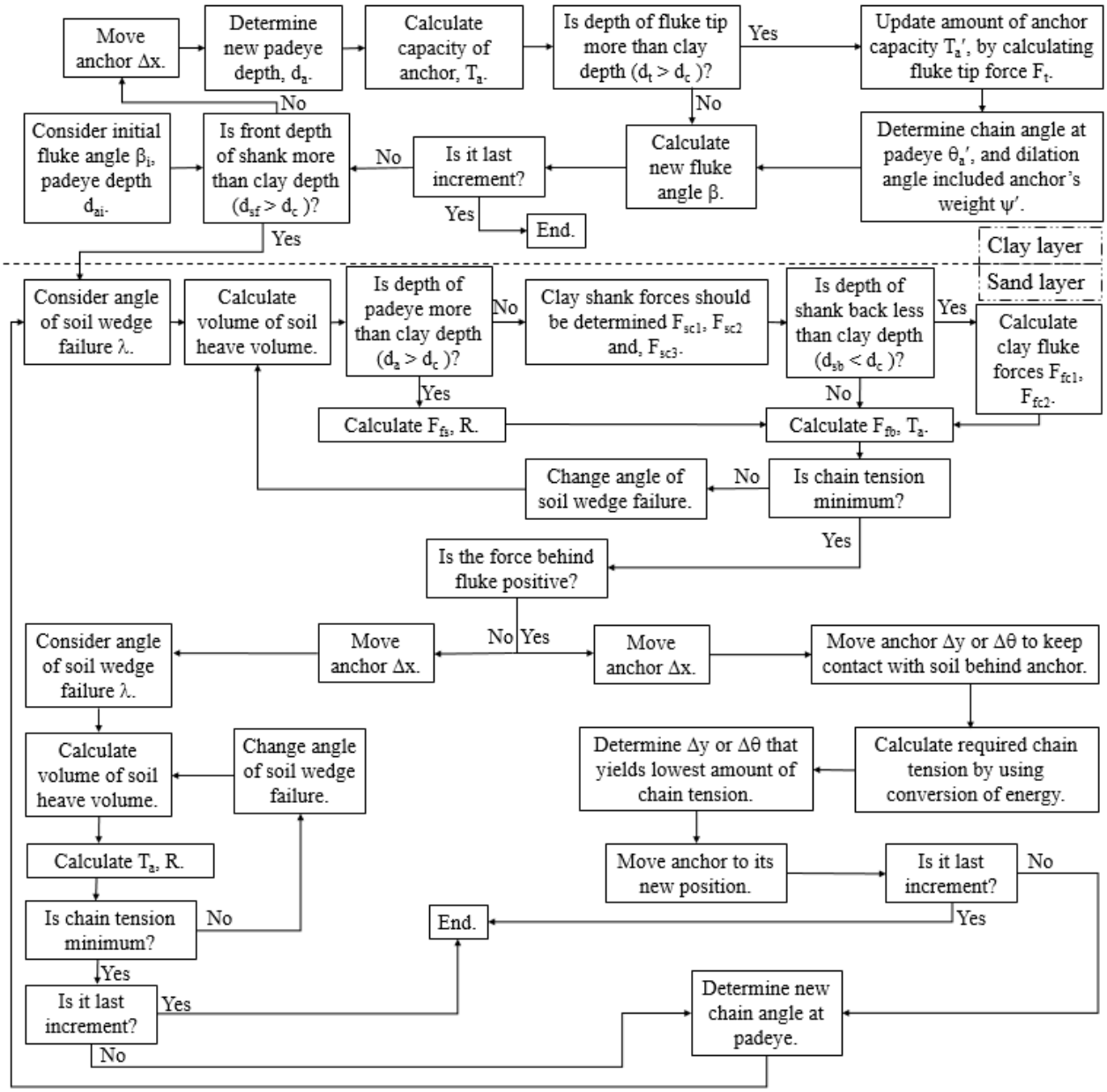

Figure 4-5. Flowchart of anchor embedment calculation in the layered seabed

The performance of the developed spreadsheet was verified against the published experimental and analytical studies O'Neill (2000). The anchor, chain, and layered soil input parameters for the validation study are summarized in Table 4-1.

Table 4-1. Soil and anchor input parameters in the current analysis

Parameter	Value
Anchor dry weight, W_a (kN)	313.6
Fluke length, L_f (m)	4.97
Fluke width, b_f (m)	4.23
Fluke thickness, d_f (m)	0.72
Shank length, L_s (m)	8.07
Shank width, b_s (m)	0.83
Fluke-Shank angle, θ_{fs} (°)	27.1
Effective chain width, b_c (m)	0.24
Chain self-weight, w_c (kN/m)	2
Chain soil friction coefficient μ	0.4
Peak friction angle, ϕ_p (°)	35
Shank bearing factor, N_{qs}	20
Dilation angle, ψ (°)	8.5
Effective unit weight, γ_s' (kN/m3)	10
Fluke tip bearing factor, N_t	0.1
Surface undrained shear strength, s_{u0} (kPa)	0
Undrained shear strength gradient,	1.5
Effective clay unit weight, γ_c' (kN/m3)	7.19
Clay bearing capacity factor, N_c	9
Clay layer depth, d_c (m)	5.31

Figure 4-6 shows a perfect agreement between the developed spreadsheet and the existing experimental and analytical studies.

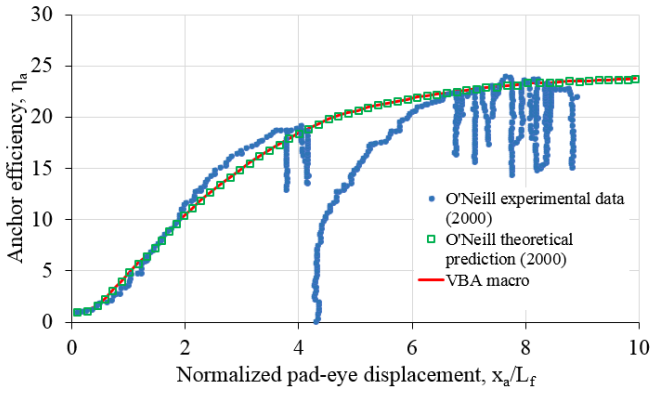

Figure 4-6. Comparison between anchor efficiency results

4.3.4 Anchors Selected for Reliability Studies

Stevpris Mk5 and Mk6 were used for reliability analysis in the current study. These anchors are widely used for permanent and temporary station keeping of floating systems. Also, the selection of these anchors enabled an effective comparison of the reliability results with earlier studies conducted in homogenous clay and sand (Moharrami and Shiri (2018) and Aslkhalili et al. (2019)). The ratio of fluke length to fluke thickness (L_f/d_f) in these anchors are 6.67 and 3.09 for Mk5 and Mk6, respectively. Figure 4-7 indicates the plan and side view of these anchors with geometrical properties given in Table 4-2.

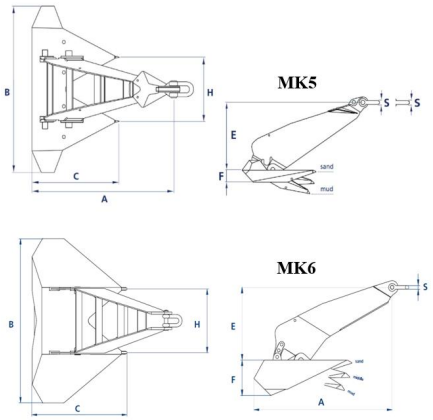

Figure 4-7. Schematic plan and side view of the modeled anchor in the present study

Table 4-2. Main dimensions for 12 t anchors (Vryhof Anchors, 2010)

	Mk5 (L_f/d_f = 6.67)	Mk6 (L_f/d_f = 3.09)
A (mm)	5908	5593
B (mm)	6368	6171
C (L_f), (mm)	3624	3961
E (mm)	3010	2642
F (d_f), (mm)	543	1282
H (mm)	2460	2394
S (mm)	150	140
Fluke-shank angle(θ_{fs}), (°)	32.00	32

Using the soil properties presented in Table 4-1, the holding capacities or design resistance ($R_{d,a}$) and the corresponding line tension angle (θ_a) at the pad-eyes were calculated for both Mk5 and Mk6, and the results were summarized in Table 4-3.

Table 4-3. Properties of the modeled drag anchors

Anchor type	L_f/d_f	L_f (mm)	d_f (mm)	$R_{d,a}$ (kN)	θ_a (˚)
Mk5	6.67	4297	644	2275	13.0
Mk6	3.09	4534	1468	2267	12.9

4.4 Finite Element Mooring Analysis

A generic semisubmersible platform in the Flemish Pass Basin, Newfoundland offshore, was considered with a catenary spread mooring consisting of eight mooring legs. Each line includes three segments; the upper, middle, and lower parts which are made up of chain, wire rope, and chain, respectively. The dynamic line tensions at the touchdown point (TDP) were obtained using a finite element model developed in OrcaFlex. Performing a three hours time-domain simulation revealed that the environmental loads with a 100 years return period (i.e., H_s = 9.5 m, T_P = 12.8 s, and U_{10} = 29 m/s) results in the most heavily loaded line. The incorporated response amplitude operator (RAO) of the platform for the head sea indicated in Figure 4-8.

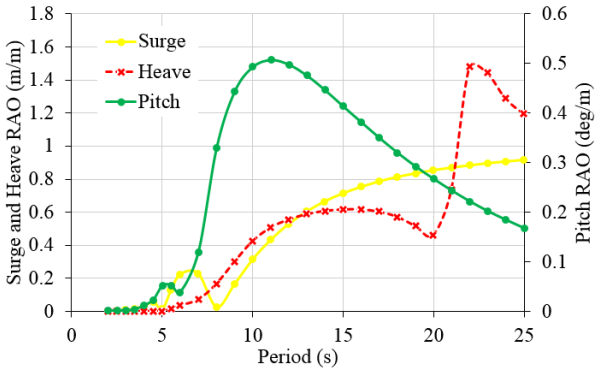

Figure 4-8. Generic semisubmersible RAO, the head sea

Table 4-4 shows the primary outcome of dynamic mooring analysis including T_d (design line tension), θ_o (line angle at mudline), $T_{mean\text{-}C}$ (characteristic mean tension), and $T_{dyn,max\text{-}C}$ (characteristic mean maximum dynamic tension). These results were used in reliability analysis.

Table 4-4. Characteristic of the catenary mooring system

H_s (m)	T_P (s)	U_{10} (m/s)	$T_{mean\text{-}C}$ (kN)	$T_{dyn,max\text{-}C}$ (kN)	T_d (kN)	θ_o (°)
9.5	12.8	29	846	623	2493	1.3

4.5 Reliability Analysis

The first order reliability method (FORM) was used through an iterative technique to get the probabilistic results by consideration of uncertainties in the seabed properties and environmental loads. The limit equilibrium method proposed by O'Neill et al. (1997) was adopted for probabilistic modeling of the anchor capacity in layered soil (clay over sand). The embedment trajectory and the chain frictional capacity were accounted for in the ultimate holding capacity calculations. The uncertainties related to environmental loads and metocean variables like wind velocity, spectral peak period, significant wave height, and consequently the stress distribution throughout the catenary lines were considered by defining appropriate probability density function and the response surface approach. Based on recommendations of DNV-RP-E301 (2012), a target failure probability and consequence class of 10E-5 and 2 were set in this study.

4.5.1 Limit State Function

The anchor holding capacity and the mooring line tensions at mudline were used to construct the limit state function (DNV-RP-E301, 2012):

$$M = R_d - T_d \tag{4-9}$$

where T_d and R_d are the design line tension and design anchor and chain system capacity at mudline, respectively. The design line tension, T_d, was formulated as the sum of the characteristic mean line tension, $T_{mean\text{-}C}$, and the characteristic dynamic line tension, $T_{dyn,max\text{-}C}$. The characteristic mean line tension, $T_{mean\text{-}C}$, is the result of the line pretension and mean environmental loads. The maximum dynamic line tension, $T_{dyn,max\text{-}C}$, is representing the low-frequency and wave-frequency vessel motions. The dynamic and characteristic mean line tensions were multiplied by relevant partial safety factors, γ_{dyn} and γ_{mean}, respectively.

$$T_d = T_{mean-C} \cdot \gamma_{mean} + T_{dyn-C} \cdot \gamma_{dyn} \quad (4\text{-}10)$$

The partial safety factors for mean and dynamic line tension was taken as 1.4 and 2.1 for consequence class 2 (DNV-RP-E301, 2012). The significant wave height (H_s), peak period (T_p), and wind velocity (U_{10}) were used as primary parameters of the extreme sea-state. Both $T_{mean\text{-}C}$ and $T_{dyn,max\text{-}C}$ were expressed as a function of those parameters at the mudline; therefore, the limit state function can be written as:

$$M\left(R, H_s, T_p, U_{10}\right) = R_d - T_{mean-C} \cdot \gamma_{mean} - T_{dyn,max-C} \cdot \gamma_{dyn} \quad (4\text{-}11)$$

The failure probability p_F for a given extreme sea state was defined as:

$$p_F = P\left[M\left(R, H_s, T_p, U_{10}\right) \leq 0\right] \quad (4\text{-}12)$$

The annual probability of failure (p_{Fa}) for the incidence of extreme sea states was defined by adopting a Poisson model and using an exponential function of failure probability (p_F) (Silva-González et al., 2013):

$$p_{Fa} = 1 - exp(-\lambda p_F) \quad (4\text{-}13)$$

where λ indicates the number of occurred extreme sea states throughout the observation period in years.

4.5.2 Probabilistic Modelling of Anchor Capacity

The anchor capacity database in the layered seabed (clay over sand) was constructed by using the key anchor-seabed interaction factors including undrained shear strength (s_{ug}), the side shear factor (α_s), effective clay and sand weight (γ'_c, γ'_s), fluke bearing factor (N_c), sand friction angle (ϕ_p), and dilation angle (ψ). For the homogeneous clay domain, the properties used by Moharrami and Shiri (2018) were adopted. A lognormal distribution with mean value (μs_{ug}) of 1.5 kPa/m and a coefficient of variation (δs_{ug}) of 0.2 was used for undrained shear strength. A bivariate lognormal distribution was used for fluke bearing and side friction factors with a mean values $\mu_{\alpha s}$ of 0.7 and μ_{Nc} of 9. A coefficient of variation $\delta_{\alpha s}$ equal to 0.2 and δ_{Nc} of 0.25 was used with a correlation coefficient of -0.8, (ρ). The effective clay weight was considered by using a normal distribution with a mean value ($\mu_{\gamma'_c}$) of 7.19 and a coefficient variance ($\delta_{\gamma'_c}$) of 0.07 (Phoon, 1999). For the homogeneous sand layer, the magnitudes suggested by Aslkhalili et al. (2019) were used. A lognormal distribution was set for peak friction angle with the mean (μ_{ϕ_p}) and coefficient of variation (δ_{ϕ_p}) equal to 35° and 0.05, respectively. For dilation and sand unit weight, a normal distribution was adopted with the following properties. The mean value for soil density ($\mu_{\gamma_s'}$) and the related coefficient variance ($\delta_{\gamma_s'}$) were taken as 10.07 and 0.02, respectively. The magnitude of these parameters for dilation angle (μ_ψ and δ_ψ) were set to 8.49° and 0.28. The database for holding capacity of anchor in layered soil was constructed by performing 8750 simulations and using different values for s_{ug}, α_s, γ'_c, γ'_s, N_c, ϕ_p, ψ.

In order to investigate the effect of clay layer depth on holding capacity of anchor, two different clay layer depths (d_c) of $1.07L_f$ and $1.39L_f$ were studied. Figure 4-9 shows the curve fits for distribution and the histograms of the anchor capacities at mudline for both Mk5 with $L_f = 4.297$ (Left) and Mk6 with $L_f = 4.534$ (Right) in layered soil ($d_c = 1.39L_f$).

(a)

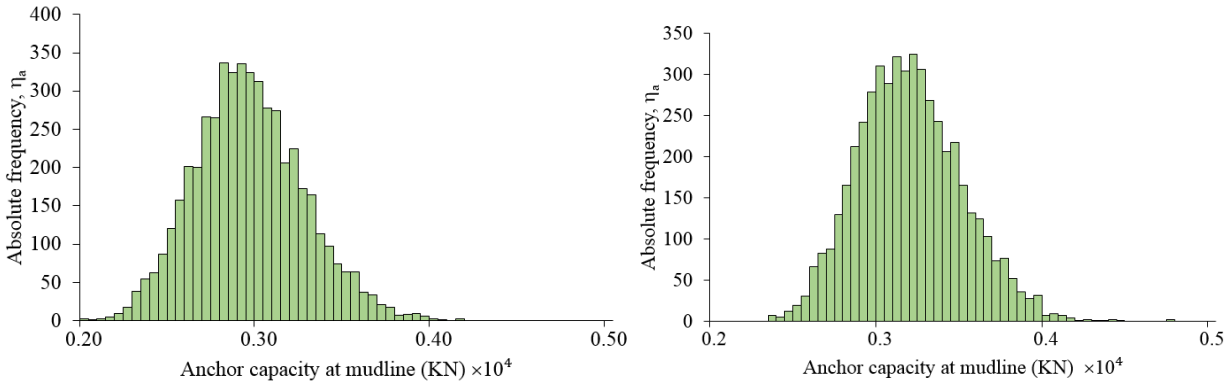

(b)

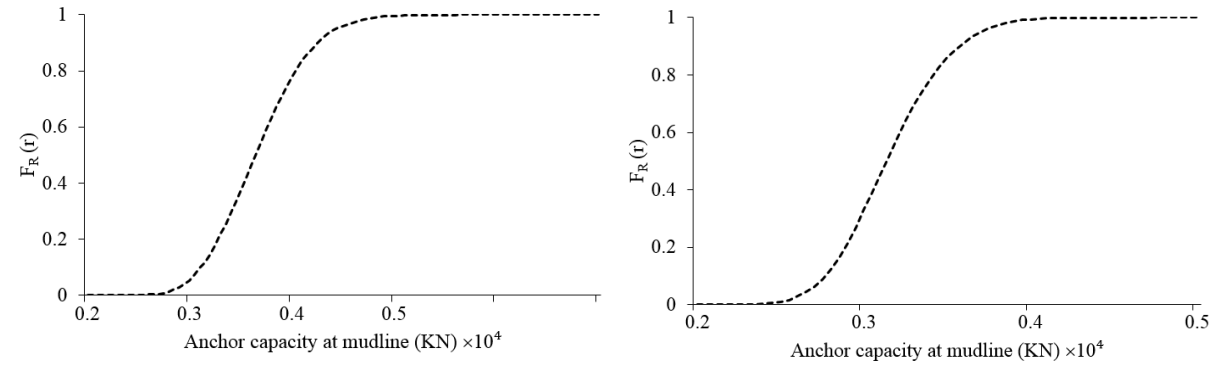

Figure 4-9. Histograms of simulated capacities at mudline, (a) absolute frequency, (b) cumulative frequency

Table 4-5 has summarized the statistical properties of anchor capacities at pad-eye and mudline for MK5 (with fluke length of 3.904, 4.149, 4.297, and, 4.436) and MK6 (with fluke length of 4.267, 4.534, 4.696, and, 4.848) with a clay layer depth of $1.39L_f$. These parameters are including the mean (μ), standard deviation (σ), median value (m), and coefficient of variation (δ). Figure

4-10 shows the variation of the mean and standard deviation of anchor capacity at pad-eye and mudline against the fluke length for MK6 anchor family in two different clay layer depth (d_c=1.07L_f and 1.39L_f).

Table 4-5. Statistical properties of anchor capacity at pad-eye and mudline

Model	L_f/d_f	L_f (m)	Padeye				Mudline				μ_{Ra}/μ_R
			μ_{Ra} (kN)	σ_{Ra} (kN)	δ_{Ra}	m_{Ra} (kN)	μ_R (kN)	σ_R (kN)	δ_R	m_R (kN)	
MK5	6.67	3.904	2672.6	309.87	0.115	2646.0	2847.2	331.26	0.1163	2809.0	0.93
MK5	6.67	4.149	3127.3	360.30	0.115	3080.0	3312.4	396.29	0.1196	3263.0	0.94
MK5	6.67	4.297	3472.0	426.97	0.122	3403.0	3674.4	446.85	0.1216	3600.0	0.94
MK5	6.67	4.436	3772.6	456.76	0.121	3709.5	3988.2	480.92	0.1205	3922.5	0.94
MK6	3.09	4.267	3082.5	360.77	0.117	3022.5	3294.6	376.08	0.1141	3218.5	0.93
MK6	3.09	4.534	3684.3	399.84	0.108	3624.0	3914.0	423.45	0.1081	3852.0	0.94
MK6	3.09	4.696	4106.2	493.49	0.120	4025.5	4356.9	522.16	0.1198	4275.0	0.94
MK6	3.09	4.848	4507.4	516.49	0.114	4426.0	4777.0	546.03	0.1143	4695.0	0.94

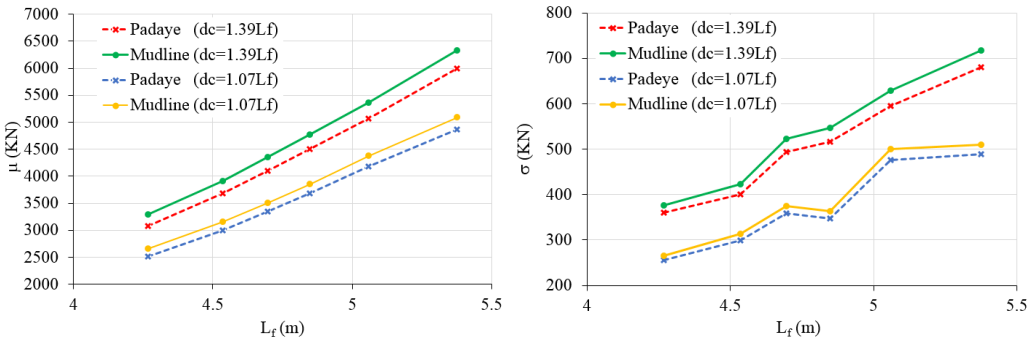

Figure 4-10. The mean and standard deviation of anchor capacity against fluke length for MK6

The results show that the mean capacity at pad-eye is 5% to 7% less than the mean capacity at mudline. Overall, in all MK5 and MK6 anchor models, the difference between capacity (median or mean) at the pad-eye and mudline rises by an increment of the fluke length and thickness. The coefficient of variation of capacity at mudline and pad-eye are about 11-12% for MK5 and 10-12% for MK6 anchor families, respectively.

4.5.3 Probabilistic Model of Line Tension

To develop the response surfaces, an approach proposed by Silva-González et al. (2013) was adopted. The dynamic line tensions were defined by using a Gaussian process (Choi, 2007; Sarkar and Eatock Taylor, 2000) by expressing its maximum magnitude during an extreme sea state using the model proposed by Davenport (1964). The extreme sea state (Θ) was represented by using a random vector of r uncertain environmental variables:

$$\mathrm{E}\left[T_{dyn,max}\right]_{\Theta} = \mu_{Tdyn,max} = \left[\sqrt{2\ln\left(\nu_{\Theta}\Delta t/2\right)} + \frac{0.5772}{\sqrt{2\ln\left(\nu_{\Theta}\Delta t/2\right)}}\right]\sigma_{T,\Theta} \qquad (4\text{-}14)$$

where, Δt is the duration of extreme sea state; $\sigma_{T,\Theta}$ (or $\sigma(\Theta)$) is the standard deviation; and ν_{Θ} (or $\nu(\Theta)$) is the mean crossing rate of the dynamic line tension. The predicted maximum dynamic line

tension at mudline ($T_{dyn,max}$) and the mean line tension (T_{mean}) were formulated using a second-order polynomial expansion in terms of Θ:

$$Y(\Theta) = c + a^T\Theta + \Theta^T b\Theta \quad (4\text{-}15)$$

where Θ and Y(Θ) are the r × 1 vector of environmental variables and the response of interest, respectively. Response analysis was adopted to determine the subsequent unknown coefficients c, a (r ×1), and b (r ×r). The response surfaces were developed by using seven critical environmental parameters obtained from the mooring system in the Flemish Pass Basin located in the East Newfoundland offshore region. A database comprised of 8100 different combinations of environmental variables was constructed by using of different environmental variables including significant wave height (H_s), the direction of wave (d_w), peak period (T_p), the velocity of wind (U_{10}), direction of wind (d_{ww}), speed of the surface current (U_c), and current direction relative to wave direction (d_{wc}). The mooring line going under the highest load was investigated to get the response surface. Figure 4-11 indicates the response surface of both maximum and mean expected line tension for domains of peak wave period and significant wave height.

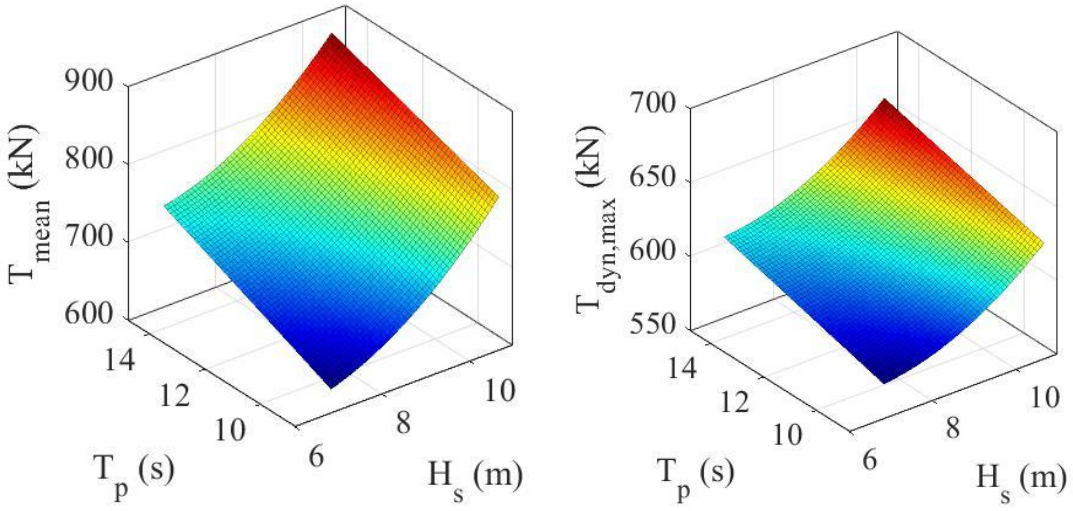

Figure 4-11. Response surfaces of Tmean and Tdyn, max

A storm event was used to identify the extreme sea states. A time window was defined around the peak period by using clustering and de-clustering (t_{peak} - $\Delta T_{cluster}$, t_{peak} - $\Delta T_{cluster}$). The extreme sea state occurs if a significant wave height is reached at t_{peak} which is higher than the threshold amount ($H_s \geq H_s^{th}$). The other environmental variables were determined based on the peak period (t_{peak}). The marginal probability distribution of Θ (or $[H_s, T_p, U_{10}]^T$) was generated by using the peaks over the threshold approach and a set of 24 extreme sea states within the hindcast time series. The amount of mean annual rate λ is 1.25, (30/24), per year according to the maximum probability estimate. Table 4-6 and Table 4-7 summarize the best fitted marginal distributions, the parameters related to maximum likelihood estimate, and correlation coefficients for main environmental variables.

Table 4-6. Distribution parameters of environmental variables

Variable	Probability distribution	Distribution parameters	
H_s	Weibull	Scale	9.5351
		Shape	10.1552
T_p	Lognormal	μ_{lnT_p}	2.4966
		σ_{lnT_p}	0.1196
U_{10}	Lognormal	$\mu_{lnU_{10}}$	3.4827
		$\sigma_{lnU_{10}}$	0.1095

Table 4-7. Estimated correlation coefficients

	H_s	T_p	U_{10}
H_s	1.0	0.9728	0.9905
T_p	0.9728	1.0	0.9935
U_{10}	0.9905	0.9935	1.0

4.5.4 Results of Reliability Analysis

Figure 4-12 illustrates the variation of annual reliability index versus fluke length (plot a) and dry anchor weight (plot b) in two different clay layer depth ($1.07L_f$, $1.39L_f$). Each point on plot A linked to an equivalent point on plot B and vice versa. For instance, in both plots of Figure 4-12, point 3 represents an MK6 anchor with a length of 4.696 m and a weight of 20 t in clay layer depth of $1.39L_f$ with an annual reliability index of 4.89.

(a)

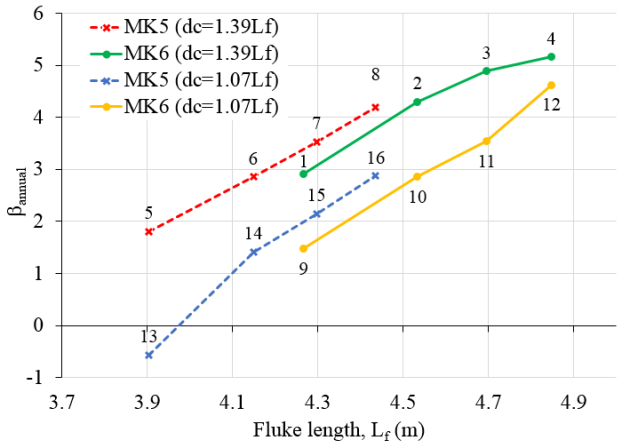

(b)

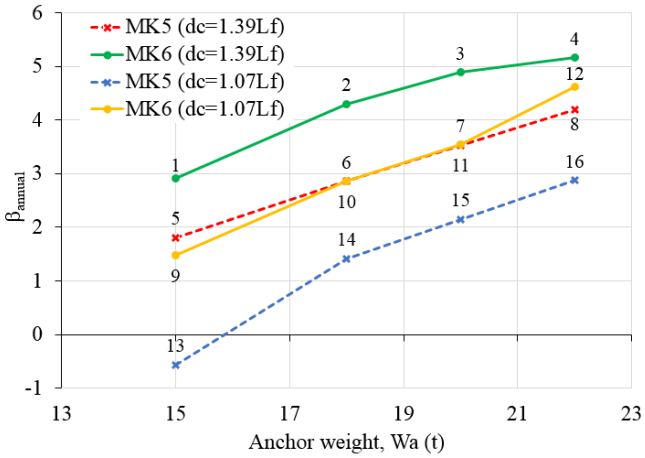

Figure 4-12. Annual reliability index versus (a) fluke length, and (b) anchor weight

As shown in Figure 4-12, at any clay depth, different anchor families with different weights and fluke lengths could be used to reach a specified reliability target. For instance, at a clay layer depth (d_c) of $1.39L_f$ for target reliability index of $\beta_{annual} = 3$, either MK5 with $L_f = 4.149$ m and $W_a = 18$ t (point 6) or MK6 with $L_f = 4.267$ m and $W_a = 15$ t (point 1) could be selected. These trends show

that same as homogeneous clay (Moharrami and Shiri, 2018), anchors with different weights, but identical fluke lengths produce very close reliability levels. For achieving target failure probabilities between 10^{-4} and 10^{-5} (with $d_c=1.39L_f$), the existing weight and fluke length for MK5 is 22 t and 4.436 m and for MK6 is 18 t and 4.534 m. The mentioned target failure probabilities are generally used as the ultimate limit state design in offshore systems (DNV-OS-E-301 2010; DNV-OS-F201, 2010; DNVGL-ST-F101, 2019). Also, at a given clay layer depth, two different anchor families with the same weight and different fluke length result in different annual reliability indices. For a weight of 15 t (with $d_c=1.39L_f$) by changing fluke length from 3.904 m (point 5) in MK5 to 4.267 m (point 1) in MK6, the annual reliability index increases from 1.80 to 2.91 which corresponds to a reduction of annual failure probability by one order of magnitude from 0.0355 to 0.0018. Similar to homogeneous clay condition (Moharrami and Shiri, 2018), the capacity of deeply embedded anchors in layered soil (clay over sand) is significantly affected by fluke length, while the anchor weight is not a significant factor. In each anchor family, the annual reliability index increases when the clay layer depth increases. For instance, the annual reliability index of an MK5 anchor with a fluke length of 4.297 m increases from 2.15 to 3.532 when clay layer depth (d_c) increases from $1.07L_f$ to $1.39L_f$.

The logarithmic variation of failure probability (log (P_{Fa})) against anchor weight and fluke length with their linear curve fit in two different clay layer depth (d_c) for MK5 and MK6 anchor families are shown in Figure 4-13.

(a)

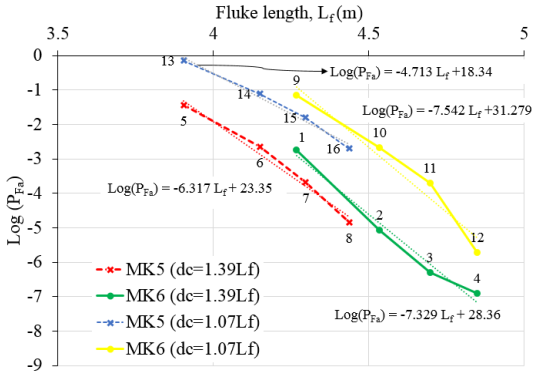

(b)

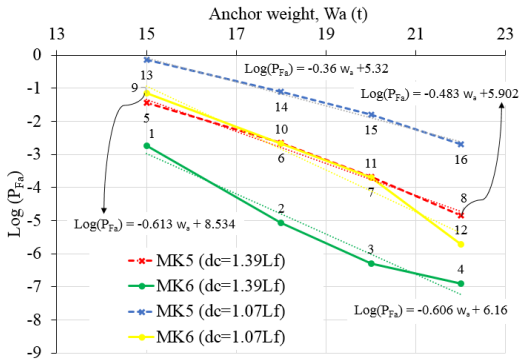

Figure 4-13. The logarithm of failure probability versus (a) fluke length, and (b) anchor weight

The required increment of anchor fluke length and weight to decrease the annual failure probability for one order of magnitude (by a factor of 10) could be achieved by finding the slope of each curve. These outcomes are useful in the life cycle cost-benefit analysis, where finding the initial cost model as a function of the failure probability is required. By increasing the weight and fluke length of the anchor, which are associated with the mass and volume of the anchor, the initial cost and failure probability will increase and decrease respectively. Figure 4-13 shows that in each clay layer depth (d_c=1.07L_f and d_c=1.39L_f) the slope of the MK6 anchor family is higher than the MK5 family. Therefore, a small deviation in fluke weight and fluke length causes considerable variation in failure probability and reliability index. The required increasing rate of the fluke length and the

anchor weight for MK5 are 0.212, 2.777 for $d_c=1.07L_f$, and 0.158, 2.070 for $d_c=1.39L_f$. In the case of MK6, the magnitude of these parameters are 0.132 and 1.631 for $d_c=1.07L_f$, and 0.136 and 1.650 for $d_c=1.39L_f$. Therefore, to increase the annual reliability index from 2.85 to 3.53 in MK5, an increment of 4% and 12% for $d_c=1.39L_f$, and 5% and 13% for $d_c=1.07L_f$ in fluke length and anchor weight are required. In the case of MK6, a corresponding increment of 3% and 11% for $d_c=1.39L_f$, and 3% and 9% for $d_c=1.07L_f$ are needed.

4.5.5 Comparison Between the Reliability of Anchors in Homogenous and Layered Soils

The results of reliability assessment in layered soil (clay over sand) were compared with the earlier reliability investigation in the homogenous soil; clay (Moharrami and Shiri, 2018) and sand (Aslkhalili et al., 2019). This was facilitated by selecting the same properties of homogenous clay and sand layers from the aforementioned studies to define the soil layers in layered stratum (clay over sand). Figure 4-14 shows the variation of annular reliability index versus anchor weight in sand, clay, and, clay over sand for MK5 and MK6, with clay layer depths of $1.07L_f$ and $1.39L_f$.

(a)

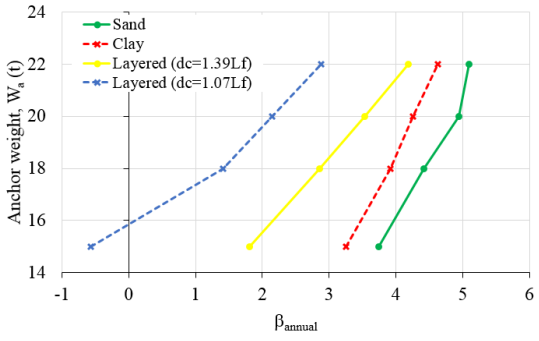

(b)

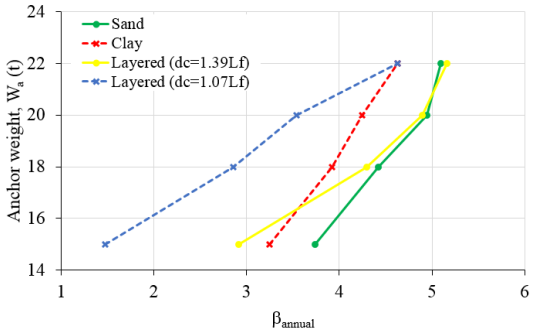

Figure 4-14. Annular reliability index versus anchor weight (a) MK5, (b) MK6

In MK5 anchor family (Figure 4-14(a)), the homogenous seabed produces reliability indices higher than layered soils by different anchor weights. However, in the MK6 anchor family (Figure 4-14(b)), the reliability indices in layered soil strata are higher in some weights. In both MK5 and MK6 anchor families, reliability indices related to the layered seabed have higher dispersion compared to the homogenous soils. For instance, in MK5 the reliability index of clay over sand with $d_c=1.39L_f$ varies from 1.8 to 4.18, but the variation range in the sand (in MK5) is from 3.73 to 5.09.

4.6 Conclusion

The reliability of drag embedment anchors supporting the catenary mooring systems in the layered seabed condition (clay over sand) was investigated by using the first order reliability method (FORM). Stevpris MK5 and MK6 anchors that are widely used in temporary and permanent applications were selected for reliability analysis. The limit state function was formulated at the mudline, and the frictional capacity of chain-soil interaction was accounted for calculation of ultimate holding capacity. Dynamic mooring analysis was conducted by assuming a generic semisubmersible platform in the Flemish Pass Basin, Newfoundland offshore, to obtain the dynamic mooring line tensions. The response surface method was employed for probabilistic

modeling of the line tensions at the mudline. The ultimate holding capacity and the anchor trajectory were calculated by developing an Excel spreadsheet integrated with VBA macros for iterative analysis. The annual reliability indices and failure probabilities in layers soil strata were obtained and compared with earlier studies in homogenous clay and sand layers. The primary outcomes of the study are summarized as follow:

- The seabed soil stratum and its configuration (individual layer thickness) have a significant influence on reliability indices. Overall, the probability of failure is higher for the layered clay over sand stratum compared with homogeneous clay and sand layers. This suggests that the recommended practices that are currently considering only homogeneous soil should be re-assessed and possibly improved for complex, layered seabed soil strata.
- The geometrical anchor configuration, particularly the fluke length, was found to have a significant effect on holding capacity and consequently the reliability indices. The anchor weight showed a positive influence on reliability results, but less effective than the fluke length. The geometrical improvement of the anchors can effectively improve their reliability. In addition, the current design practice is identical for all of the different anchor families. This approach does not account for the significant influence of anchor geometry and the uncertainties associated with different anchor families, environmental, and operational loads. The reliability-based refinement of the design procedure can considerably improve the reliability and cost-effectiveness of anchor design.
- The configuration of layered soil strata, particularly the depth and thickness of layers showed a significant effect on ultimate holding capacity and reliability indices. Thicker clay layers resulted in higher reliability indices. Different range of layer thickness still needs to be investigated to generalize the obtained results.

Although the analytical and numerical solutions are quite beneficial to assess the parameters affecting the reliability of drag embedment anchors. However, the reliability assessment of anchors can be significantly improved by having access to in-field test databases, related seabed properties, and, statistical data of failures. The current study was limited to specific anchor families performing in clay over sand seabed strata with two instances of layer thickness. Further investigations are necessary for different layer configurations such as sand over clay, sand over sand, and clay over the clay; and also different anchor families.

Acknowledgments

The authors gratefully acknowledge the financial support of this research by the Memorial University of Newfoundland through VP start-up fund and school of graduate studies (SGS). The technical advice of Mr. Mohammad Javad Moharrami and Mr. Rahim Shoughi is also kindly acknowledged.

References

Aslkhalili, A., Shiri, H., Zendehboudi, S., 2019. Reliability assessment of drag embedment anchors in sand and the effect of idealized anchor geometry. Saf. Extrem. Environ. 1, 39–57. https://doi.org/10.1007/s42797-019-00006-5

Choi, Y.J., 2007. Reliability Assessment of Foundations for Offshore Mooring Systems under Extreme Environments.

Clukey, E.C., Gilbert, R.B., Andersen, K.H., Dahlberg, R., 2013. Reliability of Suction Caissons for Deep Water Floating Facilities 1991, 456–474. https://doi.org/10.1061/9780784412763.035

Davenport, A.G., 1964. Note on the Distribution of the Largest Value of a Random Function With Application To Gust Loading. Proc. Inst. Civ. Eng. 28, 187–196. https://doi.org/10.1680/iicep.1964.10112

DNV-OS-E-301, 2010. Position Mooring. Offshore Standard.

DNV-OS-F201, 2010. Dynamic Risers. Offshore Standard.

DNV-RP-E301, 2012. Design and Installation of Fluke Anchors.

DNVGL-ST-F101, 2019. Submarine Pipeline Systems. Offshore standartd.

Duggal, A., Ma, K., Shu, H., Smedley, P., L'Hostis, D., 2013. A Historical Review on Integrity Issues of Permanent Mooring Systems 3. https://doi.org/10.4043/24025-ms

Dunnavant, T.W., Kwan, C.-T.T., 1993. Centrifuge Modelling And Parametric Analyses Of Drag Anchor Behavior, in: Offshore Technology Conference. https://doi.org/10.4043/7202-ms

Moharrami, M.J., Shiri, H., 2018. Reliability assessment of drag embedment anchors in clay for

catenary mooring systems. Mar. Struct. 58, 342–360. https://doi.org/10.1016/j.marstruc.2017.12.005

Montes-Iturrizaga, R., Heredia-Zavoni, E., 2016. Reliability analysis of mooring lines using copulas to model statistical dependence of environmental variables. Appl. Ocean Res. 59, 564–576. https://doi.org/10.1016/j.apor.2016.07.008

Neubecker, S.R., 1995. The behaviour of drag anchor and chain systems, PhD Thesis, Department of Civil Engineering, The University of Western Australia.

Neubecker, S.R., Randolph, M.F., 1996a. The performance of drag anchor and chain systems in cohesive soil. Georesources Geotech. 14, 1–7.

Neubecker, S.R., Randolph, M.F., 1996b. The kinematic behaviour of drag anchors in sand. Can. Geotech. J. 33, 584–594. https://doi.org/https://doi.org/10.1139/t96-084-306

Neubecker, S.R., Randolph, M.F., 1996c. The static equilibrium of drag anchors in sand. Can. Geotech. J. 33, 574–583.

Neubecker, S.R., Randolph, M.F., 1995a. Profile and frictional capacity of embedded anchor chains. Geotech. Eng. 121, 797–803.

Neubecker, S.R., Randolph, M.F., 1995b. Performance of Embedded Anchor Chains and Consequences for Anchor Design. https://doi.org/10.4043/7712-ms

O'Neill, M.P., 2000. The behaviour of drag anchors in layered soils, PhD Thesis, Department of Civil Engineering, The University of Western Australia.

O'Neill, M.P., Bransby, M.F., Randolph, M.F., 2003. Drag anchor fluke–soil interaction in clays. Can. Geotech. J. 40, 78–94. https://doi.org/10.1139/t02-096

O'Neill, M.P., Randolph, M.F., House, A.R., 1997. A preliminary assessment of the behaviour of drag anchors in layered soils 9.

Phoon, K.K., 1999. Characterization of geotechnical variability. Can. Geotech. J. 624, 612–624.

Rendón-Conde, C., Heredia-Zavoni, E., 2016. Reliability analysis of suction caissons for moored structures under parameter uncertainties. Struct. Saf. 60, 102–116. https://doi.org/10.1016/j.strusafe.2016.02.004

Sarkar, A., Eatock Taylor, R., 2000. Effects of mooring line drag damping on response statistics of vessels excited by first- and second-order wave forces. Ocean Eng. 27, 667–686. https://doi.org/10.1016/S0029-8018(99)00014-1

Silva-González, F., Heredia-Zavoni, E., Valle-Molina, C., Sánchez-Moreno, J., Gilbert, R.B., 2013. Reliabilitystudy of suction caissons for catenary and taut-leg mooring systems. Struct. Saf. 45, 59–70. https://doi.org/10.1016/j.strusafe.2013.08.011

Valle-molina, C., Heredia-zavoni, E., Silva-gonzález, F.L., 2008. Reliability analyses of suction caissons for FPSO systems, in: International Conference on Offshore Mechanics and Arctic Engineering. pp. 1–6.

Vryhof Anchors, 2010. Anchor manual. Krimpen ad Yssel, The Netherlands.

Chapter 5. Probabilistic Assessment of Lateral Pipeline-Backfill-Trench Interaction

Amin Aslkhalili[1], Hodjat Shiri [1], Sohrab Zendehboudi[2]

1. Civil Engineering Dept., Faculty of Engineering and Applied Science, Memorial University of Newfoundland, A1B 3X5, St. John's, NL, Canada.

2. Process Engineering Dept., Faculty of Engineering and Applied Science, Memorial University of Newfoundland, A1B 3X5, St. John's, NL, Canada.

This chapter is currently under review as a journal manuscript

Abstract

In seismic regions, the buried pipelines may be at risk of fault displacement that applies massive lateral pipe movements and jeopardizes the mechanical integrity of the buried pipes. Trenching and the burial of pipelines is a common practice for physical protection. The lower stiffness of the remoulded backfilling material relative to the native ground has a significant impact on lateral soil resistance against large pipeline displacements that is rarely considered in the current design practice. Finding a safe, reliable, and cost-effective trench configuration is a key aspect of design practice that is affected by pipeline-backfill-trench interaction. In this analysis, a probabilistic approach was employed to investigate the trenching/backfilling effect on the response of the buried pipelines to large lateral displacements. A three-dimensional beam-spring model subjected to a strike-slip fault was developed and the effect of trenching/backfilling was incorporated by using non-linear springs. Two limit state criteria were set to identify the safe and failure regions. A Python code was developed to perform iterative analysis by variation of pipe specifications, native and backfill soil properties, trench width, trench depth, and lateral displacements. The first order reliability method (FORM) was used to estimate the exceedance probability of failure by using the identified limit states. The study showed that the trenching/backfilling of the pipeline results in lower lateral soil resistance against the displaced pipe. Also, it was observed that the advantage of load reduction could be used for mitigation of trench dimensions and reduction of the construction costs without jeopardizing the safety and integrity requirements.

5.1 Introduction

Onshore and offshore buried pipelines have been widely used for the transportation of hydrocarbons. Buried pipelines may be endangered due to different hazards sources like landslides, ice gouging, slope slides, seismic activity, frost heave, thaw settlement of permafrost, or a variety of other sources. The engineering design of buried pipelines should account for the mentioned sources of hazards, which results in significant technical challenges and uncertainty. These hazards induce pipeline-backfill-trench interaction that affects the lateral response of the buried pipeline to large displacements. Pipelines are usually buried by trenching and backfilling for physical protection against the environmental and operational loads. Pre-excavated soils are commonly used as a cost-effective backfilling material to bury the pipeline inside the trench. The lower stiffness of the remoulded backfilling material relative to the native ground has a significant impact on failure mechanisms and the lateral soil resistance against large pipeline displacements (see Figure 5-1).

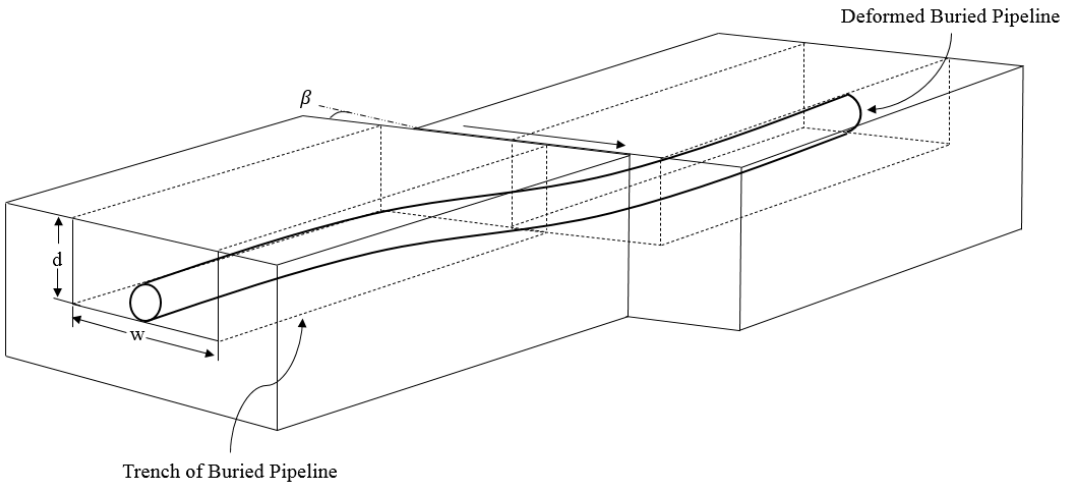

Figure 5-1. Schematic illustration of the trenched buried pipeline subjected to a strike-slip fault

The trenching/backfilling effect is rarely considered in the current design codes (e.g., DNVGL-RP-F114, 2017; PRCI, 2009; ALA, 2005; ASCE committee, 2014). The solutions that has been proposed based on various earlier studies on lateral pipe-soil interaction (Tschebotarioff, 1973; Wantland et al., 1979; Paulin, 1998) or anchor soil interactions (Hansen, 1948, Hansen and Christensen, 1961; Smith, 1962; Ovesen, 1964; Kostyukov, 1963; Ovesen and Stroman, 1972; Neely et al., 1973; Das and Seeley, 1975; Rowe and Davis, 1982; Merifield et al., 2001). However, the number of studies considering the pipeline-backfill-trench interaction effect on lateral pipe response is quite limited (Paulin, 1998; C-CORE, 2003, 2004, 2005; Phillips et al., 2004; Kianian et al., 2018; Kianian and Shiri, 2019; Kianian and Shiri, 2020).

Considering a broad range of uncertainties affecting the pipeline response to large lateral displacments, probabilistic design methods have been recently recommended by design codes (e.g., DNVGL-ST-F101, 2019) as a reasonable and alternate design approach. There are a few studies in the literature that has used probabilistic approaches to investigate this challenging area of engineering (e.g., Nobahar et al., 2007; Cheng and Akkar, 2017). However, neither of these studies have accounted for the uncertainties arising from the trenching/backfilling effects.

In this study, a probabilistic approach was utilized to study the mechanical integrity of buried pipelines exposed to massive lateral soil displacement due to seismic fault movement in clay with the incorporation of the trenching/backfilling effects. A 3D beam/spring finite element model was developed in ABAQUS and the effect of trenching/backfilling was incorporated by non-linear later spring extracted from the published centrifuge model tests (i.e., Paulin, 1998). Two different pipeline failure envelopes were considered based on serviceability and ultimate limit state design to identify failure zones and calculate failure probabilities. A Python code was developed for iterative computations and performing the probabilistic assessment of the pipeline mechanical

integrity using the FORM. Different trench geometries, fault displacement, and pipe geometrical properties were examined to obtain the annual failure probability and the corresponding trench configurations. It should be mentioned that the angle of the pipe-fault intersection (β) assumed to be zero as it causes the maximum stress-strain states throughout the pipeline and considers as the worth case scenario.

5.2 Finite Element Model

The pipeline-soil interaction can be model by continuum and beam-spring models. Each approach has its pros and cons. The continuum models produce more accurate results using high computational resources. The beam-spring approach is more cost-effective and fairly accurate which is more used in daily engineering practice. However, the beam-spring analysis decoupled the soil interaction in three directions and does not account for some of the complex soil behaviors such as dilatancy, stress path dependency, and rate effects. Depending on the objectives, either of these approaches can be selected to produce the desired outputs.

In the current study, since the probabilistic analysis requires a large number of FE model runs, the beam-spring approach was adapted for a cost-effective analysis with acceptable level of accuracies.

A three-dimensional beam-spring finite element model was developed in ABAQUS to model the pipeline-backfill-trench interaction in the probabilistic analysis using three-node quadratic PIPE32 elements. Each node of the pipeline element has six degrees of freedom (three displacements and three rotations), and quadratic shape function was used to define pipe elements. Additionally, other variables represent average hoop stress regarding the thin-wall pipeline theory. A total length of 1000 m, 762 mm pipeline was modeled with assuming a 100 m fault zone in the center (50 m on

both sides of the fault crossing). The length of the pipe was selected long enough to prevent the boundary effects of the pipe ends, as suggested by earlier studies (Takada et al., 2001; Karamitros et al., 2007).

Using mesh sensitivity analysis, the mesh size was selected to be 10 m throughout the pipe, and 1 m in the fault zone. The stress-strain constitutive relationship of the pipeline was identified by isotropic, elastoplastic behavior with a von Mises yield surface, and isotropic hardening rule. The stress-strain formulation proposed by Ramberg-Osgood was employed to define the stress-strain relationship (Walker and Williams, 1995).

5.2.1 Pipe-Soil Model

Two-node nonlinear SPRINGA elements with hyperbolic responses were used in three directions to model the elastoplastic soil interactions in axial, transverse horizontal, and transverse vertical directions (see Figure 5-2).

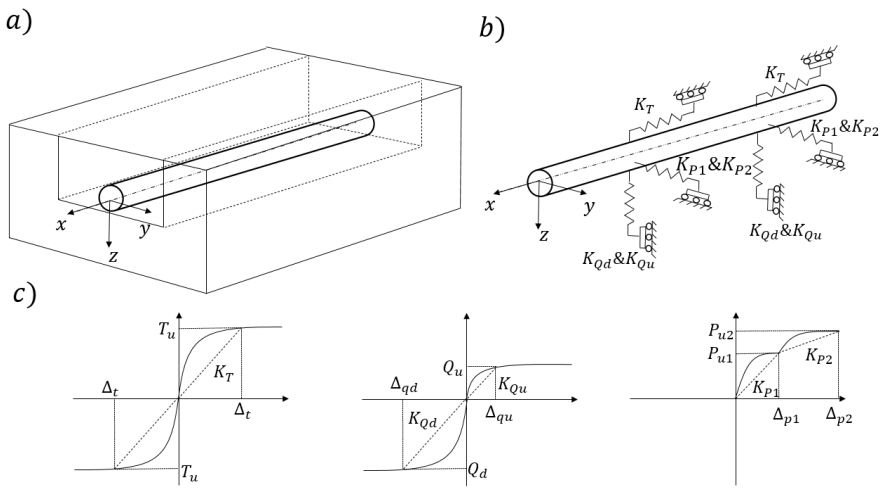

Figure 5-2. Trenched buried pipe-soil interaction in a) continuum analysis, b) idealized structural model, and c) soil load-displacement response curves in three directions

The induced seismic ground movements were applied as displacement boundary conditions to the base of the soil spring elements. This simplified model is obtained from the subgrade reaction concept initially proposed by Winkler (1867). In the beam-spring model, the soil resistance function in each direction (axial t-x, transverse horizontal p- y, and transverse vertical q- z) defines the analytical expression which relates the maximum clay soil spring forces and corresponding displacements. These resistance functions implicitly integrate the geomechanically and geometrical properties of the pipeline-backfill trench interaction into the model.

A few lateral response of the trenched/backfilled pipelines in clay has been proposed in the literature based on theoretical, numerical, and experimental studies (e.g., Paulin, 1998; C-CORE, 2003; Phillips et al., 2004; Kianian and Shiri, 2019; ASCE, 2005; PRCI, 2009). In the current study, the pipeline-soil interaction model recommended by PRCI (2009) guideline was incorporated.

5.2.2 Pipe Properties

The API 5L X65 grade material was chosen for the pipe. Three different nominal outside pipeline diameter to wall thickness ratios (D/t) were studied to represent the D/t range that may be employed in offshore pipeline designs (API, 2018). The pipeline parameters are presented in Table 5-1.

Table 5-1. Pipeline properties for the current analysis

Parameter	Value
Nominal outside diameter	762 mm (30.0 in.)
Nominal wall thicknesses	15.9 mm (0.625 in.)
	22.2 mm (0.875 in.)
	32 mm (1.25 in.)
Pipeline diameter to wall thickness ratios	48
	34
	24
Material grade	API 5L X65
Internal pressure	15 MPa
Pipe length	1 km

The internal pressure of the pipe was set to provide a hoop stress of 35-70% of the yield stress based on earlier studies (Nobahar et al., 2007).

5.3 Probabilistic Model

To perform a probabilistic analysis, a set of uncertain parameters involved in the problem is represented by $X = \{X_1, X_2, \dots, X_n\}$, where $X_1, X_2, \dots, X_n$ and $f(X)$ are the probability density function for each parameter and the joint probability function of X, respectively. The performance function $G(X)$ of the system can be expressed as a function of loading $R(X)$ and capacity $S(X)$ as follows:

$$G = R(X) - S(X) \tag{5-1}$$

The probability of failure corresponding to the performance criteria can be defined as follows, where $G(X) < 0$ declares a failure state ($S(X) > R(X)$):

$$P_F = Prob[G(X) < 0] = \int_{G(X)\leq 0} f(X)\, \mathrm{dX} \tag{5-2}$$

In a real engineering problem, this integral could be too complicated to solve. Therefore, different approximation methods are developed to resolve this issue, such as the first-order reliability

method (FORM), the second-order reliability method (SORM), etc. Moreover, there are other solutions like sampling methods (Monte Carlo) that are required a large number of samples to reach a reasonable answer, which is not computationally efficient on some occasions.

In this study, the maximum von Mises stress and compressive strain obtained from the FE analysis were used to generate the loading of the system $R(X)$ to satisfy two different levels of safety: i) serviceability and ii) ultimate state design. According to two different safety levels, two limit state criteria based on von Mises stress and compressive strain were used to define the capacity of the system, $S(X)$. The probability of failure during a fault event was identified using the following set of equations:

$$P_F = Prob[\text{Max von Mises(X)}>\text{von Mises limit state}] \rightarrow \text{serviceability design} \quad (5\text{-}3)$$

$$P_F = Prob[\text{Max Compressive strain(X)}>\text{Compressive strain limit}] \rightarrow \text{ultimate design} \quad (5\text{-}4)$$

The annual probability of failure P_{Fa} relates to the probability of failure P_F using a Poisson model for the occurrence of the active fault along the pipeline:

$$P_{Fa} = 1 - \exp(-\lambda P_F) \quad (5\text{-}5)$$

where λ is the occurrence rate of active faults, and P_{Fa} approximately equals to λP_F for small amounts of λP_F.

The annual target safety levels for serviceability, ultimate limit state, and active fault occurrence rate were selected as 10^{-3}, $10^{-4,}$ and 10^{-2} based on the DNVGL-ST-F101 (2019) recommendation.

The RT software (Mahsuli and Haukaas, 2013) was used in the first-order reliability method (FORM) analysis to obtain probabilistic results.

5.3.1 Limit State Criteria

A buried pipeline subjected to strike-slip fault undergoes structural loads such as bending and axial compressive force that may threaten the mechanical integrity of the pipeline. The application of strain-based design scenarios in these circumstances is required to obtain a feasible and cost-effective design. The load effects on the mechanical integrity of the pipe are assessed by defining limit state criteria and identification of deformation-based failure and safe envelopes. Serviceability, ultimate, fatigue, and accidental loads limit states can be considered to assess the pipeline integrity. In the current study that investigates the trenching/backfilling effect on mechanical integrity, serviceability and ultimate states were set as of the limit state criteria. The serviceability limit state-controlled the yielding and ovalization, while the ultimate limit state monitored the local buckling, collapse, and tensile fracture.

To ensure the normal operation of the pipeline according to the serviceability limit state, a von Mises stress criterion was used to limit the design stress to 90% of the specified minimum yield stress (SMYS) (Nobahar et al., 2007). Different compressive strain limits for the serviceability criterion have been proposed by design codes (BS 8010, 1993; CSA Z662, 2003; DNVGL-ST-F101, 2019). A comparison of these limit state functions concerning local buckling of pipelines was presented by Kenny et al. (2004). In this study, the recommendation provided by DNVGL-ST-F101 (2019) was used to set a compression strain limit and secure the pipe pressure integrity for local buckling. The recommended limit state criteria for local buckling caused by displacement-controlled events in the internal overpressure pipeline can be written as follows (DNVGL-ST-F101, 2019):

$$\varepsilon_d < \frac{\varepsilon_c}{\gamma_\varepsilon} \tag{5-6}$$

where ε_d is design compression strain, γ_ε is resistance strain factor equals to 2.6 (Normal safety class) and ε_c is compression strain.

$$\varepsilon_c = 0.78\left(\frac{t}{D} - 0.01\right)\left(1 + 5\frac{\sigma_h}{f_y}\right)\frac{\alpha_{gw}}{\alpha_h^{1.5}} \tag{5-7}$$

where $t, D, \sigma_h, f_y, \alpha_{gw}$, and α_h are the wall thickness; diameter; hoop stress; steel yield stress; girth weld factor, $\min(1, 1.2 - 0.01(D/t))$; and strain hardening parameter, respectively. The compression strain limit has different uncertainties, which will be further discussed in the pipeline probabilistic fragility section.

5.3.2 Probabilistic Characterization of Seismic Hazard

Using seismic hazard curves, the fault induced ground displacement is usually defined as a function of the related frequency of occurrence. However, to overcome the shortage of seismic hazard fault data, the equation proposed by Wells and Coppersmith (1994) was used to determine the fault displacement that is varied between 0.05 to 8 m for strike-slip faults:

$$\log \delta_{fs} = -6.32 + 0.9M \tag{5-8}$$

where δ_{fs}, M are average fault displacement and the moment magnitude of the earthquake. The fault displacements of $1D$, $2D$, $4D$, and $6D$ (D is the diameter of the buried pipe) were selected to cover the possible fault displacement in the proposed range.

5.3.3 Probabilistic Fragility of the Pipeline

The uncertainties of the pipeline resistance are usually characterized by the fragility curves in the form of cumulative probabilistic distributions. Other practical methods could be employed to create fragility curves in case of a lack of experimental or field data. The first solution is to use a

two-parameter lognormal distribution for the resistance, where the distribution can be defined by mean and coefficient of variation. Mohr et al. (2004) performed a strain-based design review using a complete data set for buckling strain on the pipeline. The results revealed that equation 5-7 almost indicates the average of the data but creating a probability distribution of compressive strain capacity for different D/t ratio and internal pressure ranges require more available experimental data. Some of the factors causing uncertainty in the experimental data are: the different test conditions and experimental methods; different curvature and strain measurement on global and local scale; and axial load application to refute end cap effects caused by internal pressure during displacement controlled procedures (Nobahar et al., 2007). The second method is representing the resistance by a simplified deterministic approach, such as using a factored resistance. Some of the basis for developing equation 5-7 was reviewed by Vitali et al. (1999) using finite element assessment, and the results were compared with other available formulations and data. The study showed that the fitted equation has an error of mean and coefficient of variation of about 0.9 and 20%, respectively. This error only involves uncertainty related to the regression equation and does not incorporate other sources of ambiguities. Becker (1996) performed a series of calculations and indicated that by using a resistance strain factor (γ_ε) equal to 2.6 (DNVGL-ST-F101, 2019), the coefficient of variation expected to be 35%.

Based on these investigations, there are two possible approaches to characterize the strain limits: i)using a logarithmic distribution with mean value defined by equation 5-7 and coefficient of variation of 35%, ii)using factored compression strain limit defined by equation 5-6. Table 5-2 represents the key parameters of both methods.

Table 5-2. Strain limits characterization

	Logarithmic distribution of strain limit		Factored compression strain limit
D/t	Mean (%)	COV (%)	$\varepsilon_c/\gamma_\varepsilon$ (%)
48	3.12	35	1.20
35	5.07	35	1.95
24	7.37	35	2.83

In the current study, the factored compression strain limit with the parameter values given in Table 5-2 was utilized to characterize the strain limits.

5.3.4 Probabilistic Characterization of Soil and Trench

The uncertain parameters related to native, and backfill soil along with the trench geometry was characterized by undrained shear strength of backfill (C_{ub}), undrained shear strength of native (C_{un}), soil density (γ), trench width (w), and trench depth (d) to construct the database.

The uncertainties regarding systematic test variations and spatial alteration of soil properties were incorporated by using the lognormal distribution for defining undrained shear strength of backfill (C_{ub}), undrained shear strength of native (C_{un}), and soil density (γ). The mean and coefficient of variation were respectively set to 3.06 kPa ($\mu_{C_{ub}}$), 2.541 kPa ($\delta_{C_{ub}}$) for undrained shear strength of backfill (C_{ub}); 31.72 kPa ($\mu_{C_{un}}$) and 0.98 kPa ($\delta_{C_{un}}$) for undrained shear strength of native (C_{un}); and 17.5 kN/m^3 (μ_γ) and 0.09 kN/m^3 (δ_γ) for soil density (γ) (Ching and Phoon, 2012).

The variation of trench geometry (trench width and depth) were addressed by defining distinct quantities based on the study conducted by Paulin (1998). For studying trench geometry, two groups of analyses were conducted with constant trench depth (varying trench width) and constant trench width (varying trench depth). The trench dimensions for both groups of studies are summarized in Table 5-3.

Table 5-3. The variation of trench geometry (depth and width)

Groups	Trench width	Trench depth
Group 1 (constant trench depth & varying trench widths)	1.57 D	1.84 D
	2.10 D	
	2.63 D	
	3.15 D	
Group 2 (constant trench width & varying trench depths)	2.63 D	1.26 D
		1.84 D
		2.42 D
		3.00 D

To have a better understanding of trench effects, the pipeline without trench in different depth (same as a trenched condition) were also considered in this study.

5.3.5 Iterative Procedure

A Python code was developed to conduct iterative FE simulations in ABAQUS and construct the loading database (von Mises and compressive strain). In each iteration different values of C_{ub}, C_{un}, and γ were set for each group of trench geometry (width and depth) under various fault movements to obtain the maximum von Mises and compressive strain of the pipeline. During the FE analysis, the active fault was modeled by applying lateral displacements to the half of the spring elements on the pipeline, while the other half had no movements. The probabilistic analysis was performed by using the first-order reliability method (FORM). Figure 5-3 illustrates the procedure employed to obtain the probability of failure based on the defined serviceability and ultimate limit state criteria.

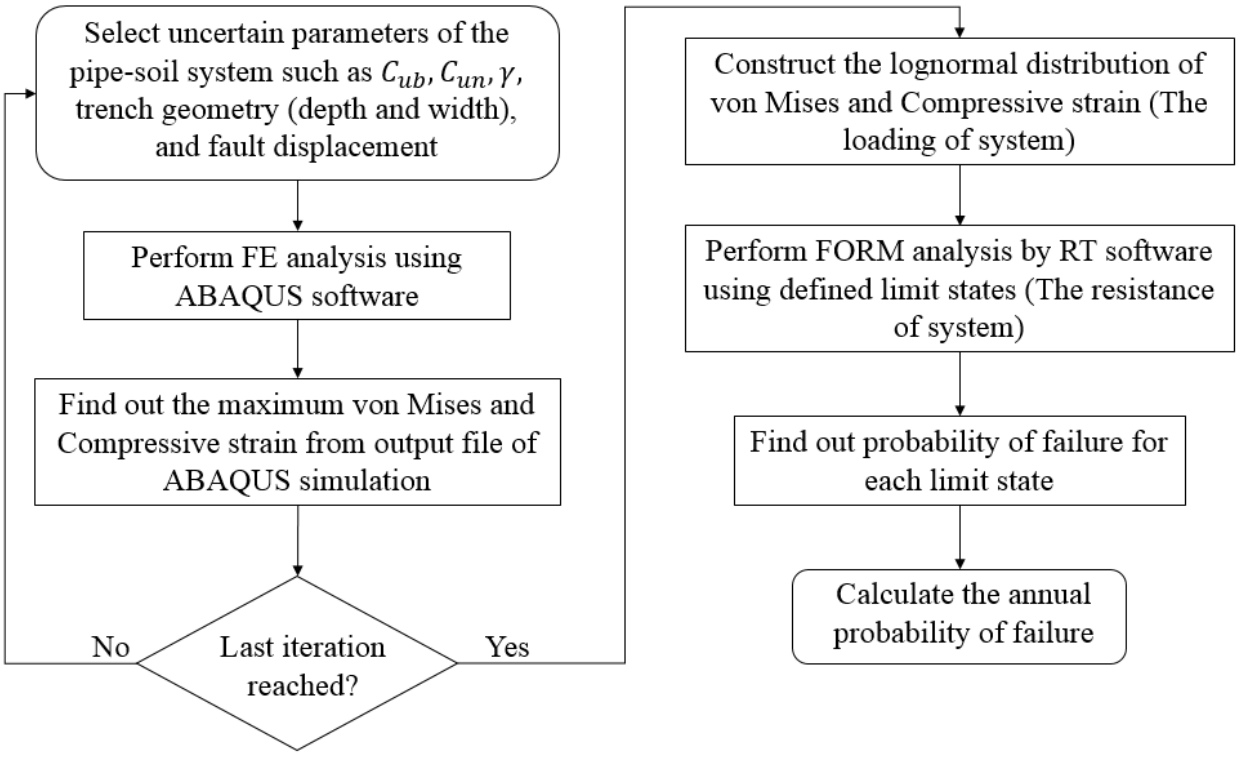

Figure 5-3. Flow chart of probabilistic analysis

Samples of fitted von Mises stress and compressive strain distributions and histograms are shown in Figure 5-4 where the trenched/backfilled pipeline (wall thickness of 15.9 mm) has a 2D lateral displacement, a trench width of 2.63D, and a trench depth of 1.26D. The Pipeline without a trench (wall thickness of 22.2 mm) has a 4D lateral displacement and a pipe burial depth of 3D.

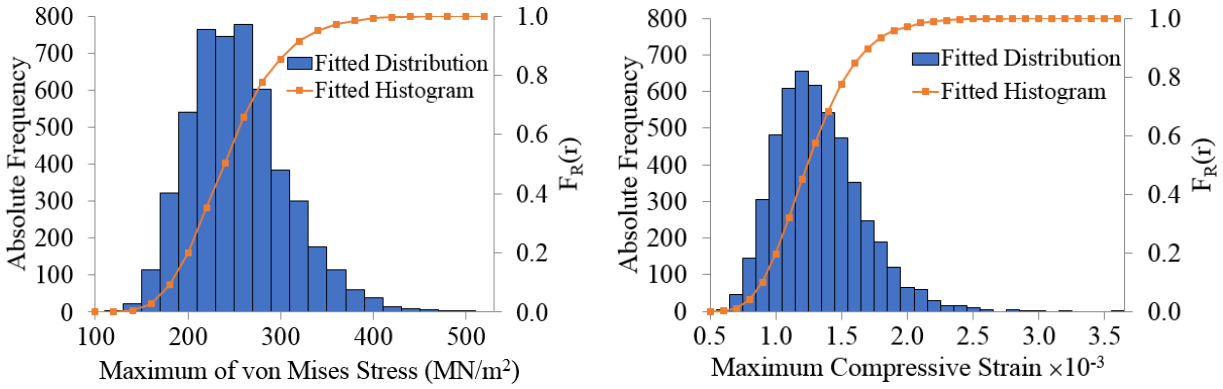

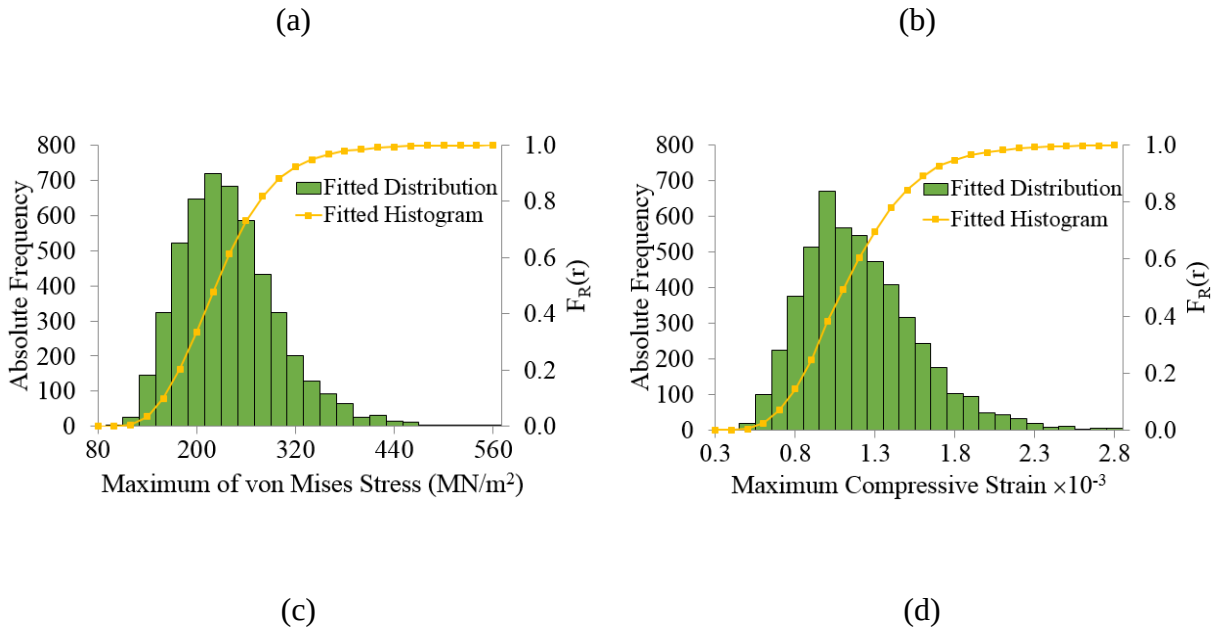

Figure 5-4. The fitted distribution and histogram of maximum von Mises stress and compressive strain for the trenched (a, b) and no trench pipe (c, d)

The statistical properties (mean, standard deviation, and coefficient of variation) of maximum compressive strain and maximum von Mises stress of pipeline with trench configurations, different pipe thickness, and lateral displacements are presented in Table 5-4. Means and standard deviations increase by an increment of lateral displacement in each group of pipe thickness. For a constant lateral displacement, the mean and standard deviation of both strain and stress increase as the pipe wall thickness increases.

Table 5-4. Statistical properties (mean, μ; standard deviation, σ; coefficient of variation, δ) of Maximum compressive strain for trench geometry of (width = 2.631D, depth = 3D) and Maximum von Mises stress for trench geometry of (width = 3.158D, depth = 1.842D)

D/t	Lateral Dis. (D)	Max compressive strain			Max von Mises stress		
		μ	σ	δ	μ (MN)	σ (MN)	δ
48	1	9.68E-04	2.25E-04	0.23	175.93	37.62	0.21
	2	1.75E-03	5.07E-04	0.28	273.34	54.04	0.20
	4	3.60E-03	1.43E-03	0.39	398.15	65.19	0.16
	6	5.70E-03	2.50E-03	0.43	473.37	68.18	0.14
	1	8.18E-04	1.86E-04	0.22	149.87	32.57	0.21
	2	1.44E-03	3.85E-04	0.26	236.16	49.60	0.21

34	4	2.78E-03	1.02E-03	0.36	353.96	63.37	0.18
	6	4.27E-03	1.81E-03	0.42	427.28	67.82	0.16
24	1	6.82E-04	1.54E-04	0.22	125.52	27.64	0.22
	2	1.18E-03	2.97E-04	0.25	199.71	43.95	0.22
	4	2.15E-03	7.17E-04	0.33	307.72	60.37	0.19
	6	3.17E-03	1.26E-03	0.39	377.99	66.16	0.17

Figure 5-5 and Figure 5-6 show the variation of the mean and standard deviation of maximum von Mises stress and compressive strain for the pipeline with 4D lateral displacement.

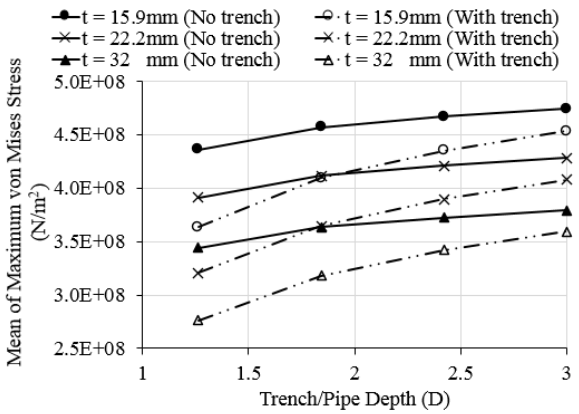

(a)

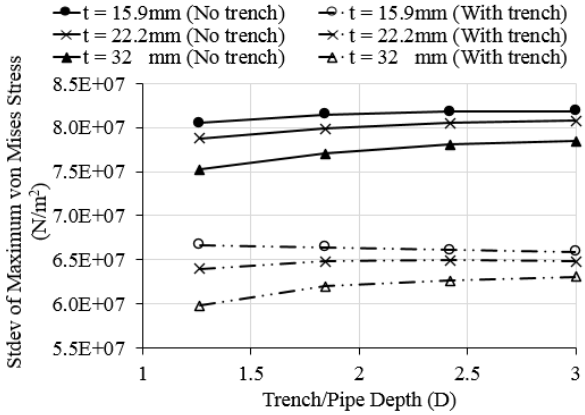

(b)

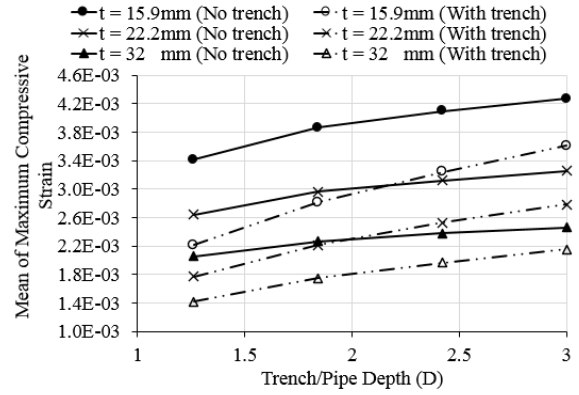

(c)

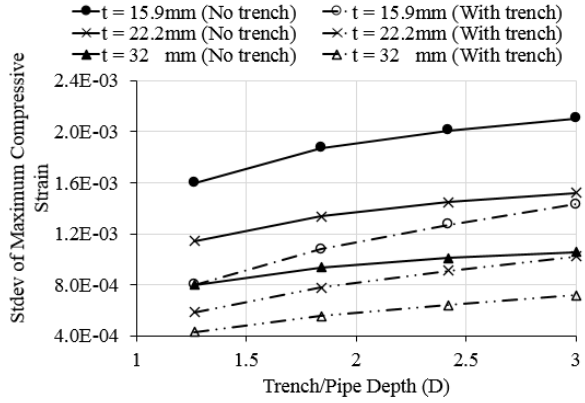

(d)

Figure 5-5. Mean and Stdev of maximum von Mises stress (a, b) and compressive strain (c, d) with the variation of trench/pipe depth

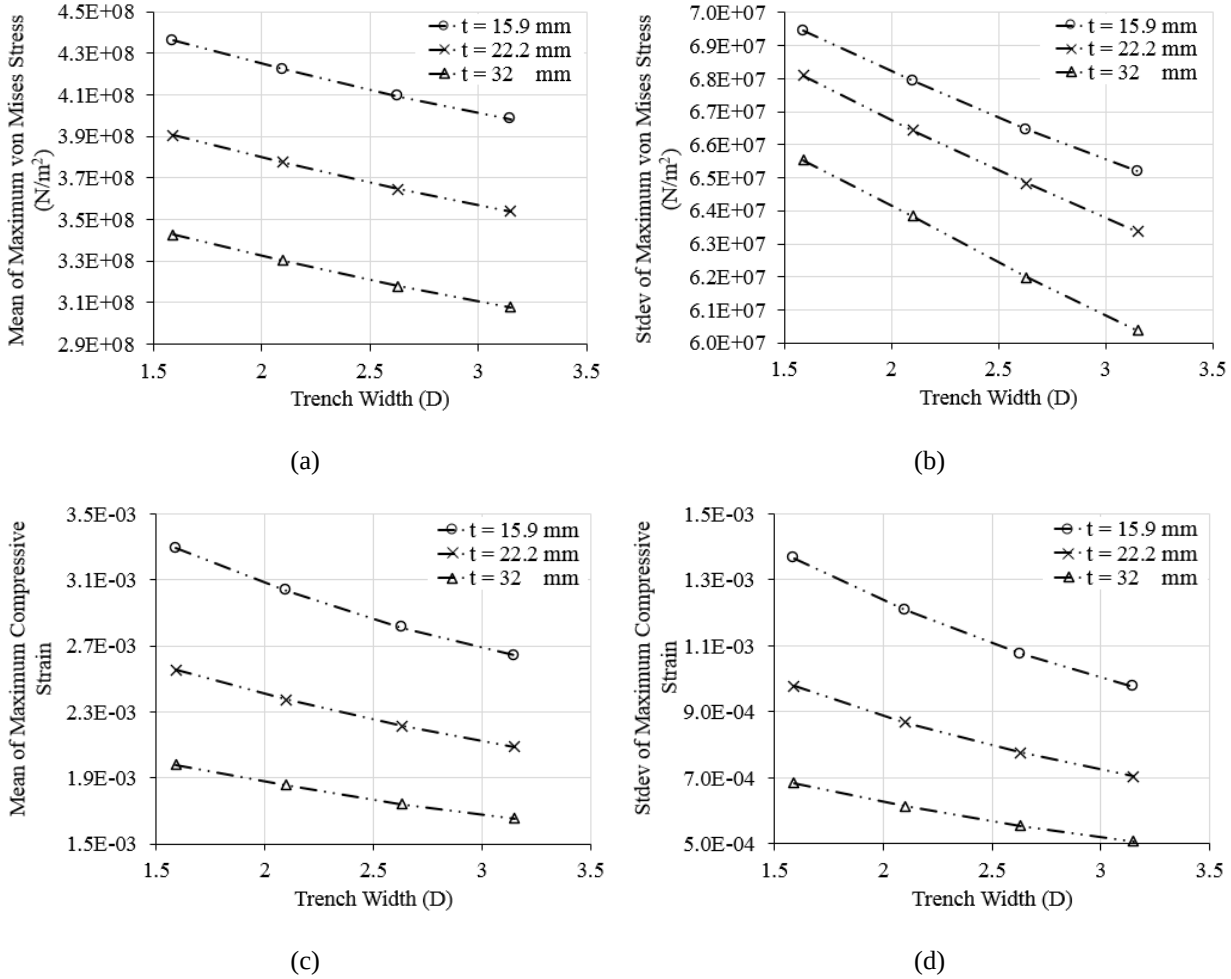

Figure 5-6. Mean and Stdev of maximum von Mises stress (a, b) and compressive strain (c, d) with the variation trench width

Figure 5-5 and Figure 5-6 show that both mean and standard deviation of maximum von Mises and compressive strain have proportional and reverse relation with the increment of trench depth and width, respectively. Figure 5-5 implies that a pipeline without trench undergoes a higher amount of von Mises and compressive strain compared to a trenched pipeline with the same configurations. These results are all in agreement with published numerical and experimental studies (e.g., Paulin, 1998; Kianian and Shiri, 2019; Kianian and Shiri, 2020).

5.4 Results and Discussion

The probabilities of exceedance were obtained as a function of trench geometry (trench width and depth) for both limit state criteria during a single fault event. Figure 5-7 shows the logarithmic exceedance curves versus trench width and depth with lateral displacement of 6D for both limit states.

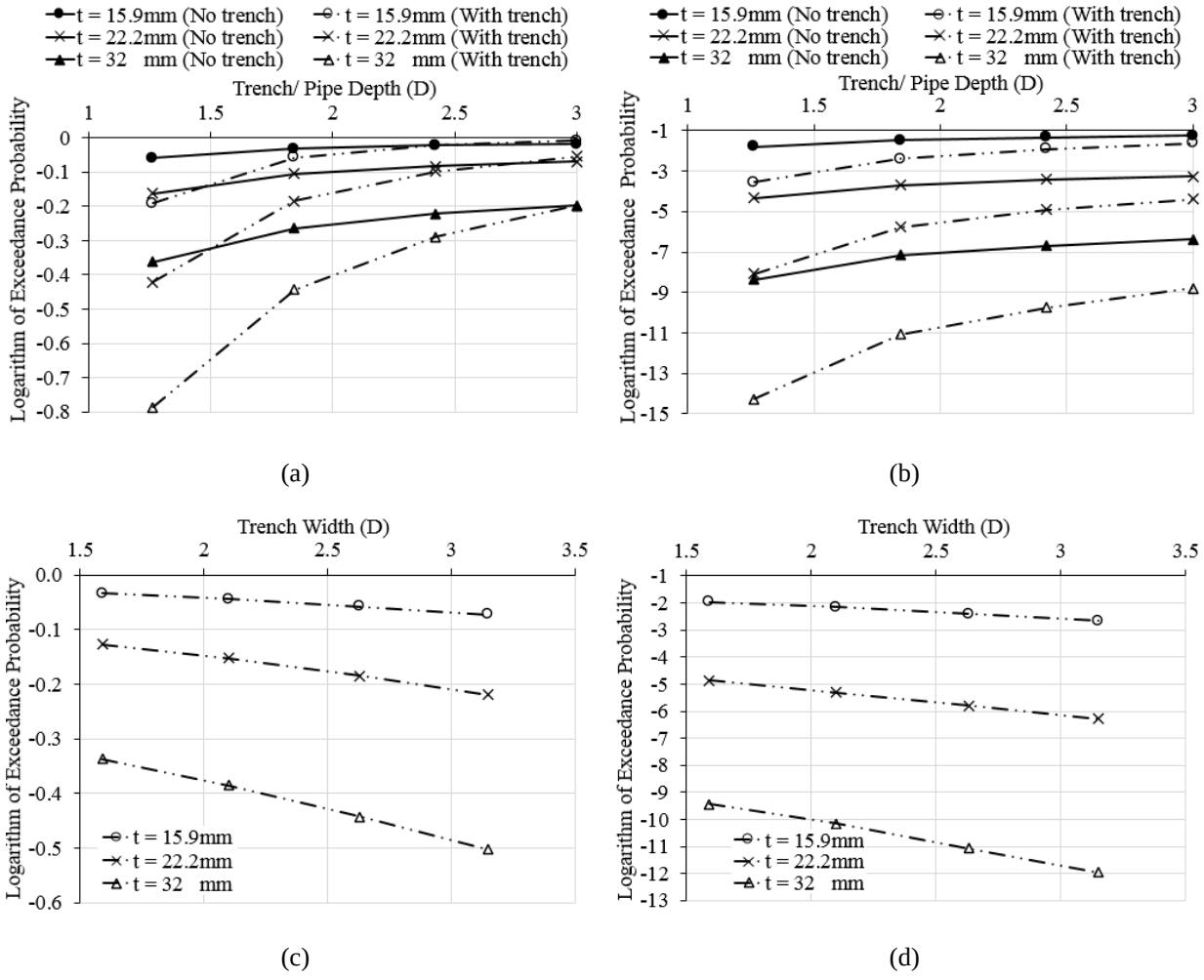

Figure 5-7. Logarithmic probability of exceedance for serviceability (left) and ultimate (right) limit states with the variation of trench depth (a, b) and trench width (c, d)

Figure 5-7 shows that the exceedance probability increases with the trench depth. This is in agreement with earlier studies showing that the lateral soil resistance is increased with deeper pipe embedment. The probability of exceedance is decreased for wider trenches larger trench width.

This reduction shows that a wider trench results in a less pipeline interaction with the trench wall that has a higher stiffness. This, in turn, reduces the mobilized soil resistance against the pipe. Also, Figure 5-7 shows that the non-trenched pipe buried in a uniform soil stratum encounters higher exceedance probability compared to the trenched pipe. This is in agreement with earlier studies, where the pipeline-backfill-trench interaction reduces the ultimate lateral soil resistance against the pipe. This ultimate load reduction is related to the failure mechanism in the backfill and native soil surrounding the pipeline. With the large displacements, pipe is penetrating to the trench wall and causes wall collapse into the trench that is filled with a soft backfill. The soft backfill mobilizes less passive pressure against the collapsing wall and results in a lower lateral soil resistance that, in turn, results are a lower probability of exceedance. A more significant variation of exceedance probability with trench depth and trench width takes place as the thickness of pipe increases and a larger structural resistance is achieved.

Figure 5-8 shows the variation of logarithmic annual probability of exceedance versus trench depth and width with 6D lateral displacement of the pipeline. Figure 5-8 (a, b) and (c, d) are corresponding to the serviceability and ultimate limit states, respectively.

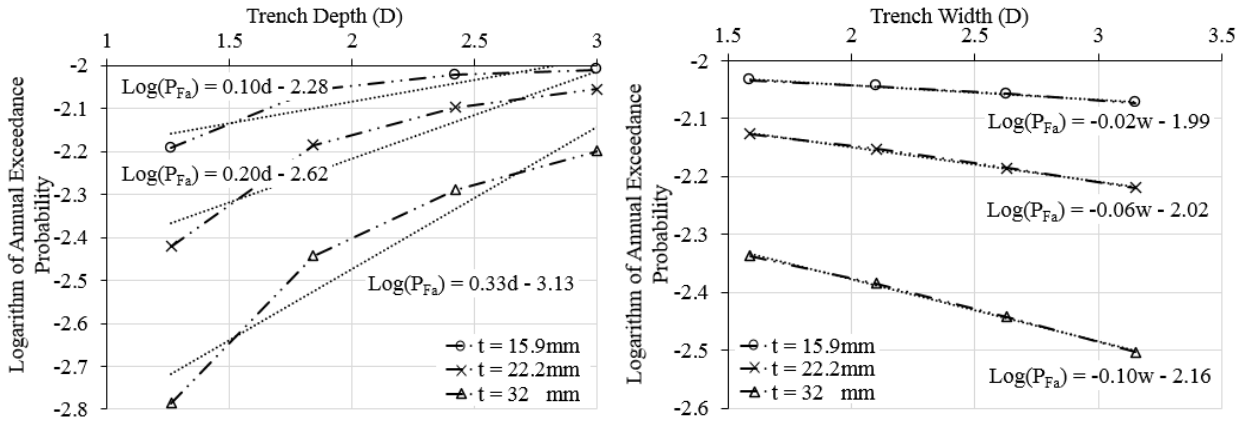

(a) (b)

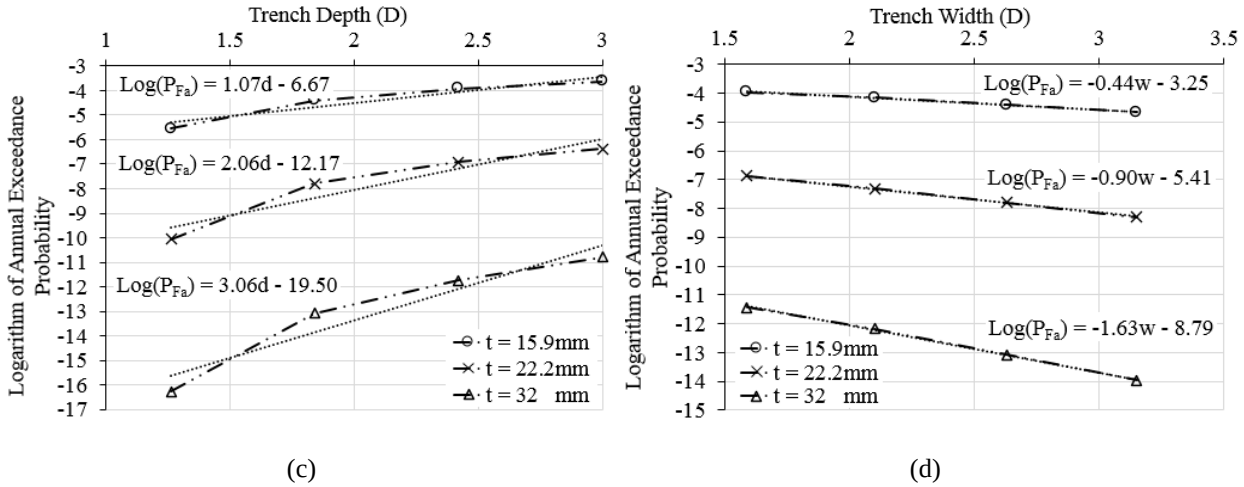

(c) (d)

Figure 5-8. The logarithm of annual exceedance probability against trench depth and width for serviceability (a, b) and ultimate limit states (c, d)

For each pipe thickness, a linear curve fit was proposed between the log (P_{Fa}) and trench depth/width. The slope of each curve in trench width/depth variations plots indicates the required increment/decrement of trench width/depth to reduce the annular probability of exceedance for one order of magnitude (by a factor of 10). It was observed that for both limit states, one order of magnitude reduction of annular exceedance probability required a higher amount of trench depth reduction compared to trench width increase. This suggests that the trench width variation may have a higher effect on the failure probability of the pipe system compared to trench depth. For example, pipe with a thickness of 15.9 mm requires 1.07D reduction of trench depth and 0.44D increment of trench width to reduce the annular probability of failure for one order of magnitude. In all curves, the slope of trendline increases with the increment of pipe thickness. So, the annual possibility of failure in pipes with higher thickness is more related to the variation of trench geometry (width/depth).

The annual exceedance probabilities against trench depth/width for remaining lateral displacement (1D, 2D, 4D) were produced to find the trench geometry satisfying the required annular safety

level (serviceability and ultimate) (see Table 5-5). The least possible trench depth was considered to achieve the lowest probability of exceedance.

Table 5-5. The desired trench geometry for different design scenarios

		Serviceability Design ($P_{Fa}<10^{-3}$)	Ultimate Design ($P_{Fa}<10^{-4}$)
D/t	Lateral Dis. (D)	Desired trench width (D)	Desired trench width (D)
48	1	<1.57	<1.57
	2	2.10	<1.57
	4	3.15	<1.57
	6	>3.15	2.10
34	1	<1.57	<1.57
	2	1.57	<1.57
	4	>3.15	<1.57
	6	>3.15	<1.57
24	1	<1.57	<1.57
	2	<1.57	<1.57
	4	2.63	<1.57
	6	>3.15	<1.57

In this study, only four trench width (i.e., 1.57D, 2.10D, 2.63D, and 3.15D) were investigated. Therefore, only (> 3.15) and (<1.57) was used for the cases where the required width was outside of these ranges. However, by increasing the lateral displacement and pipe thickness, the probability of failure increases and decreases, respectively. Consequently, the required trench width (e.g., >3.15D) for the case with, e.g., D/t=24 and lateral displacement of 6D is smaller than the case with D/t=34 and the same lateral displacement.

The study showed that the pipeline diameter/thickness ratio (D/t) and acceptance criteria have a considerable impact on the trench geometry. A larger trench is required if a stress criterion (serviceability design) is considered in a displacement-controlled event with a more significant acceptable annual limit state probability (e.g., 10^{-3}). This confirms that the strain-based criteria (ultimate design) are preferable for displacement-controlled events in the pipeline.

It is worth mentioning that the construction expenses can be optimized by using the results of the current study for the appropriate selection of pipeline and trench configurations. As material cost is often less than trenching cost, the observation in the current study shows that the selection of robust D/t ratios to mitigate fault movement hazards can result in a cost-effective design using practical trench geometries. Although, there are other engineering and economic criteria like material selection, welding, seabed bathymetry, etc. that should be accounted for the design optimization.

5.5 Conclusions and Recommendations

The probabilistic analysis of buried pipelines under seismic fault hazards was investigated using the FORM method. A finite element beam-spring model was developed to simulate the pipeline response to strike faults events. Nonlinear hyperbolic springs were used to model the trenching/backfilling effects in the lateral pipe-soil interaction. Two limit states based on von Mises stress and compressive strain of pipeline were employed to differentiate the failure and safe regions. A phyton code was developed to perform iterative probabilistic analysis with the variation of native and backfill soil properties, pipe specifications (D/t), and trench geometry under the different magnitude of lateral fault displacements. The annual probabilities of failure pipeline were calculated using the Poisson model. The key findings are summarized below:

- Deeper pipe embedment in narrow trenches results in a higher ultimate soil resistance and a higher annual probability of failure, where the trench width showed a greater impact.
- Pipe diameter to wall thickness ratio (D/t) and the limit state criteria have the most significant influence on the desired trench geometry.

- The proposed probabilistic approach could be used in real pipeline design projects in seismic regions to optimize pipe specification and trench geometry to have safe and cost-effective construction.

For a practical application, the methodology developed in the current study can be improved by deterministic selection of seismic occurrence frequency and fault displacement, incorporation of the axial and vertical effects of trenching/backfilling in the finite elements analysis, using the factored method for limit state criteria, and examining a wider range of trench configurations.

Acknowledgment

The authors gratefully acknowledge the financial support of this research by Wood PLC via establishing the Wood Group Chair in Arctic and harsh environment engineering at Memorial University, the NL Tourism, Culture, Industry and Innovation (TCII) via CRD collaborative funding program, the Natural Sciences and Engineering Research Council of Canada (NSERC) via Engage funding program, the in-kind technical supports and advice of TechnipFMC, NL, Canada, the Memorial University of Newfoundland through VP start-up fund, and the school of graduate studies (SGS) baseline fund.

References

ALA, 2005. Guidelines for the design of buried steel pipe. Am. Socoiety Civ. Eng. 2001, 29-32,68-72.

API, A.P.I., 2018. API 5L Specification for line pipe. Api Spec 5L Forty Four, 1–40. https://doi.org/10.1520/G0154-12A

ASCE Committee, 2014. Soil Parameters for Assessing Axial and Transverse Behavior of Restrained Pipelines-Part 2: Transverse Behavior. Pipelines 2014: From Underground to Forefront of Innovation and Sustainability.

Becker, D.E., 1996. Eighteenth Canadian Geotechnical Colloquium: Limit States Design For Foundations. Part II. Development for the National Building Code of Canada. Can. Geotech. J. 33, 984–1007.

BS 8010, 1993. Code of Practice for Pipelines Part 3. Pipeline Subsea: Design, Construction and Installation. Br. Stand. 8010.

C-Core, 2005. Extended model for pipe soil interaction.

C-Core, 2004. Extended model for pipe soil interaction.

C-CORE, 2003. Extended model for pipe soil interaction.

Cheng, Y., Akkar, S., 2017. Measuring bias in structural response caused by ground motion scaling. Earthq. Eng. Struct. Dyn. 605–620. https://doi.org/10.1002/eqe

Ching, J., Phoon, K.K., 2012. Modeling parameters of structured clays as a multivariate normal distribution. Can. Geotech. J. 49, 522–545. https://doi.org/10.1139/T2012-015

CSA Z662, 2003. Oil and Gas Pipeline Systems. Can. Stand. Assoc. 2003.

Das, B.M., Seeley, G.R., 1975. Pullout resistance of vertical anchors. Geotech. Eng. Div. Soc. Civ. Eng. 87–91.

DNVGL-RP-F114, 2017. DNVGL RP F114 Rules for pipe-soil interaction for submarine pipelines. Dnvgl Rp F114 97.

DNVGL-ST-F101, 2019. Submarine Pipeline Systems. Offshore standartd.

Hansen, J.B., 1948. The Stabilizing Effect of Piles in Clay., in: CN Post No. 3, Christiani and Nielson, Copenhagen, Denmark, November. pp. 14–15.

Hansen, J.B., Christensen, N.H., 1961. The ultimate resistance of rigid piles against transversal forces. Geoteknisk Institut, Copenhagen 1961.

Karamitros, D.K., Bouckovalas, G.D., Kouretzis, G.P., 2007. Stress analysis of buried steel pipelines at strike-slip fault crossings. Soil Dyn. Earthq. Eng. 27, 200–211. https://doi.org/10.1016/j.soildyn.2006.08.001

Kenny, S., Bruce, J., King, T., McKenna, R., Nobahar, A., Phillips, R., 2004. Probabilistic design methodology to mitigate ice gouge hazards for offshore pipelines, in: International Pipeline Conference.

Kianian, M., Esmaeilzadeh, M., Shiri, H., 2018. Lateral response of trenched pipelines to large deformations in clay. Proc. Annu. Offshore Technol. Conf. 5, 3487–3504. https://doi.org/10.4043/28842-ms

Kianian, M., Shiri, H., 2020. The effect of backfilling stiffness on lateral response of the shallowly trenched-backfilled pipelines in clay. Mar. Georesources Geotechnol. 0, 1–13. https://doi.org/10.1080/1064119X.2020.1736699

Kianian, M., Shiri, H., 2019. The influence of pipeline–trenchbed interaction intensity on lateral soil resistance and failure mechanisms. Int. J. Geotech. Eng. https://doi.org/10.1080/19386362.2019.1709948

Kostyukov, V.D., 1963. DISTRIBUTION OF THE DENSITY OF SAND IN THE SLIDING WEDGE IN FRONT OF ANCHOR PLATES. Soil Mech. Found. Eng. 12–13.

Mahsuli, M., Haukaas, T., 2013. Computer program for multimodel reliability and optimization analysis. J. Comput. Civ. Eng. 27, 87–98. https://doi.org/10.1061/(ASCE)CP.1943-5487.0000204

Merifield, R.S., Sloan, S.W., Yu, H.S., 2001. Stability of plate anchors in undrained clay. Géotechnique 51, 141–153.

Mohr, B., Gordon, R., Smith, R., 2004. Strain Based Design Guidelines for Pipelines, in: Pipeline Technology Conference. pp. 291 – 311.

Neely, W.J., Stewart, J.G., Graham, J., 1973. Failure loads of vertical anchor plates in sand. Soil Mech. Found. Div. Am. Soc. Civ. Eng. 669–685.

Nobahar, A., Kenny, S., King, T., McKenna, R., Phillips, R., 2007. Analysis and design of buried pipelines for ice gouging hazard: A probabilistic approach. J. Offshore Mech. Arct. Eng. 129, 219–228. https://doi.org/10.1115/1.2426989

Ovesen, N.K., 1964. Anchor slabs, calculation methods and model tests, in: Danish Geotech. Inst., Copenhagen, Denmark.

Ovesen, N.K., Stroman, H., 1972. Design methods for vertical anchor plates in sand, in: Proceedings of Specialty Conference on Performance of Earth at Earth Supported Structures.

New York: American Society of Civil Engineers, pp. 1481–1500.

Paulin, M., 1998. An investigation into pipelines subjected to lateral soil loading." Ph.D. thesis, Ph.D. thesis, Memorial University of Newfoundland, St. John's, Canada.

Phillips, R., Nobahar, A., Zhou, J., 2004. TRENCH EFFECTS ON PIPE-SOIL INTERACTION, in: International Pipeline Conference.

PRCI, 2009. Guidelines for Constructing Natural Gas and Liquid Hydrocarbon Pipelines Through Areas Prone to Landslide and Subsidence Hazards. Des. Mater. Constr. Comm. Pipeline Res. Counc. Int. Inc.

Rowe, R.K., Davis, E.H., 1982. The behaviour of anchor plates in clay. Géotechnique 32, 25–41.

Smith, J.E., 1962. Deadman anchorages is sand. Technical report R199.

Takada, S., Hassani, N., Fukuda, K., 2001. A new proposal for simplified design of buried steel pipes crossing active faults. Earthq. Eng. Struct. Dyn. 30, 1243–1257. https://doi.org/10.1002/eqe.62

Vitali, L., Bruschi, R., Mork, K.J., Levold, E., Verley, R., 1999. Hotpipe Project: Capacity of Pipes Subject to Internal Pressure, Axial Force and Bending Moment, in: Proceedings of the Ninth International Offshore and Polar Engineering Conference. pp. 22–33.

Walker, A.C., Williams, K.A.J., 1995. Strain Based Design of Pipelines, in: 14th OMAE. pp. 345–350.

Wantland, G.M., O'Neill, M.W., Reese, L.C., Kalajian, E.H., 1979. Lateral stability of pipelines in clay, in: Proceedings of the Annual Offshore Technology Conference. pp. 1025–1034.

Wells, D.L., Coppersmith, K.J., 1994. New empirical relationships among magnitude, rupture

length, rupture width, rupture area, and surface displacement. Bull. - Seismol. Soc. Am. 84, 974–1002.

Winkler, E., 1867. Die leher von der elastizitat und festigkeit. Dominicus, Prague 1867.

Chapter 6. Summary, Conclusions and recommendations

6.1 Drag Embedment Anchor-Seabed Interaction

The reliability of drag embedment anchors in the sand and layered soil (clay over sand) were investigated for catenary mooring systems and compared with earlier studies in clay. The reliability analyses were carried out by adopting the first order reliability method (FORM) using two popular Stevpris anchor families, MK5 and MK6. The limit state function was established at the mudline, while the chain-soil interaction effects were accounted for in the calculation of ultimate holding capacities. Fully coupled time-domain analyses were conducted to simulate the station keeping of a generic semisubmersible platform to obtain the dynamic mooring line tensions. The generic semisubmersible platform located in the Caspian Sea for sand seabed and Flemish Pass Basin, Newfoundland, for clay over sandy soil were selected. The response surface method was adopted for probabilistic modeling of the line tensions at the mudline. Two Excel spreadsheets containing VBA macros were developed and validated to predict the ultimate anchor capacity and the anchor trajectory down the seabed by incorporation of a popular limit state model in the sand and layered (clay over sand) seabed. The variation of annual reliability indices and the logarithm of the failure probabilities versus the fluke length and the anchor weight were obtained and compared with existing studies in each study. The important conclusions are summarized below:

- The geometrical configuration of the anchors, particularly the fluke length, are the most influential parameters in determining the reliability indices. The anchor weight has a beneficial contribution to achieving a higher level of reliability but to a less extent. A well-designed anchor geometry can significantly dominate the weight effect. For instance, some

lighter MK6 anchors result in a higher reliability index compared to heavier MK5 models due to their superior geometrical design.

- The costly in-field testing procedure recommended by design codes for estimation of the anchor capacities are unique for all of the anchor groups, seabed soil types, environmental loads, and operation conditions. This approach ignores the reliability effects affected by a wide range of inherent uncertainties and limits the cost-effectiveness of the proposed solutions. Further reliability-based refinement of the proposed procedures can have significant cost effects on offshore projects.
- A target reliability index for a given anchor group in clay can be achieved by a heavier anchor compared to the sand. It is challenging to determine a corresponding set of soil parameters in clay and sand to result in an identical reliability index. However, further studies in this area can be beneficial in proposing a more cost-effective infield testing procedure.
- The seabed soil stratum and its configuration (individual layer thickness) have a significant influence on reliability indices. Overall, the probability of failure is higher for the layered clay over sand stratum compared with homogeneous clay and sand layers. This suggests that the recommended practices that are currently considering only similar soil should be re-assessed and possibly improved for complex, layered seabed soil strata.
- The geometrical anchor configuration, particularly the fluke length, was found to have a significant effect on holding capacity and consequently the reliability indices. The anchor weight showed a positive influence on reliability results, but less effective than the fluke length. The geometrical improvement of the anchors can effectively improve their reliability. In addition, the current design practice is identical for all of the different anchor

families. This approach does not account for the significant influence of anchor geometry and the uncertainties associated with different anchor families, environmental, and operational loads. The reliability-based refinement of the design procedure can considerably improve the reliability and cost-effectiveness of anchor design.

- The configuration of layered soil strata, particularly the depth and thickness of layers, showed a significant effect on the ultimate holding capacity and reliability indices. Thicker clay layers resulted in higher reliability indices. Different range of layer thickness still needs to be investigated to generalize the obtained results.

6.2 Lateral Pipeline-Backfill-Trench Interaction

The FORM method was utilized to perform the probabilistic analysis of buried pipelines under seismic fault movements with consideration of trench effects in clay. The mechanical response of the pipe to fault movements was captured by a three-dimensional FE element model using the nonlinear beam-spring method integrated with trench effects. Two limit states based on von Mises stress and compressive strain were anticipated. The iterative calculations were performed by variation of native soil, backfill, pipe specifications (D/t), trench geometry under the different magnitude of lateral fault displacement events using developed python code. The Poisson model was employed to calculate the annual probability of failure. The key findings are summarized below:

- Deeper pipe embedment in narrow trenches results in a higher ultimate soil resistance and a higher annual probability of failure, where the trench width showed a greater impact.
- Pipe diameter to wall thickness ratio (D/t) and the limit state criteria have the most significant influence on the desired trench geometry.

- The proposed probabilistic approach could be used in real pipeline design projects in seismic regions to optimize pipe specification and trench geometry to have safe and cost-effective construction.

6.3 Comparative Reliability of Drag Embedment Anchor and Buried Pipelines

The probabilistic results of buried pipelines in this study were compared with the earlier reliability studies of drag anchors in clay (Moharrami and Shiri, 2018) to have a comparison between the reliability of pipe and anchors. The comparative probabilistic assessment was performed to determine the anchor class (referred by their weight in ton) resulting in a similar annual probability of failure with buried pipelines. The comparison was carried out for different pipe displacement, pipe specification (thickness), and trench of pipe had the maximum and minimum trench depth and width, respectively, to have the maximum annual failure probability. The map of equivalent MK5 and MK6 anchor classes with buried pipelines are presented in Table 6-1 and Table 6-2, respectively.

Table 6-1. Equivalency map of MK5 anchor with the buried pipeline

	Minimum Trench Width			Maximum Trench Depth		
Pipe Thickness (mm) / Lateral Dis. (D)	15.9	22.2	32	15.9	22.2	32
1	28 t*	30 t	35 t*	30 t	38 t*	40 t*
2	18 t	20 t	22 t	18 t	21 t*	25 t
4	15 t	16 t*	18 t	15 t	16 t*	18 t
6	14 t*	15 t	16 t*	14 t*	15 t	16 t*

Table 6-2. Equivalency map of MK6 anchor with the buried pipeline

	Minimum Trench Width			Maximum Trench Depth		
Pipe Thickness (mm) / Lateral Dis. (D)	15.9	22.2	32	15.9	22.2	32
1	20 t	24 t*	30 t	22 t	27 t*	32 t*
2	15 t	16 t*	18 t	15 t	16 t*	19 t*
4	11 t*	12 t	13 t*	11 t*	12 t	13 t*
6	10 t	11 t*	12 t	10 t	11 t*	12 t

It should be mentioned that in both Table 6-1 and Table 6-2, anchors were identified by their weights in the unit of ton(t), and the cells with star sign(*) correspond to anchor weight which are not offered in the Veryhof anchor manual. Overall, the study showed that the conventional equations commonly used between the anchors and pipelines could be reasonably used for the reliability of anchors and pipelines in uniform soils. However, involving more realistic scenarios with non-homogenous and layered soils significantly affects the failure mechanisms and ultimate soil resistance, consequently. Therefore, further improved models to account for complex soil strata is recommended for future studies.

6.4 Recommendations for Future Studies

Most essential features that could be recommended for consideration in the future studies are as follows:

a) Suggestion for Drag Embedment Study

- The existing anchor solutions are developed based on simplified anchor geometries. The idealization of anchor geometry may have a significant impact on reliability results. However, the impact is not significant in comparative studies. Further investigations are required to determine the best practice for the idealization of anchor geometry in analytical solutions.
- The reliability models for assessing the anchor capacities can be significantly improved by having access to the in-field test databases and corresponding seabed soil properties, and the statistics of failures.
- Further studies could find a corresponding relationship between soil parameters in sand and clay to have a matching reliability index.

- Developing more robust anchor-seabed interaction models to account for the complex layered soil strata would significantly improve the results of reliability analysis.

b) Recommendation for Buried Subsea Pipelines

- Developing new models for incorporation of trenching/backfilling effect in pipe-soil interaction analysis.
- Employing deterministic seismic occurrence frequency and fault displacement. Selecting the probabilistic occurrence frequency would be a better option.
- Incorporation of the trenching/backfilling impacts on pipeline response in axial and vertical directions.
- Using the factored method for limit state criteria.
- Employing more trench geometries for better quantification of optimum trench geometry.

References

ALA, 2005. Guidelines for the design of buried steel pipe. Am. Socoiety Civ. Eng. 2001, 29-32,68-72.

Almahakeri, M., Fam, A., Moore, I.D., 2013. Longitudinal bending and failure of GFRP pipes buried in dense sand under relative ground movement. J. Compos. Constr. 17, 702–710. https://doi.org/10.1061/(ASCE)CC.1943-5614.0000340

API RP 2SK, 2008. Design and Analysis of Stationkeeping Systems for Floating Structures.

ASCE, 2001. Guidelines for the seismic design of oil and gas pipeline systems. " American Society of Civil Engineers, Committee on gas and liquid fuel life lines, Technical Council on Life line Earthquake Engineering, ASCE, New York. 1984.

Audibert, J.M.E., Lai, N.., Bea, R.G., 1979. Design of Pipelines- Sea Bottom Loads and Restraints, Pipelines in Adverse Environments: A State of the Art. ASCE 1, 187–203.

Bhushan, K., Haley, S.C., Fong, P.T., 1979. Lateral Load Tests on Drilled Piers in Stiff Clays. J. Geotech. Eng. Div. ASCE 105, 969–985.

Bjerager, R., 1991. Methods for structural reliability computation. In: Casciati F, editor. Reliability problems: general principles and applications in mechanics of solid and structures. New York; Springer Verlag, 1991. p. 89-136.

C-CORE, 2003. Extended model for pipe soil interaction.

Choi, Y.J., 2007. Reliability Assessment of Foundations for Offshore Mooring Systems under Extreme Environments.

Clukey, E.C., Gilbert, R.B., Andersen, K.H., Dahlberg, R., 2013. Reliability of Suction Caissons

for Deep Water Floating Facilities 1991, 456–474. https://doi.org/10.1061/9780784412763.035

Craig, W.H., 1994. Size effects in anchor performance. Can. Geotech. J. 31, 450–454. https://doi.org/10.1139/t94-052

Das, B.M., Moreno, R., Dallo, K., 1985. Ultimate pullout capacity of shallow vertical anchors in clay. Soils Found. 2091.

Das, B.M., Tarquin, A.J., Marino, R., 1987. Model Tests for Pullout Resistance of Vertical Anchors in Clay. Soils Found. 17, 52–56.

Degenkamp, B.G., Dutta, A., 1989. Soil resistances to embedded anchor chain in soft clay 115, 1420–1438.

Dickin, E.A., 1994. Uplift resistance of buried pipelines in sand 41–48.

Ditlevsen, O., 1981. Principle of Normal Tail Approximation. J. Eng. Mech. Div. 107, 1191–1207.

DNV, 2007. Global Buckling of Submarine Pipelines–Structural Design to High Temperature/High Pressure. Dnv-Rp-F110.

DNV, 2000. Design and installation of fluke anchors in clay. Recommended Practice RP-301. Det Nor. Verit. 28.

Dunnavant, T.W., Kwan, C.-T.T., 1993. Centrifuge Modelling And Parametric Analyses Of Drag Anchor Behavior, in: Offshore Technology Conference. https://doi.org/10.4043/7202-ms

EGIG, 2005. Gas Pipeline Incidents, European Gas Pipeline Incident Data Group, Groningen, the Netherlands 6th EGIG Report 1970-2004, No. EGIG 05-R-0002.

Felix, S., Wong, M., 1985. SLOPE RELIABILITY AND RESPONSE SURFACE METHOD. Geotech. Eng. 111, 32–53.

Fulton, T.M., Stewart, W.P., 1994. Vertical loads on drag embedment anchors. Proc. Annu. Offshore Technol. Conf. 1994–May, 233–241. https://doi.org/10.4043/7491-ms

Guo, P.J., Stolle, D.F.E., 2005. Lateral Pipe–Soil Interaction in Sand with Reference to Scale Effect. J. Geotech. Geoenvironmental Eng. 131, 987–1003. https://doi.org/10.1061/(ASCE)1090-0241(2005)131

Hansen, J.B., Christensen, N.H., 1961. The ultimate resistance of rigid piles against transversal forces. Geoteknisk Institut, Copenhagen 1961.

Hasofer, A.M., Lind, N.C., 1974. Exact and Invariant Second-Moment Code Format. J. Eng. Mech. Div. ASCE 100, 111–121.

Hohenbichler, M., Rackwitz, R., 1981. Non-Normal Dependant Vectors in Structural Safety. J. Eng. Mech. Div. 107, 1227–1238.

Jung, J.K., O'Rourke, T.D., Olson, N.A., 2013. Lateral soil-pipe interaction in dry and partially saturated sand. J. Geotech. Geoenvironmental Eng. 139, 2028–2036. https://doi.org/10.1061/(ASCE)GT.1943-5606.0000960

Kianian, M., Shiri, H., 2019. The influence of pipeline–trenchbed interaction intensity on lateral soil resistance and failure mechanisms. Int. J. Geotech. Eng. https://doi.org/10.1080/19386362.2019.1709948

Klar, A., Randolph, M.F., 2008. Upper-bound and load–displacement solutions for laterally loaded piles in clays based on energy minimisation. Géotechnique 58, 815–820.

https://doi.org/10.1680/geot.2007.00197

LeLievre, B., Tabatabaee, J., 1981. Performance of Marine Anchors With Planar Flukes in Sand. Can. Geotech. J. 18, 520–534. https://doi.org/10.1139/t81-063

Liu, P.L., Der Kiureghian, A., 1991. Optimization Algorithms for Structural Reliability. Struct. Saf. 9, 161–177. https://doi.org/10.12681/eadd/1834

Lucia Faravelli, 1990. RESPONSE-SURFACE APPROACH FOR RELIABILITY ANALYSIS By Lucia Faravelli 1. J. Eng. Mech. 115, 2763–2781.

Luscher, U., Thomas, H.P., Maple, J.A., 1979. Pipe – Soil Interaction. Trans-Alaska Pipeline." Pipelines in Adverse Environments: A State of the Art. ASCE 486–502.

Madsen, H., Krenk, S., Lind, N., 1986. Methods of structural safety. Englewood Cliffs, NJ: Prentice- Hall, Inc, 1986.

Merifield, R.S., Sloan, S.W., Yu, H.S., 2001. Stability of plate anchors in undrained clay. Géotechnique 51, 141–153.

Moharrami, M.J., Shiri, H., 2018. Reliability assessment of drag embedment anchors in clay for catenary mooring systems. Mar. Struct. 58, 342–360. https://doi.org/10.1016/j.marstruc.2017.12.005

Montes-Iturrizaga, R., Heredia-Zavoni, E., 2016. Reliability analysis of mooring lines using copulas to model statistical dependence of environmental variables. Appl. Ocean Res. 59, 564–576. https://doi.org/10.1016/j.apor.2016.07.008

NCEL, 1987a. Naval Civil Engineering Laboratory Naval Civil Engineering Laboratory (Port Hueneme, 1987. Drag embedment anchors for navy moorings (Vol. 83, No. 8).

Neubecker, S.R., 1995. The behaviour of drag anchor and chain systems, PhD Thesis, Department of Civil Engineering, The University of Western Australia.

Neubecker, S.R., Randolph, M.F., 1996a. The performance of drag anchor and chain systems in cohesive soil. Georesources Geotech. 14, 1–7.

Neubecker, S.R., Randolph, M.F., 1996b. The kinematic behaviour of drag anchors in sand. Can. Geotech. J. 33, 584–594. https://doi.org/https://doi.org/10.1139/t96-084-306

Neubecker, S.R., Randolph, M.F., 1996c. The static equilibrium of drag anchors in sand. Can. Geotech. J. 33, 574–583.

Ng, C.F., 1994. Behaviour of Buried Pipelines Subjected to External Loading.

Nobahar, A., Kenny, S., King, T., McKenna, R., Phillips, R., 2007. Analysis and design of buried pipelines for ice gouging hazard: A probabilistic approach. J. Offshore Mech. Arct. Eng. 129, 219–228. https://doi.org/10.1115/1.2426989

O'Neill, M.P., 2000. The behaviour of drag anchors in layered soils, PhD Thesis, Department of Civil Engineering, The University of Western Australia.

O'Neill, M.P., Bransby, M.F., Randolph, M.F., 2003. Drag anchor fluke–soil interaction in clays. Can. Geotech. J. 40, 78–94. https://doi.org/10.1139/t02-096

Paulin, M., 1998. An investigation into pipelines subjected to lateral soil loading." Ph.D. thesis, Ph.D. thesis, Memorial University of Newfoundland, St. John's, Canada.

Phillips, R., Nobahar, A., Zhou, J., 2004. TRENCH EFFECTS ON PIPE-SOIL INTERACTION, in: International Pipeline Conference.

Poulos, H.G., 1988. Marine Geotechnics. Unwin Hyman, London, 473p.

PRCI, 2009. Guidelines for Constructing Natural Gas and Liquid Hydrocarbon Pipelines Through Areas Prone to Landslide and Subsidence Hazards. Des. Mater. Constr. Comm. Pipeline Res. Counc. Int. Inc.

Rackwitz, R., 1982. Response surfaces in structural reliability Sonderforschungsbereich 96.

Reese, L.C., Welch, R.C., 1975. Lateral Loading of Deep Foundations in Stiff Clay. J. Geotech. Eng. 101, 633–649.

Rendón-Conde, C., Heredia-Zavoni, E., 2016. Reliability analysis of suction caissons for moored structures under parameter uncertainties. Struct. Saf. 60, 102–116. https://doi.org/10.1016/j.strusafe.2016.02.004

Rowe, R.K., Davis, E.H., 1982. The behaviour of anchor plates in clay. Géotechnique 32, 25–41.

Saurwalt, K.J., 1974. Anchors digging in and holding in a soft planar seabed.

Silva-González, F., Heredia-Zavoni, E., Valle-Molina, C., Sánchez-Moreno, J., Gilbert, R.B., 2013. Reliabilitystudy of suction caissons for catenary and taut-leg mooring systems. Struct. Saf. 45, 59–70. https://doi.org/10.1016/j.strusafe.2013.08.011

Stewart, D.., 1992. Lateral loading of piled bridge abutments due to embankment construction. Ph. D thesis, Univ. of Western Australia.

Stewart Technology Associate, 1995. STA ANCHOR.

Tabatabaee, J., 1980. Theoretical and experimental investigations on marine anchors, PhD Thesis, Department of Civil Engineering, The University of Waterloo.

0241(1998)124:10(945)

Thorne, C.P., 1998. Penetration and load capacity of marine drag anchors in soft clay. J. Geotech. Geoenvironmental Eng. 124, 945–953. https://doi.org/10.1061/(ASCE)1090-0241(1998)124:10(945)

Trautmann, C.H., O'Rourke, T.D., 1985. Lateral force-displacement of buried pipe response. J. Geotech. Eng. 111, 1077–1092. https://doi.org/0733-9410/85/0009- 1077/$01.00

Tschebotarioff, G.P., 1973. Foundations, Retaining and Earth Structures . McGraw-Hill Book Company. New York .

Valle-molina, C., Heredia-zavoni, E., Silva-gonzález, F.L., 2008. Reliability analyses of suction caissons for FPSO systems, in: International Conference on Offshore Mechanics and Arctic Engineering. pp. 1–6.

Vivatrat, V., Valent, P.J., Ponterio, A.A., 1982. The influence of chain friction on anchor pile design. Proc. Annu. Offshore Technol. Conf. 1982–May, 153–156. https://doi.org/10.4043/4178-ms

Xie, X., Symans, M.D., O'Rourke, M.J., Abdoun, T.H., O'Rourke, T.D., Palmer, M.C., Stewart, H.E., 2013. Numerical modeling of buried HDPE pipelines subjected to normal faulting: A case study. Earthq. Spectra 29, 609–632. https://doi.org/10.1193/1.4000137

Yimsiri, S., Soga, K., Yoshizaki, K., Dasari, G.R., O'Rourke, T.D., 2004. Lateral and Upward Soil-Pipeline Interactions in Sand for Deep Embedment Conditions. J. Geotech. Geoenvironmental Eng. 23, 1390–1392. https://doi.org/10.1061/(ASCE)1090-0241(2004)130

Zhao, Y.G., Ono, T., 1999. A General Procedure for First/Second-Order Reliability Method

(FORM/SORM). Struct. Saf. 21, 95–112.